PERFORMANCE CHARACTERIZATION AND OPTIMIZATION OF MICROGRID-BASED ENERGY GENERATION AND STORAGE TECHNOLOGIES

by

JOE DAVID GUGGENBERGER II

A DISSERTATION

Presented to the Faculty of the Graduate School of the

MISSOURI UNIVERSITY OF SCIENCE AND TECHNOLOGY

In Partial Fulfillment of the Requirements for the Degree

DOCTOR OF PHILOSOPHY

in

GEOLOGICAL ENGINEERING

2012

Approved by

Curt Elmore, Advisor
J.D. Cawlfield
M.L. Crow
N.H. Maerz
J.D. Rogers

Report Documentation Page		Form Approved OMB No. 0704-0188

Public reporting burden for the collection of information is estimated to average 1 hour per response, including the time for reviewing instructions, searching existing data sources, gathering and maintaining the data needed, and completing and reviewing the collection of information. Send comments regarding this burden estimate or any other aspect of this collection of information, including suggestions for reducing this burden, to Washington Headquarters Services, Directorate for Information Operations and Reports, 1215 Jefferson Davis Highway, Suite 1204, Arlington VA 22202-4302. Respondents should be aware that notwithstanding any other provision of law, no person shall be subject to a penalty for failing to comply with a collection of information if it does not display a currently valid OMB control number.

1. REPORT DATE **2012**	2. REPORT TYPE	3. DATES COVERED **00-00-2012 to 00-00-2012**

4. TITLE AND SUBTITLE	5a. CONTRACT NUMBER
Performance Characterization and Optimization of Microgrid-Based Energy Generation and Storage Technologies	5b. GRANT NUMBER
	5c. PROGRAM ELEMENT NUMBER
6. AUTHOR(S)	5d. PROJECT NUMBER
	5e. TASK NUMBER
	5f. WORK UNIT NUMBER

7. PERFORMING ORGANIZATION NAME(S) AND ADDRESS(ES) **Missouri University of Science and Technology,1870 Miner Circle,Rolla,MO,65409**	8. PERFORMING ORGANIZATION REPORT NUMBER

9. SPONSORING/MONITORING AGENCY NAME(S) AND ADDRESS(ES)	10. SPONSOR/MONITOR'S ACRONYM(S)
	11. SPONSOR/MONITOR'S REPORT NUMBER(S)

12. DISTRIBUTION/AVAILABILITY STATEMENT
Approved for public release; distribution unlimited

13. SUPPLEMENTARY NOTES

14. ABSTRACT
Renewable energy-powered microgrids have proven to be a valuable technology for self-contained (off-grid) energy systems. Characterizing microgrid system performance pre-deployment would allow the system to be appropriately sized to meet all required electrical loads at a given renewable source operational time frequency. A vanadium redox battery was empirically characterized to determine operating efficiency as a function of charging characteristics and parasitic load losses. A model was developed to iteratively determine system performance based on known weather conditions and load requirements. A case study was performed to compare modeled system performance to measurements taken during operation of the microgrid system. Another iterative model was developed to incrementally predict the microgrid operating performance as a function of diesel generator operating frequency. Calibration of the model was performed to determine accurate PV panel and inverter efficiencies. A case study was performed to estimate the constant loads the system could power at varying diesel generator operating frequencies. Typical Meteorological Year 3 (TMY3) data from 217 Class I locations throughout the United States was inserted into the model to determine the quantity of external AC and DC load the system could supply at intermittent diesel generator variable operational frequencies. Ordinary block Kriging analysis was performed using ArcGIS to interpolate AC and DC load power between TMY3 Class I locations for each diesel generator operating frequency. Figures representing projected AC and DC external load were then developed for each diesel generator operating frequency.

15. SUBJECT TERMS

16. SECURITY CLASSIFICATION OF:			17. LIMITATION OF ABSTRACT	18. NUMBER OF PAGES	19a. NAME OF RESPONSIBLE PERSON
a. REPORT **unclassified**	b. ABSTRACT **unclassified**	c. THIS PAGE **unclassified**	**Same as Report (SAR)**	**152**	

PUBLICATION DISSERTATION OPTION

This dissertation has been prepared in publication format. Section 1.0, pages 1-29, has been added to supply background information for the remainder of the dissertation. Paper 1, pages 28-55, is entitled "Performance Prediction of a Vanadium Redox Battery for Use in Portable, Scalable Microgrids", and is prepared in the style used by the *Institute of Electrical and Electronics Engineers (IEEE) Transactions on Smart Grid Special Issue on Microgrids* as submitted on November 30, 2011. Paper 2, pages 56-80, is entitled "Microgrid Load Characterization using Long-Term Weather Data", and is prepared in the style used by the *IEEE Transactions on Sustainable Energy* as submitted on March 29, 2012. Paper 3, pages 81-101, is entitled "Predicting performance of a renewable energy-powered microgrid throughout the United States using typical meteorological year 3 data", and is prepared in the style used by the *Journal of Renewable Energy* as submitted on April 17, 2012. Pictures of the renewable energy-powered microgrid system at Fort Leonard Wood, Missouri are included in Appendix A, from pages 102-112. Additional figures representing AC and DC external load the renewable energy-powered microgrid could supply at various generator operating frequencies are included in Appendix B, from pages 113-124. Additional material on wind and solar energy theory is included in Appendix C, from pages 125-135.

ABSTRACT

Renewable energy-powered microgrids have proven to be a valuable technology for self-contained (off-grid) energy systems. Characterizing microgrid system performance pre-deployment would allow the system to be appropriately sized to meet all required electrical loads at a given renewable source operational time frequency. A vanadium redox battery was empirically characterized to determine operating efficiency as a function of charging characteristics and parasitic load losses. A model was developed to iteratively determine system performance based on known weather conditions and load requirements. A case study was performed to compare modeled system performance to measurements taken during operation of the microgrid system. Another iterative model was developed to incrementally predict the microgrid operating performance as a function of diesel generator operating frequency. Calibration of the model was performed to determine accurate PV panel and inverter efficiencies. A case study was performed to estimate the constant loads the system could power at varying diesel generator operating frequencies. Typical Meteorological Year 3 (TMY3) data from 217 Class I locations throughout the United States was inserted into the model to determine the quantity of external AC and DC load the system could supply at intermittent diesel generator variable operational frequencies. Ordinary block Kriging analysis was performed using ArcGIS to interpolate AC and DC load power between TMY3 Class I locations for each diesel generator operating frequency. Figures representing projected AC and DC external load were then developed for each diesel generator operating frequency.

ACKNOWLEDGMENTS

I would like to express my sincere appreciation to my major advisor Dr. Curt Elmore for his guidance and support during the development of this dissertation. I would like to thank Dr. Mariesa Crow for her leadership and obtaining the grants to finance this research and for three years of stipend, as well as The Leonard Wood Institute and the U.S. Air Force Research Laboratory for providing that funding. I would also like to thank the other members of my committee, Dr. Cawlfield, Dr. Maerz, and Dr. Rogers for their guidance, time, and years of hard work at the Missouri University of Science and Technology.

Special thanks go out to my office mates John Conroy, Yovanna Cortes Di Lena, Erica Collins, Chris Redell, Gavin Risley, Allison Sperber, and Jenna Vujic for their support and entertainment over my time at Missouri University of Science and Technology. I want to thank all members of my research group consisting of Jerry Tichenor, Tu Nguyen, Xin Qiu, Thoshitha Gamage, Yaxi Liu, Stefani Moore, and Dr. Bruce McMillan for providing key support during the development of this project.

I want to thank my sons, Grant and Austin, for providing constant entertainment during this process, and thank my Mom, Dad, and Mother-in-Law Elaine for watching Grant and Austin to allow me to get some work done. Finally, I would like to thank my wife, Monica, for her constant support and encouragement during this process. Without her, none of this would be possible.

TABLE OF CONTENTS

SECTION

APPENDICES

LIST OF ILLUSTRATIONS

LIST OF TABLES

NOMENCLATURE

1. PREVIOUS AND PRELIMINARY WORK

1.1 PURPOSE

The function of this document is to fulfill the requirements for the Ph.D. degree in Geological Engineering and to present for faculty review the areas of research and subsequent peer reviewed papers.

1.2 INTRODUCTION

Funding was obtained by the Energy Research and Development Center at the Missouri University of Science and Technology from the Leonard Wood Institute (LWI) of the United States (U.S.) Army under Grant LWI-191-060. The primary goal of this funding was to develop a portable, scalable renewable energy-powered microgrid at Training Area (TA)-246 in Fort Leonard Wood, Missouri (FLW) which could be used to replicate energy generation at forward operating bases (FOBs). This microgrid operated using a variety of energy generation and charging sources in order to optimize system performance. Construction of this microgrid occurred from March 2010 through July 2011. This microgrid is described in detail in Section 1.5. Additional funding was obtained from the U.S. Air Force Research Laboratory (AFRL) under grant FA 4819-09-C-0018 to install a separate renewable energy-powered microgrid at Hypoint Industrial Park (Hypoint) in Rolla, Missouri. Construction of this microgrid occurred from July 2011 through September 2011.

Long-term weather data was obtained from both locations, as well as the Missouri State Highway Patrol Troop I Headquarters (Troop I) in Rolla, Missouri. Due to

differences in components (i.e. Vanadium Redox Battery [VRB] as energy storage at FLW and hydrogen fuel cell as energy storage at Hypoint) and operational issues at Hypoint, all system power analysis was performed using the microgrid system at FLW.

1.3   PROBLEM STATEMENT

The U.S. Department of Energy Information (EIA) has estimated that worldwide energy use is expected to increase to 678 quadrillion British thermal units (BTU's) by 2030, a 44 percent increase from 2006 (U.S. EIA 2010). This projected growth will result in a 39 percent worldwide increase in energy-related CO_2 emissions from 29.1 billion metric tons in 2005 to 40.4 metric tons in 2030. In order to meet these predicted future demands, the U.S. EIA predicts renewable energy used for electricity generation will grow by an average of 2.9 percent annually from 2006 to 2030, with hydropower and wind power the major sources (U.S. EIA 2010).

Wind and solar power produce intermittent power. These power sources have little impact on grid operations when in small doses, but introducing the predicted increases of intermittent power will require our transmission system to be significantly upgraded or perhaps completely redesigned. There are approximately 5,400 power plants (US EIA 2011a) supplying energy throughout the U.S. via more than 700,000 miles of electrical transmission lines (Anderson 2004). Nationally retrofitting the entire electrical grid to meet these needs would be both cost and time prohibitive.

One solution to meeting future energy requirements that would not require extensive grid reconfiguration is developing decentralized microgrids, which generate power closer to the end user rather than transmitting it from remote power plants.

Intermittent power would be generated and stored locally, and work in parallel with the main grid. This would allow intermittent power sources such as wind and solar to be effectively added to meet future energy demands without requiring extensive grid reconfiguration.

Natural disasters impact every region of the U. S., and have increased in frequency and severity over the last 40 years (Deering and Thorton 1999). Common natural disasters that occur throughout the U.S. include extreme weather events such as hurricanes, flooding, tornadoes, earthquakes, volcano eruptions, and landslides. In 2011, the U.S. government set a record for disaster declarations with aggregate damage totaling approximately $55 billion (National Oceanographic and Atmospheric Administration [NOAA] National Climatic Data Center 2012). Power outages are common during natural disasters. These occurrences can last up to several months if connection to the utility grid is interrupted during the event (Congress of the U.S. Office of Technology Assessment 1990). Approximately $150 billion is lost each year in the U.S. due to power outages and blackouts (U.S. EIA 2011b).

During blackout periods, most homeowners rely on portable gasoline or diesel-powered generators to keep their refrigerators running and perhaps operate a light and a small fan for a few hours each night (Deering and Thorton 1999). Gasoline and diesel-powered generators are commonly supplied by insurers during periods of long-term power outages resulting from natural disasters. Fossil fuel-powered generators are not cost effective due to rising fuel costs, the large quantities of nonrenewable fossil fuels required to operate, and are harmful to human and environmental health due to an increase in carbon monoxide emissions and as fire hazards (NOAA 2012). The

development of deployable renewable energy-powered microgrids as power sources during long term power outages would allow energy demands to be met with portable and effective way, while limiting diesel fuel consumption to emergency periods.

The U.S. military is an expeditionary force which depends on FOBs to project power around the world (Boswell 2007). This strategy calls for U.S. military forces to be able to rapidly deploy from the U.S. to locations throughout the world, and be operational for months to years at a time. These FOBs have proven an effective means of troop deployment, specifically in Iraq and Afghanistan, and have allowed the U.S. military to close many large permanent bases throughout the world.

FOB establishment has proven to be a taxing endeavor due to the rising fuel costs and the vulnerability of supply lines. The average price of fuels sold in fiscal year 2001 was $1.337 per gallon, but the actual cost to deliver these fuels to FOBs globally is much higher, ranging from $17.50 per gallon for US Air Force worldwide tanker-delivered fuel to hundreds of dollars per gallon for US Army forces to deliver fuel deep into battlespace (U.S. Defense Science Board 2001). According to the U.S. EIA (2011c), the current National price of fuel sold of $3.513 per gallon suggests these costs could be incrementally higher. Transporting fuel to our FOBs puts our airmen and soldiers at risk, specifically from Improvised Explosive Devices (IEDs) (Boswell 2007). The U.S. Department of Defense (DoD) recognizes the importance of reducing greenhouse gas (GHG) emissions by issuing goals for future production of GHG emissions (Booth et al. 2010). The emissions responsible for human induced global warming come primarily from the burning of fossil fuels (coal, oil, and gas) with additional contributions from the clearing of forests and agricultural activities (US Global Change Research Program

2009). Therefore, reducing fossil fuel consumption at FOBs will reduce costs, reduce

GHG consumption which will help alleviate global warming, as well as save lives.

One method of reducing fuel consumption at FOBs and during natural disasters is

using renewable energy-powered microgrids. These microgrids must be portable enough

to be dropped effectively in a battlespace, and scalable enough to be used for a variety of

power-related tasks. Installation procedures must be simplified to where soldiers can

erect and activate these microgrids in a timely manner with minimal training. The

equipment used in the installation of the microgrids must have sufficient quality to meet

the demands of a battlefield environment.

This dissertation focuses on the ability to optimize the deployment of renewable

energy-powered microgrids to FOBs around the world based on performance

characteristics and field data collected from local and regional weather stations. Using

the most effective system for the job at hand would decrease cost for both installation and

shipping of the system, alleviate the amount of fuel necessary for electricity generation,

and minimize the amount of labor for shipping and installation. This would minimize the

amount of Airmen and soldiers put in harm's way when installing in battle zones.

1.4   REVIEW OF RELEVANT LITERATURE

1.4.1. Microgrids. Microgrid technologies have been extensively researched.

This includes research focused on the individual energy generation and storage

technologies, as well as the controls and electrical layout of particular systems. Lasseter

et al. (2002) discusses the potential implementation of integrating Consortium of Electric

Reliability Solutions (CERTS) microgrids to meet customers' and utilities' electrical

needs throughout the US as a replacement of grid-connected electrical resources. These CERTS microgrids combine microturbines, fuel cells, renewable power generation including photovoltaic (PV) and wind turbines, storage technologies such as batteries and ultracapacitors (UCAPs), and heat recovery technologies. This study proved CERTS microgrids to be an alternative approach to integrate small scale distributed energy resources into electricity distribution networks, and more generally, into the current wider power system.

Illindala et al. (2004) studied operational controls of two-inverter microgrids. Associated current and future hardware, controls, and software are discussed in detail, as well as future technological challenges. A case study is discussed in detail, including modeling simulations and experimental data.

Firestone and Marnay (2005) studied the design of energy manager controls for microgrids which optimize energy generation and ensure safe operation by meeting system objectives such as cost minimization, reliability, efficiency, and emissions requirements. Marnay (2007) then described how the CERTS microgrid could evolve to meet future requirements for the high quality electrical service that modern digital economies demand, and the potential role microgrids have in delivering heterogeneous power quantity. Power quality and economic considerations were discussed based on test results from separate microgrid systems in the US and Japan. Marnay and Firestone (2007) discussed the possibility of future decentralizing of the electrical grid towards disperse control in autonomous microgrids, focusing on the ability of decentralized microgrids to meet building electricity and heat requirements with appropriate energy quality. It was concluded that microgrids have potential to provide heterogeneous

electricity security, quality, reliability, and availability to serve sensitive loads and improve energy efficiency by moving thermal generation close to possible uses. Finally, Marnay et al. (2009) performed a Distributed Energy Resources Custer Adoption Model to perform an economic analysis of implementing a CERTS microgrid at three California buildings. The results of this analysis indicated the CERTS microgrid would generate a cost savings at two of the three locations while maintaining electric security, quality, reliability, and availability.

Siddiqui et al. (2010) studied microgrids that have installed distribution energy resources in the form of distributed generation with combined heat and power applications. Economic, electrical quality and risk, and environmental considerations were examined for both microgrid and grid-connected scenarios. Greater uncertainty results in higher expected costs and higher risk exposure using the distribution energy resources microgrid.

Research was also directed at applicable renewable energy-generation technologies such as PV. Kotter et al. (2008) discussed the design and testing of a nanetenna electromagnetic collector (NEC), which is a new approach for producing electricity from solar radiation by targeting mid-infrared wavelengths to improve efficiency in locations with abundant solar radiation. This research determined that both modeling and experimental measurements of individual nantennas can absorb close to 90 percent of the available in-band energy, which is significantly more efficient than typical PV cells. Crawley and Walker (2009) studied the efficiency of employing a solar hot water collector and PV panels to offset energy consumption at Camp Pendleton Marine Corps Base.

Research has also been performed to study applicable energy storage technologies. Glavin and Hurley (2007) studied the benefit of using batteries and UCAPs for solar energy storage in order to increase the lifetime of energy systems. This hybrid storage system will optimize charge/discharge cycles due to variable solar output. The ultra-capacitor/battery hybrid system must be controlled by an energy management system to coordinate charge rates. Marnay et al. (2008) studied the effect of storage technologies such as lead-acid batteries, flow batteries, or heat storage to improve on-site electrical generation processes. This paper concludes that while storage technologies are not economical, they do significantly alter the residual load profile, which would reduce carbon emissions and decrease energy costs. Denholm et al. (2010) characterized the importance of energy storage in variable renewable energy -powered systems. This paper concentrated on variable power systems and their ability to supply typical hourly loads through various battery storage mechanisms.

1.4.2. Resource Assessment and Performance Characterization. Extensive research has also been performed to assess potential renewable energy resources for electricity generation in microgrids such as solar and wind. These publications focused on potential energy reserves at given locations, and/or characterizing potential performance of a given system based on measured or predicted resources.

1.4.2.1. Solar. Solar resources have been extensively assessed around the globe. Marion et al. (2001) calculated and modeled grid-intertie PV performance throughout the US based on historic weather data. The Department of Energy (2001) performed a climate assessment to evaluate PV energy potential in the U.S. This study focused on how solar resources, weather patterns, and microclimates affect the performance of solar

energy systems. Renné et al. (2003) performed a solar resource assessment for Sri Lanka and Maldives. This assessment was based on previous studies that estimated the daily total direct sunshine hours based on several weather and agricultural stations throughout the country, as well as hourly or three-hourly cloud cover observations made at nine weather stations in Sri Lanka and two in the Maldives. The results of the analysis indicate that the annual solar resources in Sri Lanka and Maldives vary from 4.2 to 5.6 kWh/m^2/day, with seasonal variations varying between 20 and 30 percent during any season. Renné et al. (2008) performed a solar radiation resource assessment of the US. The solar resource analysis was performed based on data obtained from the PV performance model PV Watts, which is based on data from the National Radiation Database for the period of 1961-2005. This assessment concluded that some portions of the country, particularly east of the Rocky Mountains showed solar resources during 1998-2005 to be significantly lower than during 1961-1990, while a few locations in the west showed resources during 1997-2005 to be higher than in 1961-1990. Seasonal comparisons demonstrated that most portions of the US showed greater seasonal variations between 1998 and 2005 than in the annual comparisons. Helm and Burman (2010) performed a solar resource analysis of the island of Kauai, Hawaii. This study used the In My Back Yard (IMBY) software tool to calculate how much power could be generated at a specific area of a roof or open area of land, and hourly satellite solar radiation data determine the feasibility of increasing the contributions of solar energy for energy generation. The study showed that there is potential to generate enough energy to cover the peak load as reported for Kauai in 2007.

Performance of solar-powered renewable energy generation systems were also characterized based off of projected resources available at a given site. King et al. (1998) characterized new test methods to improve modeling of PV system performance. This paper describes the required implementation for the new model and associated tests that were performed, and the new model and outdoor tests required to implement it. Five separate field tests were discussed. Sites (2009) performed characterization studies on $CuIn_{1-X}Ga_XSe_2$ (CIGS) and CdTe solar cells. Specific cells were evaluated for spatial non-uniformities using light-beam-induced-current, and detailed analysis of grain-boundary effects was performed using two-dimensional modeling. Scmid et al. (2004) studied the economic feasibility of using PV/diesel hybrid energy systems in the Brazilian Amazon. This study showed that in Northern Brazil, where transportation costs cause maximal wholesale diesel prices in it is economical to implement hybrid PV/diesel systems.

1.4.2.2. Wind. Wind resource potential has also been assessed primarily to predict energy at a particular location. Elmore et al. (2004) examined the performance of a wind turbine to power a groundwater remediation system in Mead, Nebraska. The preliminary results of this study indicated that coupling wind turbines with groundwater circulation wells could prove to be an attractive alternative in terms of system operation time, cost savings, and contaminant mass removal. Gallagher and Elmore (2008) then performed a comparative analysis between using a wind turbine disconnected from the electrical utility grid, a grid-intertie wind turbine, and electricity directly from the utility grid to power a groundwater circulation well at the subject site. This study indicated retrofitting the groundwater circulation well with the wind turbine did not economically

offset costs of the turbine unless it would be installed at remote locations without direct access to the utility grid. Later, Elmore and Gallagher (2009) used wind data gathered from regional weather stations to predict performance of a wind turbine to power a groundwater circulation well. Finally, Gallagher and Elmore (2009) performed Monte Carlo simulations of wind speed data to predict wind turbine performance efficiencies using Weibull shape and scale variables determined from historic wind speed data collected near Mead, Nebraska.

Sullivan et al. (2008) characterized the benefits of adding storage technologies to wind turbines to offset variability of wind resources. This analysis deployed the Regional Energy Deployment System model developed at the National Renewable Energy Laboratory (NREL) to estimate the cost and development path associated with 20 percent penetration of wind by 2030. Their analysis used four scenarios, current wind generation with and without storage and 20 percent wind energy by 2030 with and without storage. Storage technologies modeled included pumped hydro storage, compressed air energy storage, and batteries. Results of this study indicate storage can increase wind capacity approximately 20 percent by 2050.

Arifujjaman et al. (2009) performed a performance comparison of grid connected small scale wind turbine-powered renewable energy systems. Their study concentrated on comparing wind turbines comprised of either permanent magnet generators to wound rotor induction generators. The results of their inspection shows that wound rotor induction generators are the optimum alternative for wind turbine performance.

Wilson and Stevens (2009) discussed the social and political implications of deploying wind energy in four different US states. These states included Massachusetts,

Minnesota, Montana, and Texas. Wind resources, demographics, and policies were reviewed. Massachusetts policy looked promising for wind deployment, but high costs of offshore wind technologies and political controversy of developing wind projects on land keep projects from being deployed. Wind energy projects in Minnesota and Texas were being developed at record breaking paces. Montana's wind deployment was nascent due to low levels of political and social support.

Kwon (2010) performed uncertainty analysis of wind resources to assess the energy potential of a wind turbine. This was performed by building probability models based on the natural variability of wind resources, performing an error prediction, and a Monte Carlo-based numerical simulation. This study proved that the uncertainty analysis can predict annual energy production from different averaging periods and confidence levels.

1.4.2.3. Hybrid. Research on the performance characterization of hybrid solar and wind renewable energy systems has also been performed. Barley et al. (1997) modeled the performance of a solar, wind, and lead acid battery hybrid system to size an appropriate hybrid system to power households in Inner Mongolia. The first phase of this study concentrated on using wind speed data collected at a subject site in Inner Mongolia to compare performance of small wind turbines manufactured in China, U.S., and Germany to meet household load criteria. The second phase focused on using a hybrid wind/PV energy source to meet this critical load. This experiment concluded that Chinese wind turbines were much more cost effective than those the U.S. manufacture at the wind speeds considered. This experiment also proved that using a hybrid solar/PV system reduced the unmet load from 14 percent to 3.3 percent with a cost increase of only

22 percent. Nema et al. (2009) studied the development of a hybrid PV/wind energy

system with diesel backup for energy generation. Modeling of each of the hybrid system

components was performed, the controller energy flow and management was analyzed,

and future trends were discussed. The paper concluded that this hybrid system is a viable

alternative for grid supply or remote area power supplies all over the world.

1.5   DATA COLLECTION

　　　1.5.1. System Components and Layout. A description of the microgrid system

components, site and regional weather system components, and data collection processes

are included in this section.

　　　1.5.1.1. Microgrid layout. A portable, scalable, renewable energy-powered

microgrid system was installed at latitude 37.71 and longitude -92.15 at FLW, Missouri.

The electrical diagram for this system is presented as Figure 1.1. Table 1.1 lists the

power system components. Photographs of the system components are included in

Appendix A.

　　　The system is broken down into eight separate zones, as shown in Figure 1.1.

Zone A consists of the renewable energy sources, which includes the hybrid wind/PV

source and two separate PV sources. The hybrid wind/PV source is composed of a 1.0

kilowatt (kW) Bergey XL.1 wind turbine and a 525 watt (W) PV array which are

connected to a 24 volt (V) Bergey Power Control Center. The Bergey Power Control

Center manages power by charging UCAPs and powering a resistive dump load. The

power supplied by this source is fed through a direct current (DC)/DC converter before

being connected to the 48 V DC bus located in Zone C. Two separate PV sources are

each comprised of five series containing three 26.6 V Brightwatts 200 W panels connected in parallel. These sources are connected to separate FlexMax 80 maximum power point trackers (MPPT) before being connected to the 48 V DC bus.
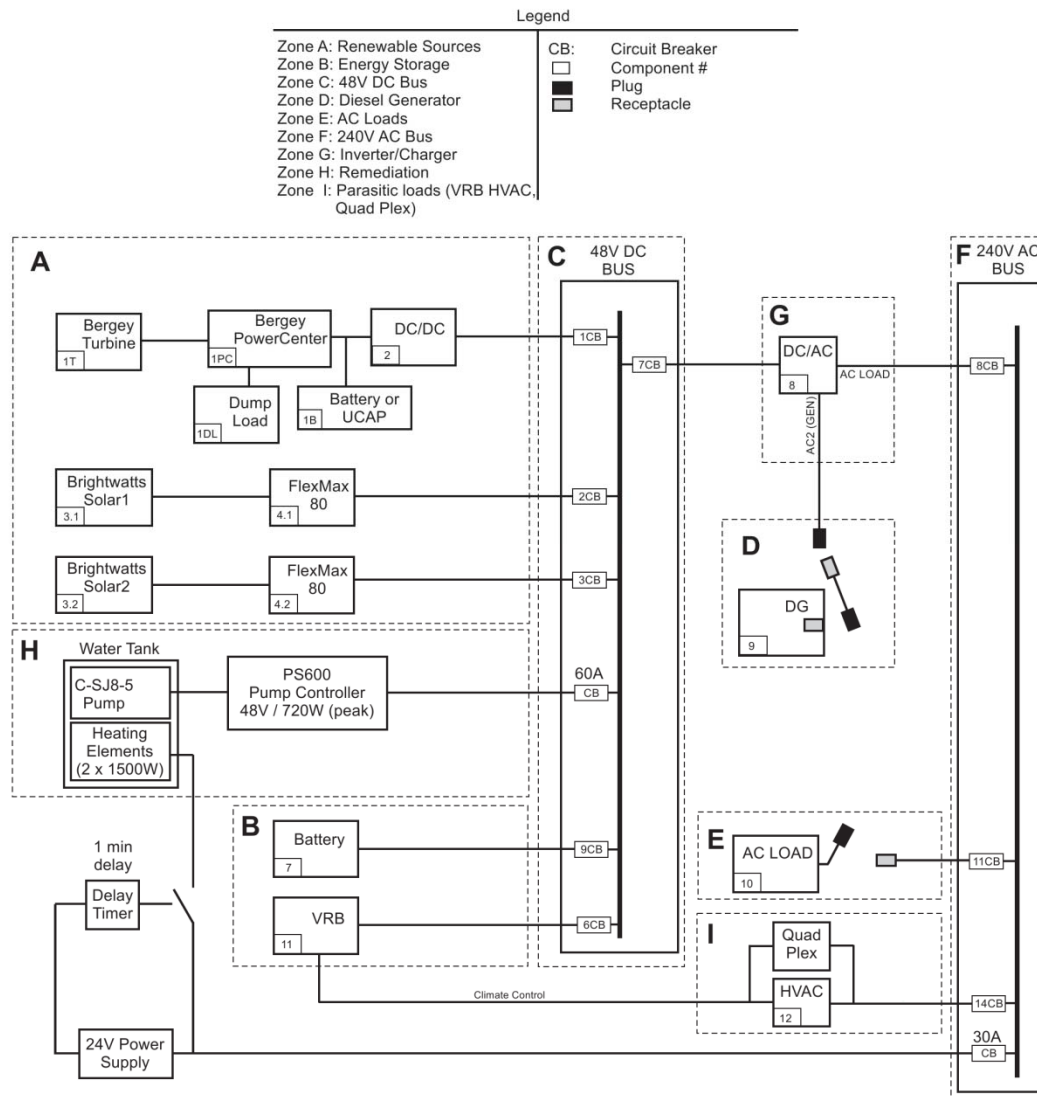
Figure 1.1: Electrical schematic for microgrid system at FLW

Table 1.1: Product summary of microgrid system components for system at FLW

ZZone[1]	NNumber[2]	Item (Quantity)	Model Number
A	1S	SunTech solar panels (3)	SUC176-STP175S
A	1T	Bergey XL.1 wind turbine (1)	BWC XL.1-24
A	1PC	Bergey Power Center controller (1)	BWC XL.1-24
A	1DL	Resistive dump load (2)	AX102KE
A	1B	Maxwell Technologies UCAP (2)	BMOD0110P016
A	2	DC/DC converter (1)	PST-SR700-24
A	3.1	Brightwatts 200 watt solar panel (15)	BW-156-200w
A	3.2	Brightwatts 200 watt solar panel (15)	BW-156-200w
A	4.1	Outback Power FlexMax 80 MPPT (1)	3510605
A	4.2	Outback Power FlexMax 80 MPPT (1)	3510605
B	5	Maxwell Technologies UCAP (4)	BMOD0165
B	6	Zahn boost DC/DC converter (1)	CH63120F-SU
B	7	Sun-Xtender sealed absorbed glass mat (AGM) battery (4)	PVX-2580L
G	8	Zantrex DC/AC inverter charge controller (1)	XW048-120/240-60
D	9	8 kW Leroy Somer generator	LSA-37M7-A-1/4
E	10	Lorentz PS600 HR/C Pump With Controller	C-SJ8-5
B	11	VRB (1)	VRB/EES
B	12	Heating Ventilation / Air Conditioner for VRB (1)	Lenox Sun Source Heat/AC

[1]The zone listed corresponds to the applicable power system category described in Figure 1.1.

[2]The number listed corresponds with the equipment identification number located in Figure 1.1.

Zone B contains the energy storage components of the system. Four 48 V UCAPs are connected in parallel to the 48 V DC bus. Power flow from the UCAP bank to the DC bus was unidirectionally controlled by a DC/DC converter. Four 12 V absorbed glass mat (AGM) batteries are connected in parallel to the 48 V DC bus. The VRB is also

connected through the 48 V DC bus. Due to temperature restrictions, the VRB

temperature is controlled by a heating ventilation and air conditioning (HVAC) unit

which is connected to the system through the 240 V alternating current (AC) bus, located

in Zone F.

Power flow between the AC and DC buses are managed by a DC/AC

inverter/charger controller located in Zone G. Power flow from the 8 kW diesel generator

located in Zone D is managed through the DC/AC inverter/charge controller. The AC

load located in Zone E is connected to the system through the 240 V AC bus.

Circuit breakers were used to manually connect/disconnect the various items for

charging and discharging. Voltage and current sensors were installed on each power and

battery source for continuous monitoring through a Campbell Scientific CR1000 data

logger. Each voltage and current censor was manually calibrated prior to data collection.

1.5.1.2. Load. The primary load used during experimental analysis was a

Lorentz PS600 centripetal submersible pump. The flow rate of the pump was controlled

through an associated controller/inverter. This pump was installed in a 55 gallon

polyvinyl chloride (PVC) drum and was plumbed to simulate a continuous loop, which

would recharge the drum at the bottom to prevent turbulence. A restrictor ball valve and

associated pressure gauges were installed to simulate the pump being submersed at given

depths in an aquifer. A gauge was installed to continuously monitor the flow rate of the

pump. This gauge was connected to the Campbell Scientific CR1000 data logger for

continuous flow rate monitoring. The pump was connected to the 48 V DC bus, which

was powered directly from the VRB. A voltage and current sensor was installed and

connected to the data logger for continuous monitoring of the pump's associated power.

Heating elements were used in order to simulate treatment processes associated with the purged water such as air sparging or carbon filtration. These two-1500 W heating elements were installed on the continuous loop system as a known constant load, and were connected to the 240 V AC bus to maximize their power. Since typical groundwater treatment processes are performed on water immediately after it is pumped from the formation, a delay timer was installed to simulate the start of the treatment processes approximately one minute after initial pumping of the well. A voltage and current sensor was installed and connected to the data logger for continuous monitoring of the heating element's associated power.

1.5.1.3. FLW weather station. A weather station was installed to monitor Site weather conditions in the vicinity of the microgrid system in FLW. The weather station consisted of components listed in Table 1.2. One anemometer were installed approximately 10 foot (ft) directly below the wind turbine head at 50 ft above ground surface, which is approximately one rotor diameter below the wind turbine head as directed by NREL (Jonkman et al. 2004). Both anemometers, the wind sentry set, one temperature probe, and a barometer were installed directly on the weather station, which was located approximately 30 ft upwind of the weather station per National Renewable Energy Laboratory requirements (Jonkman et al. 2004). Another temperature probe was added inside the VRB container at a later date in July 2012. Readings of each component were performed every five seconds, and averages of these readings were recorded every 10 minutes on a Campbell Scientific CR1000 data logger. These readings are downloaded and analyzed using PC400 software from Campbell Scientific.

Table 1.2: Product summary of FLW weather station components

Installed Height	Item (Quantity)	Model Number
50 ft	RM Young Wind Sentry Anemometer	03101-L100
3 m	RM Young Wind Sentry Set (Anemometer and Wind Vane)	41303-5A
3 m	Temperature Probe (Weather Station)	107-L8
3 m	Apogee SP-110 Pyranometer (Horizontal Mount)	CS300-L12
3 m	Apogee SP-110 Pyranometer (Tilt Mount)	CS300-L12
2 m	Sentra 278 Barometer	CS100
2 m	CR800 Measurement and Control Datalogger	CR1000-ST-SW-NC
2 m	Temperature Probe (VRB container)	107-L8

1.5.1.4. Regional weather stations. A weather station was installed at latitude 37.98 and longitude -91.72 at Hypoint, Rolla, MO. Components of this weather station are listed in Table 1.3 below. Each weather sensor was mounted on a 50 ft tall Universal Tower 5-50 freestanding aluminum tower. Heights of each sensor are listed in Table 1.3 below, with wind sensors installed at 50 ft, 10 m and 3 m to calculate wind shear. Tilt and horizontal pyranometers were installed to measure radiation directly at ground surface as well as the site latitude, which is the angle PV panels would be mounted to maximize power output annually. Readings of each component was performed every five seconds, and averages of these readings were recorded every 10 minutes on a Campbell Scientific CR1000 data logger. These readings were downloaded and analyzed using PC400 software from Campbell Scientific.

Table 1.3: Product summary of Hypoint weather station components

Installed Height	Item (Quantity)	Model Number
50 ft	RM Young Wind Sentry Anemometer	03101-L100
50 ft	RM Young Wind Vane	024A-L
10 m	RM Young Wind Sentry Anemometer	03101-L100
3 m	RM Young Wind Sentry Anemometer	03101-L100
3 m	Temperature Probe	107-L8
3 m	Apogee SP-110 Pyranometer (Horizontal Mount)	CS300-L12
3 m	Apogee SP-110 Pyranometer (Tilt Mount)	CS300-L12
3 m	Sentra 278 Barometer	CS100
3 m	CR1000 Measurement and Control Datalogger	CR1000-ST-SW-NC

Measurements from a weather station installed at Troop I at latitude 37.96 and longitude -91.78 in Rolla, Missouri during a previous research project were also used. Components of this weather station are listed in Table 1.4 below. Sensors were mounted on a 30 meters (m) Bergey Excel wind turbine tower, with heights of each sensor listed in Table 1.4 below. Readings of each component will be performed every five seconds, with averages of these readings being recorded every 1 hour on a Campbell Scientific CR1000 data logger. These readings are downloaded using Fat Spaniel online software.

Table 1.4: Product summary of Troop I weather station components

Installed Height	Item (Quantity)	Model Number
20 m	RM Young Wind Monitor	050103-L
10 m	RM Young Wind Monitor	050103-L
3 m	RM Young Wind Monitor	050103-L
3 m	Temperature Probe	107-L8
3 m	Apogee SP-110 Pyranometer (Horizontal Mount)	CS300-L12

1.5.2. Data Collection. Weather data was collected at FLW, Hypoint, and Troop I. All weather data was collected at FLW from November 2010 through February 2012 except VRB temperature, which was collected from July 2011 through February 2012. This data included wind speed at 50 ft and 3 m, wind direction, horizontal and tilt solar radiation, temperature, and barometric pressure at 3 m. Weather data was also collected at Hypoint, Rolla, Missouri from November 2010 through February 2012, although ambient temperature was only collected through July 2011. This data included horizontal solar radiation at 3 m height, wind speed at 50 ft, 10 m, and 3 m height, wind direction at 50 ft height, and temperature and barometric pressure at 3 m height. The third weather station located at Troop I collected wind speed, solar radiation, and barometric pressure data from January 2010 through February 2012 with a gap from July 2010 through October 2010 due to sensor malfunction. Data parameters collected at this site include horizontal radiation, temperature, and wind speed and direction.

Microgrid performance was also characterized through voltage and current data collected before and after each energy source, storage device, and load. Voltage and current sensors manufactured and calibrated on campus were installed in the circuit directly after each PV series and after each MPPT to determine power provided by the PV arrays as well as efficiency of the tracker. Voltage and current sensors were also be installed to the circuit coming from the VRB to instantaneously measure the power supplied from the VRB, and attached to the circuit to measure the power used by the pump and associated hardware. Measurements at each sensor were taken every five seconds and averaged every 10 minutes. Timing of these measurements was synchronized to match climatic data collected at FLW.

1.6   RESEARCH OBJECTIVES AND OUTLINE

This dissertation was separated into three distinct papers which were submitted separately to peer-reviewed journals. The first paper, which is entitled "Performance prediction of a VRB for use in portable, scalable microgrids", was submitted to the Institute of Electrical and Electronics Engineers (IEEE) Transactions on Smart Grids Special Issue on Microgrids on November 30, 2011. This paper is included in Section 2. The objectives of this paper were to:

- Characterize performance of a VRB for use in a renewable energy-powered microgrid. This included characterizing the following:

  - VRB HVAC usage

  - VRB parasitic pump and controller usage

  - VRB performance as a function of state of charge (SOC) and charging / discharging power

- Develop a model to iteratively calculate microgrid system performance assuming a PV array is charging the VRB.

- Compare the modeled values of parasitic loads, VRB efficiency, and total system efficiency versus the manufacturer's recommended values.

The second paper, which is entitled "Microgrid load characterization using long-term weather data", was submitted to IEEE Transactions on Sustainable Energy on March 29, 2012. This paper is included in Section 3. The objectives of this paper were to:

- Develop a model to empirically characterize microgrid system performance based on known weather conditions and load requirements.

- Predict intermittent periods where backup generator is necessary to meet a given load as a function of time and VRB SOC.

- Calibrate the microgrid system to determine actual PV panel efficiency and inverter efficiency compared to manufacturer's recommendations.

- Predict the constant power supplied by the FLW microgrid as a function of variable diesel generator operating frequencies.

- Characterize the constant AC and DC external loads the microgrid could supply as a function of diesel generator operating frequency at Hypoint and Troop I based on long term weather data collected at each location.

The third paper, which is entitled "Predicting performance of a renewable energy-powered microgrid throughout the United States using Typical Meteorological Year 3 data", was submitted to the Journal of Renewable Energy on May 17, 2012. This paper is included in Section 4. Objectives of this paper were to:

- Collect Global Horizontal Irradiance (GHI) data from 217 Typical Meteorological Year 3 (TMY3) weather stations throughout the U.S.

- Convert GHI data to Global Incidence Irradiance (GII) data based on the latitude of each location using the Systems Analysis Model (SAM).

- Predict AC and DC load that could be constantly supplied by the PV-powered microgrid at each location as a function of diesel generator operating frequency.

- Perform Kriging analysis to interpolate power between each TMY3 location using ArcMap 9.3 software.

- Develop figures that characterize AC and DC loads the microgrid could constantly supply at each location at a variety of diesel generator operating frequencies.

- Compare these figures to solar radiation maps developed by NREL to determine the effectiveness of the model.

Pictures of the microgrid system are included in Appendix A. Additional figures depicting constant AC and DC loads that could be provided by the microgrid based on differing generator operational frequencies are included in Appendix B. Additional information depicting the theory behind wind and solar energy generation are included in Appendix C.

1.7   REFERENCES

Anderson, R.N. (2004). *The Distributed Storage-Generation "Smart" Electric Grid of the Future.* 10-50 Workshop Proceedings: Technologies and Policies for a Low-Carbon Future, Pew Center on Global Climate Change and the National Commission on Energy Policy. March 25-26.

Arifujjaman, M.D., , Iqbal, M.T., Quiacoe, J.E. (2009). Performance comparison of grid connected small wind energy conversion systems. Wind Engineering ; 33(1):1-18.

Barley CD, Lew DJ, Flowers LT. (1997). *Sizing Wind/Photovoltaic Hybrids for Households in Inner Mongolia.* Presented at Windpower '97 Conference. National Renewable Energy Laboratory, Golden, Colorado.

Booth, S., Barnett, J., Burman, K., Hambrick, J., and Westby, R. (2010). *Net Zero Energy Military Installations: A Guide to Assessment and Planning.* National Renewable Energy Laboratory Technical Report NREL/TP-7A2-48876.

Boswell, R.L. (2007). *The Impact of Renewable Energy Sources on Forward Operating Bases.* Unpublished Thesis Approved for Public Release, Air Command and Staff College, Air University.

Congress of the U.S. Office of Technology Assessment. (1990). *Physical Vulnerability of Electric Systems to Natural Disasters and Sabotage.* Technical Report OTA-E-453.

Crawley, A.S. and Walker, A. (2009). *U.S. Marine Corps Base Camp Pendleton: Using the Sun for Hot Water and Electricity.* U.S. Department of Energy & Renewable Energy Federal Energy Management Program. Technical Report DOE/GO-102009-2910.

Deering, A. and Thornton, J.P. (1999). *Applications of solar technology for catastrophe response, claims management, and loss prevention.* National Renewable Energy Laboratory, Retrieved April 10, 2012, from http://www.nrel.gov/docs/fy99osti/25866.pdf

Denholm, P., Ela, E., Kirby, B., and Milligan, M. (2010). *The Role of Energy Storage with Renewable Electricity Generation.* National Renewable Energy Laboratory Technical Report NREL/TP-6A2-47187.

Elmore, A.C., Gallagher, R., and Drake, K.D. (2004). Using Wind to Power a Groundwater Circulation Well – Preliminary Results. Remediation; 14(4):49-65

Elmore, A.C. and Gallagher, R. (2009). Using regional climate center data to predict small wind turbine performance. *Practice Periodical of Hazardous, Toxic, and Radioactive Waste Management,* 13(1):14-19.

Firestone, R. and Marnay, C. (2005). Energy Manager Design for Microgrids. East Orlando Lawrence Berkely National Laboratory. Report LBNL-54447 prepared for California Energy Commission.

Gallagher, R. and Elmore, A.C. (2008). Groundwater Circulation Well Operation Using Wind Turbine – Generated Energy. Remediation; 18(3):31-39.

Gallagher, R. and Elmore, A.C. (2009). *Monte Carlo Simulations of Wind Speed Data.* Wind Engineering; 33(6):661-673.

Glavin, M.E. and Hurley, W.G. (2007). Ultracapacitor/battery hybrid for solar energy storage. Solar Energy 2007; 30(2):212-218

Helm, C. and Burman, K. (2010). *Kauai, Hawaii: Solar Resource Analysis and High-Penetration PV Potential.* National Renewable Energy Laboratory Technical Report NREL/TP-7A2-47956

Illindala, M.S., Piagi, P., Zhang, H., Venkataramanan, G., Lasseter, R.H. (2004).Hardware Development of a Laboratory-Scale Microgrid Phase 2: Operation and Control of a Two-Inverter Microgrid. National Renewable Energy Laboratory Report No. NREL/SR-560-35059.

Jonkman, J.M., Buhl Jr., M.L. (2004). FAST's User's Guide. National Renewable Energy Laboratory Technical Report NREL/EL-500-38230.

Kotter, D.K., Novack, S.D., Slafer, W.D., and Pinhero, P. (2008*). Solar Nantenna Electromagnetic Collectors.* Idaho National Laboratory 2nd International Conference on Energy Sustainability. INL/CON-08-13925

Kwon, S.D. (2010). Uncertainty analysis of wind energy potential assessment. *Applied Energy* 87:856-865.

Lasseter, R., Akhil, A., Marnay, C., Stephens, J., Guttromson, R., Meliopoulous, A.S>, Yinger, R., and Eto, J. (2002). *Integration of Distributed Energy Resources: The CERTS MicroGrid Concept.* Consortium for Electric Reliability Technology Solutions White Paper Prepared for Transmission Reliability Program, Office of Power Technologies, U.S. Department of Energy.

Marion, B., Andeberg, M., George, R., Gray-Hann, P., and Heimiller, D. (2001). *PVWatts Version 2 – Enhanced Spatial Resolution for Calculating Grid-Connected PV Performance.* Presented at NCPV Program Review Meeting. National Renewable Energy Laboratory Technical Report NREL/CP-650-30941.

Marnay, C. (2007). *Microgrids and Heterogeneous Security, Quality, Reliability, and Availability.* Ernest Orlando Lawrence Berkely National Laboratory Environmental Energy Technologies Division. LBNL-62460.

Marnay, C. and Firestone, R. (2007). Microgrids: An Emerging Paradigm for Meeting Building Electricity and Heat Requirements Efficiently and with Appropriate Energy Quality. Ernest Orlando Lawrence Berkely National Laboratory Environmental Energy Technologies Division. LBNL-62572.

Marnay, C., Stadler, M., Aki, H., Coffey, B., Firestone, R., Lai, J., and Siddiqui, A. (2008). *Microgrid Selection and Operation for Commercial Buildings in California and New York States.* Ernest Orlando Lawrence Berkely National Laboratory Environmental Energy Technologies Division.

Marnay, C., Lai, J., Stadler, M., and Siddiqui, A. (2009*). Added Value of Reliability to a Microgrid: Simulations of Three California Buildings.* Ernest Orlando Lawrence Berkeley National Laboratory Environmental Energy Technologies Division.

National Oceanographic and Atmospheric Administration National Climatic Data Center. (2012). Billion dollar U.S. weather / climate disasters. Retrieved April 10, 2012, from http://www.ncdc.noaa.gov/soa/reports/billionz.html

Nema, P., Nema, R.K., and Rangnekar, S. (2009*). A current and future state of art development of hybrid energy system using wind and PV-solar: a review.* Renewable and sustainable Energy Reviews 2009; 13(8):2096-2103

Renné, D., George, R., Marion, B., Heimiller, D., and Gueymard, C. (2003*). Solar Resource Assessment for Sri Lanka and Maldives.* National Renewable Laboratory Technical Report NREL/TP-710-34645.

Renné, D., George, R., Wilcox, S., Stoffel, T., Myers, D. and Heimiller, D. (2008). *Solar Resource Assessment.* National Renewable Energy Laboratory Technical Report NREL/TP-581-42301.

Schmid AL, Augusto C, Hoffman A. Replacing diesel by solar in the Amazon: short-term economic feasibility of PV-diesel hybrid systems. Energy Policy 2004; 32(7):881-898

Siddiqui, A., Stadler, M., Marnay, C., and Lai, J. (2010). *Optimal Control of Distributed Energy Resources and Demand Response under Uncertainty.* Ernest Orlando Lawrence Berkeley National Laboratory Environmental Energy Technologies Division.

Sites, J.R. (2009). Characterization and Analysis of CIGS and CdTe Solar Cells: December 2004 – July 2008. NREL Subcontract Report NREL/SR-520-44811.

Sullivan, P., Short, W., and Blair, N. (2008), Modeling the Benefits of Storage Technologies to Wind Power. Wind Engineering 2008; 32(6):603-615

U.S. Defense Science Board. (2001). More Capable War Fighting Through Reduced Fuel Burden. Task Force on Improving Fuel Efficiency on Weapons Platforms. Office of the Under Secretary of Defense for Acquisition, Technology and Logistics, Washington, D.C.

U.S. Department of Energy. (2001). *Assessing Climate to Improve Solar Design*. Energy Efficiency and Renewable Energy Clearinghouse, U.S. Department of Energy Technical Report DOE/GO-120001-1171.

U.S. Energy Information Administration. (2010). International Energy Outlook 2010:World Energy Demand and Economic Outlook [online], available: http://www.eia.doe.gov/oiaf/ieo/world.html.

U.S. Energy Information Administration. (2011a). Count of Electric Power Industry Power Plants, by Sector, by Predominant Energy Sources within Plant [online], available: http://www.eia.gov/cneaf/electricity/epa/epat5p1.html [report generated 4 Jan 2011].

U.S. Energy Information Adminstration. (2011b). Electric Power Annual 2009 – State Data Tables [online], available http://www.eia.gov/electricity/data/state/.

U.S. Energy Information Administration. (2011c). Independent Statistics and Analysis: Gasoline and Diesel Fuel Update [online], available: http://tonto.eia.doe.gov/oog/info/gdu/gasdiesel.asp [assessed 8 Feb 2011].

U.S. Global Change Research Program. (2009). Global Climate Change Impacts in the U.S. [electronic resource]. Government Document Number PREX 23.14: G 51/3.

Wilson, E.J, and Stephens, J.C., (2009). Wind Deployment in the U.S.: States, Resources, Policy and Disclosure. Environmental Science & Technology 2009; 43(24):9063-9070.

PAPER

I. PERFORMANCE PREDICTION OF A VANADIUM REDOX BATTERY FOR USE IN PORTABLE, SCALABLE MICROGRIDS

J.D. Guggenberger[1], A.C. Elmore[1], J.L. Tichenor[2], and M.L. Crow[2]

[1]Department of Geological Engineering, Missouri University of Science and

Technology – Rolla, Missouri, U.S.A. 65401

[2]Department of Electrical and Computer Engineering, Missouri University of Science

and Technology – Rolla, Missouri, U.S.A. 65401

Email: jguggenb@mst.edu, elmoreac@mst.edu, ticheno@mst.edu, crow@mst.edu

ABSTRACT

VRBs have proven to be a viable energy storage technology for portable

microgrids due to their rechargeability and high energy density. VRBs exhibit parasitic

load loss during operation due to pumping of electrolyte across the membrane during

charging and discharging cycles, as well as required temperature control in the form of

HVAC. This paper focuses on empirically characterizing VRB efficiency based on

known climatic operating conditions and load requirements. A model was created to

determine system performance based on known climatic and load data collected and

analyzed over an extended time period. A case study was performed using known data

for a week time period to characterize system performance, which was compared to

actual system performance observed during this same time period. This model allows for appropriate sizing of the PV array and discretionary loads based on required energy density of the system.

INDEX TERMS

Batteries, energy management, energy storage, load management, load modeling, performance evaluation, predictive modeling, statistical analysis

I. INTRODUCTION

Renewable-powered microgrids have proven a valuable technology for self-contained (off-grid) energy systems. These microgrids have proven effective in reducing fuel consumption and are cost effective in locations without grid access [1]. The U.S. military establishes FOBs globally as an effective method of temporary troop deployment in active battlefields [2]. These FOBs are typically powered by gasoline or diesel generators, which are not cost effective due to rising fuel and fuel transportation costs, and put soldiers in harm's way due to fuel transportation in battlefields proving to be an effective target of enemies' improvised explosive devices [3]. Renewable energy-powered microgrids are proving to be a potentially valuable tool to meet future energy demands at these FOBs in a portable and effective manner. These microgrids also allow the user to employ a variety of energy generation and storage devices such as PV and wind turbines to optimally meet site-specific needs.

Energy storage technology is a critical aspect of future development of portable, scalable microgrid technology [4]. Current energy storage technologies such as lead acid

batteries contain low energy density at a high mass, which prohibits effective transportation of these microgrids to overseas FOBs. VRBs have proven to be a viable energy storage technology for portable, scalable microgrids due to their high efficiency, high scalability, fast response, long life, and low maintenance requirements [5].

VRBs are a type of rechargeable battery that consists of an assembly of power cells that requires two electrolytes separated by a proton exchange membrane [6]. Each electrolyte contains vanadium based in a sulfuric acid solution. The positive electrolyte half-cell contains VO_2^+ and VO^{2+} ions, and the negative electrolyte half-cell contains V^{3+} and V^{2+} ions. When the vanadium battery is charged, the VO^{2+} ions in the positive half-cell are converted to VO_2^+ ions when electrons are removed from the positive terminal of the battery. During this period, the electrons are introduced which converts the V^{3+} ions into V^{2+} ions in the negative half cell. During this process, electrolyte is circulated through the cell using a series of pumps. These pumps must be in operation during charging and discharging cycles, resulting in a parasitic load loss, which is a function of the flow rate of the electrolyte. VRBs must also have temperature control in the form of HVAC to ensure the electrical equipment is not exposed to extreme ambient temperatures (i.e. between 4 degrees Celsius [°C] and 29°C. HVAC usage also results in a parasitic load loss during operations in extreme ambient temperature ranges. Therefore, HVAC load loss is a function of ambient temperature.

Characterizing performance of microgrid technology allows optimization of the system pre-deployment, allowing the system design to meet all necessary critical and noncritical loads without including unnecessary hardware, which increases costs of both system components and transportation. Past researches focused on electrochemical

characterization of VRB performance [5] and modeling VRB terminal voltage output for use in power smoothing in wind systems [6]. This paper focuses on empirically characterizing system performance using known climatic and electrical operating conditions over an extended time period, from June 2011 through October 2011. Sources of energy losses during system operation are analyzed to determine stochastic relationships to allow accurate calculations of system performance based on known climatic data. A model was created to determine the peak AC/DC load available, as well as VRB efficiencies during operation based on sample interval, solar insolation, ambient temperature, VRB container temperature, and the VRB SOC. A case study was then performed based on known data collected over a week in June 2010, and the results of the model were compared to actual field measurements collected during the same time period. Power, cumulative energy production/consumption, and VRB efficiency were compared between modeled and actual system performance to determine the effectiveness of this model. System performance was then analyzed during this case study.

II.   MICROGRID DESCRIPTION

A microgrid was constructed at a FOB training area at FLW at latitude 37.71 degrees and longitude -92.15 degrees. This system, which is outlined in Fig. 1, is composed of multiple energy generation and storage systems to allow various experimental scenarios. The energy generation configuration to collect data for analysis included a 6 kW PV array consisting of 30 - 200 W Brightwatts Inc. solar panels (model BI-156-200W-G27V) connected to two Outback FlexMax 80 charge controllers. The PV

array was electrically separated into two 3 kW arrays, and was mounted at a fixed horizontal angle of 38 degrees facing south. These controllers were used to charge a nominal 5 kW Prudent Energy VRB rated at an energy density of 20 kilowatt-hours (kWh). VRB SOC is a measurement (recorded in V) that can be used to calculate energy capacity of the VRB, where 0.5 V SOC equals 0 kWh of capacity and 9.5 V SOC equals 20 kWh of capacity. A three cylinder Kubota diesel engine was connected to the Leroy Somer 8 kW brushless self-regulated type generator, which is connected to the VRB through a Xantrex DC/AC inverter charge controller. Variable loads used during experimentation included a Lorentz PS600 HR/C submersible water pump with controller, two 1,500 W heating elements, and the HVAC of the VRB.

Solar insolation was measured using one Apogee SP-110 pyranometer mounted at 38 degrees and a second pyranometer mounted horizontally on a nearby 3 m weather station. One Campbell Scientific 107-L temperature probe was located on the 3 m weather station, and a second temperature probe was located inside the VRB. Power was measured using LEM LA55-P current and LEM LV25-P voltage sensors for various power uses including PV, charge controlled PV, diesel generation, VRB HVAC, VRB pumps, submersible pump, and heating elements. The pyranometers and power sensors were connected to a Campbell Scientific Model CR1000 datalogger. Sensor readings were measured at 5 second intervals, and 10 minute average values were recorded to the datalogger.

Fig. 1. Microgrid system layout

III. DATA COLLECTION

Data collection was performed using two separate power generation sources to charge the VRB under three variable load conditions over an extended time period. The first power generation scenario, completed in May 2011, involved using the 8 kW diesel generator to charge the VRB to simulate emergency power conditions. The second power generation scenario involved using the 6 kW PV array to charge the VRB to simulate normal operations, which were used during both charging conditions to simulate variable load requirements for the microgrid. The first load consisted of an

approximately 600 W submersible pump. The second load consisted of the submersible

pump combined with one 1,500 W heating element (2,100 W total load). The third load

consisted of the submersible pump combined with two 1,500 W heating elements (3,600

W total load). The HVAC temperature set point was adjusted variably to determine the

most energy efficient setting that keeps the VRB container temperature below 29°C.

Voltage and current of each power generation, storage device, parasitic load, and

required load were continuously monitored and analyzed to determine power usage of

each component of the microgrid system during both charging and discharging

conditions. Ambient temperature and the temperature of the VRB container were

continuously measured and correlated to the power usage of the VRB HVAC.

IV.   DATA ANALYSIS

Empirical data analysis was performed to determine efficiencies and associated

losses of each system component, which includes the available PV power to the system,

MPPT losses, inverter losses, and parasitic losses including VRB pumps, HVAC, and

sensors. The power balance equation for the microgrid system is shown in (1),

$$P_{Out\ MPPT} + P_{VRB} + P_{DC\ Load} = (P_{HVAC} + P_{AC\ Load}) * h_{Inverter} \qquad (1)$$

where $P_{Out\ MPPT}$ is the power available to the system after the MPPT, P_{VRB} is the power

charged/discharged from the VRB, $P_{DC\ Load}$ is the peak DC load available to the system,

P_{HVAC} is the power used by the HVAC of the VRB, $P_{AC\ Load}$ is the peak AC load

available to the system, and $h_{Inverter}$ is the efficiency of the inverter. Data analysis

characterization is described in separate sections detailing the calculations of available

power to the system, VRB power, VRB loads, and VRB HVAC power.

A. Available Power. Power generated by the PV array prior to heat loss is calculated using (2),

$$P_{Predicted} = I_{Solar} * h_{panel} * A_{array} \tag{2}$$

where $P_{Predicted}$ is the power produced by the panels which is available to the system, I_{Solar} is the solar insolation in units of power per unit area (kW/m²), h_{panel} is the panel efficiency, which is approximately 15.5 percent [7], and A_{array} is the area of the PV array.

Increases in cell temperature above normal operating conditions cause a decrease of the open circuit voltage of a panel, which will decrease the power produced by a panel [8].

The cell temperature, T_c, is calculated using (3),

$$T_c - T_A = \frac{NOTC - 25°C}{0.8} * G \tag{3}$$

where T_A is the ambient temperature, $G = 0.8$ kW/m², and $NOTC$ is the temperature the cells will reach when operated at open circuit in an ambient temperature of 20°C. $NOTC$ was estimated to be approximately 40°C. The wind speed must be assumed to be less than 1 m/s.

Power loss (P_{loss}) associated with cell temperature increases (T_c) is calculated using (4),

$$P_{loss} = (T_c - 25°C) * (TS_{panel}) \text{ when } T_c > 25°C \tag{4}$$

where TS_{panel} is the temperature sensitivity of the panel, which is approximately -1.00

W/°C [7]. The efficiency loss at high temperatures can be noticeable because the highest

temperatures of solar PV panels recorded are about 70°C [9]. Total power available to

the system prior to MPPT ($P_{After\ HL}$) can then be calculated by using (5).

$$P_{after\ HL} = P_{Predicted} - P_{loss} \tag{5}$$

Projected array power ($P_{after\ HL}$) was calculated for data collected during system

operation from June 2011 through October 2011. This data was plotted as a function of

the VRB SOC in Fig. 2. The projected array power varied from 0 to approximately 7,000

W and does not appear to be a function of VRB SOC. Array power measured prior to the

MPPT was then plotted as a function of VRB SOC in Fig. 2. The maximum power

accepted prior to MPPT appears to be a linear function of VRB SOC, which ranges from

approximately 1,800 W at a VRB SOC of 9.5 V to approximately 5,000 W at a VRB

SOC of 0.5 V. As the VRB stack voltage gets closer to the 59 V charging voltage as the

SOC increases, the voltage drop is decreased which lowers the current draw, and

therefore the power demand. The maximum power accepted prior to MPPT can be

calculated as a function of VRB SOC using the equation (6).

$$P_{In\ MPPT} = -380.98 * (VRB\ SOC) + 5.227.8 \tag{6}$$
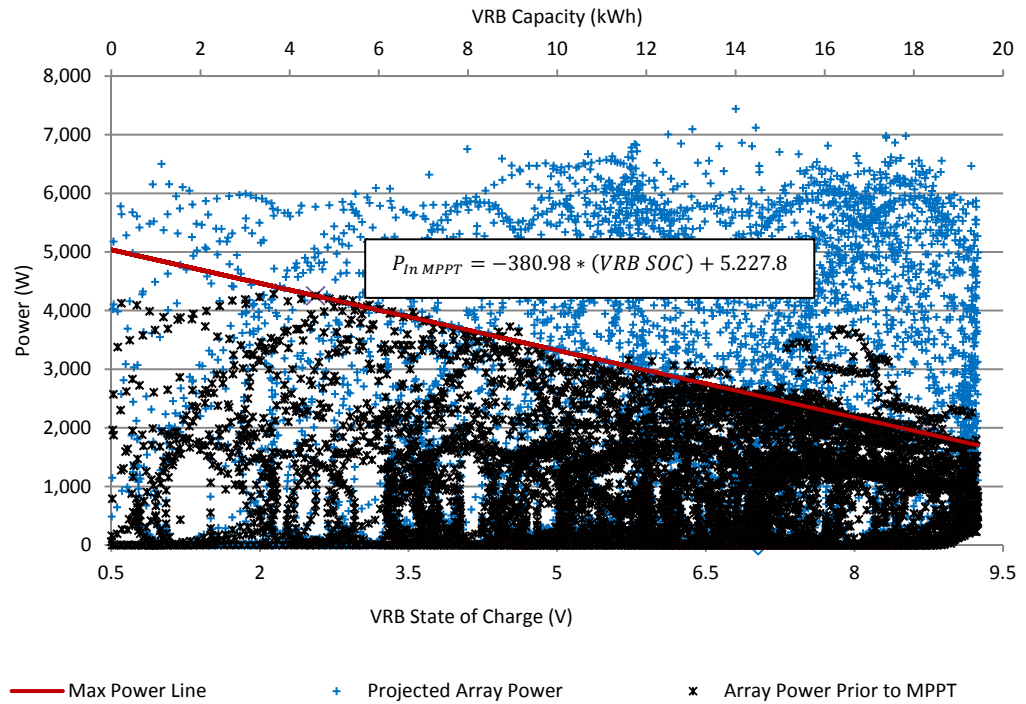
Fig. 2. PV power generation analysis

Under conditions of high power demand, such as when the SOC is low, both MPPT's will provide as much power as is required. As SOC increases and power produce approaches the maximum charging line calculated in Fig. 2, the MPPT's will no longer provide the same power and one of them, i.e. the slave, will provide less power. The other, i.e. the master, remains near its capacity. Therefore, variation in power produced by MPPT series 1 and MPPT series 2 can be used to identify if power production approaches the maximum charging line, which is assumed to have a power production variation of greater than ±10 percent during calculations. $P_{In\ MPPT}$, the array power prior to the MPPT, is plotted as a function of the projected PV power during

periods when $P_{In\ MPPT}$ is below the maximum charging line, as seen in Fig. 3. A linear correlation between array power prior to MPPT and projected PV power follow the line y = 0.5861x + 44.758 with coefficient of determination (R^2) of 0.89, where y is the array power prior to the MPPT and x is the projected array power.
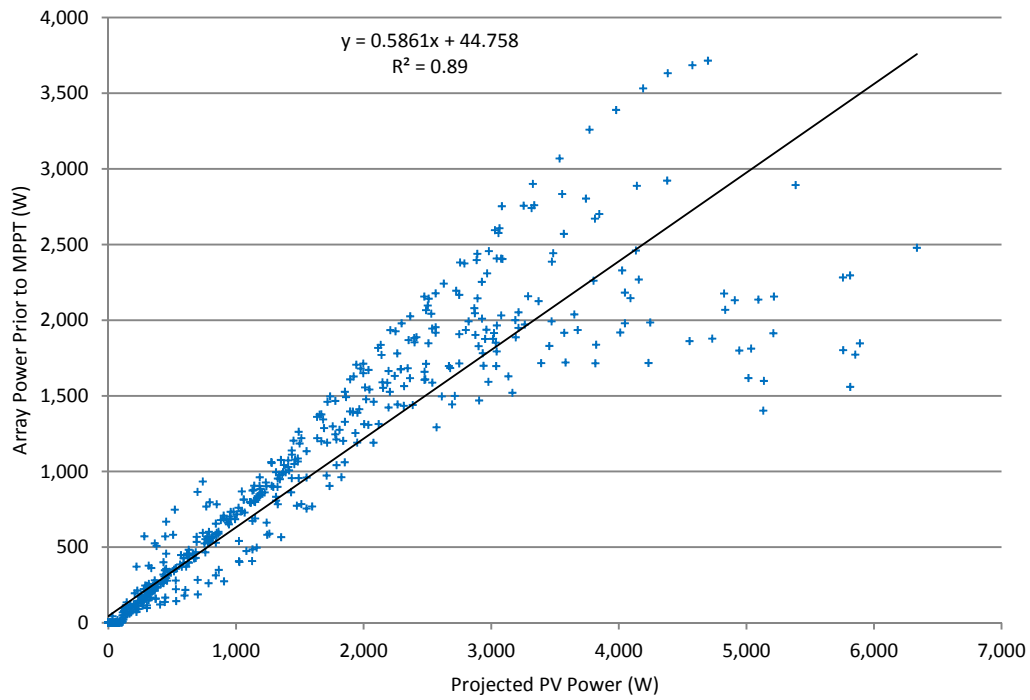
Fig. 3. System energy efficiency when below the maximum charging line

Efficiency of the MPPT (h_{MPPT}) is calculated using (7),

$$h_{MPPT} = \frac{P_{Out\ MPPT}}{P_{In\ MPPT}} \qquad (7)$$

where $P_{Out\ MPPT}$ is the power after the MPPT. Array power after the MPPT is plotted as a function of array power prior to the MPPT on Fig. 4. A linear correlation follows the line y = 0.9676x + 11.589 with a R² of 1.0. Based on (7), the slope of 0.9676 represents the MPPT power conversion efficiency, which is approximately equal to the manufacturer's specification of 0.975 [10].
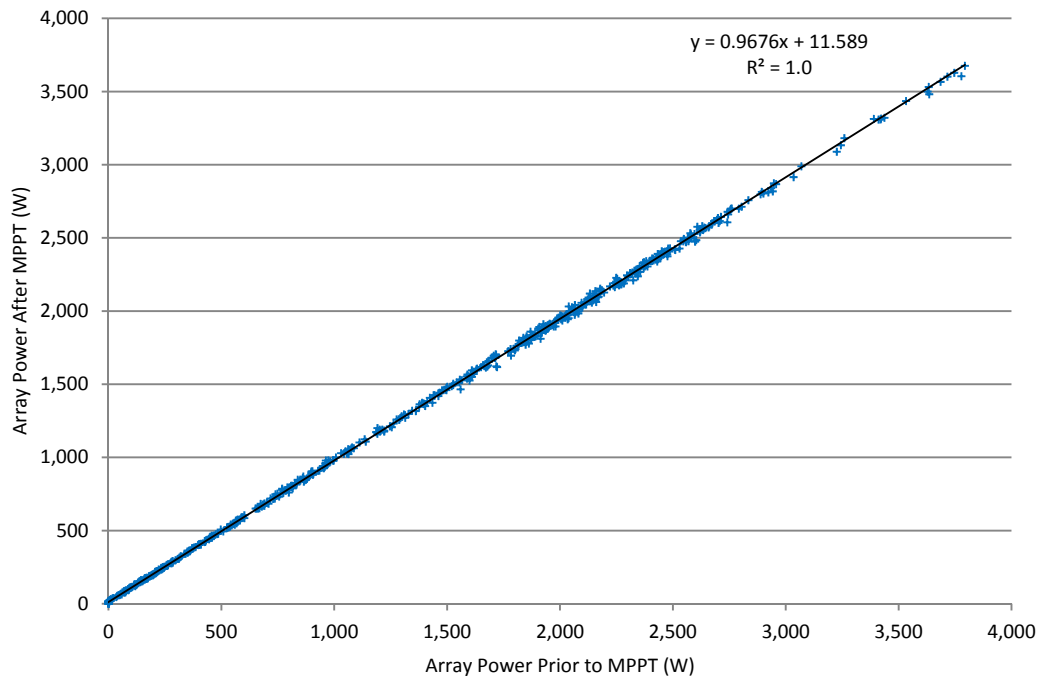
Fig. 4. MPPT efficiency determination.

B. VRB Power. VRB power represents the power going into/out of the VRB during charging/ discharging. VRB power (P_VRB) is calculated using (8),

$$P_{VRB} = f\{\Delta SOC\} \qquad (8)$$

where ΔSOC is the change in SOC over a known time period. VRB terminal power is

plotted as a function of hourly change in VRB SOC, as seen in Fig. 5. A linear

correlation between VRB terminal power and hourly change in VRB SOC follows the

line y = -3197x - 379.33 with a R^2 of 0.85, where y is the VRB terminal power and x is

the hourly change in VRB SOC.
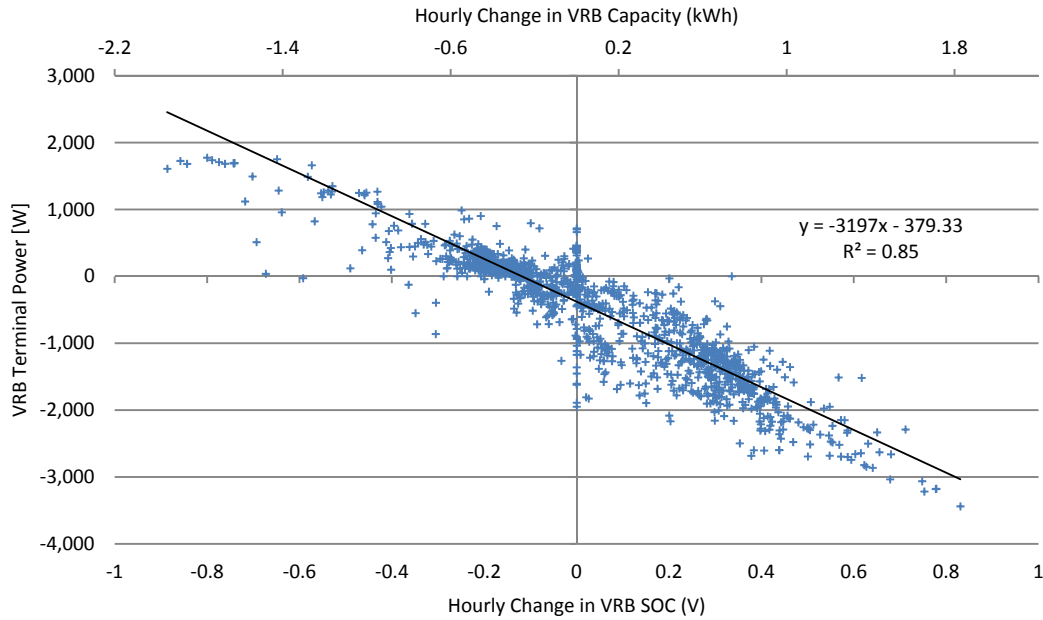
Fig. 5. VRB terminal power as a function in hourly change in SOC.

C. VRB Loads. Parasitic power associated with VRB performance included a

constant load for the controller and a variable load for the pumps which are required to

circulate the electrolyte across the membrane. VRB circulation pump power (P_{pumps})

was calculated using (9) during both charge and discharge periods.

$$P_{pumps} = f\{SOC, P_{VRB}\} \tag{9}$$

The VRB circulation pumps' characterization was performed using an analysis of pump loads. Programmable pump logic dictates the correct pump stage with the associated VRB SOC. The circulation pumps appeared to be five stage gear pumps. Combined circulation pump power and controller power were estimated to be approximately 212 W in the first stage, 273 W in the second stage, 286 W in the third stage, 316 W in the fourth stage, and 445 W in the fifth stage. Gear staging appeared to be a function of SOC and VRB power and consistent during both charge and discharge periods. Analysis of circulation pump data identified four ranges of VRB SOC which are defined by differing pump stages as a function of VRB terminal power. The first VRB SOC range is 0-3, the second range is 3-6.65, the third range is 6.65-7.05, and the fourth range is 7.05-10. Noise during empirical analysis characterization is due to the pumps switching gears during sampling periods of one minute, as well as a delay of approximately one to two minutes between VRB terminal power changes and associated changes in circulation pump powers.

Characterization of the VRB controller and circulation pumps during charging and discharging with an SOC between 0 and 3 is presented in Fig. 6. During this SOC period, the pumps appear to be operating in stage 3 at approximately 286 W when VRB terminal power is between 0 and 1,500 W. The pumps then appear to switch to stage 5 at approximately 445 W when the VRB terminal power is between 1,500 and 4,000 W.

Characterization of the VRB controller and circulation pumps during charging and discharging when the VRB SOC is between 3 and 6.65 is shown in Fig. 7. During this SOC range, when the VRB terminal power is between 0 and 1,500 W, the pumps and controller appear to be in stage 1 at approximately 212 W. The pumps then appear to switch to stage 4 at approximately 316 W total load when the VRB terminal power is between 1,500 and 3,000 W. Finally, the pump appears to switch to stage 5 at approximately 445 W total power when the VRB terminal power is between 3,000 and 4,000 W.
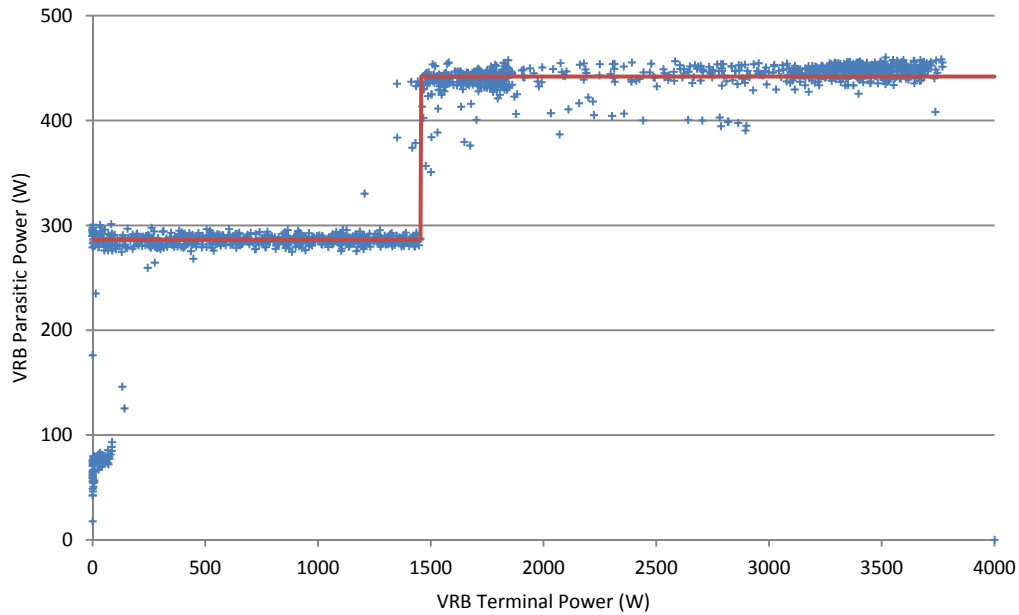
Fig. 6. VRB circulation pump and controller power characterization during charging/ discharging, SOC 0-3.
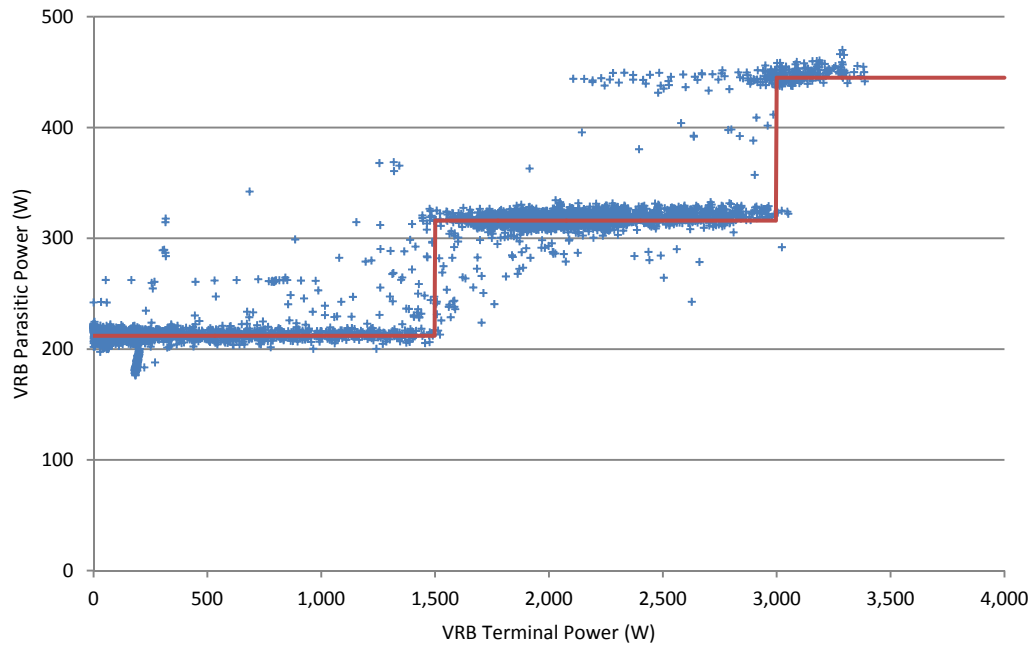
Fig. 7. VRB circulation pump and controller power characterization during charging/ discharging, SOC 3-6.65.

VRB circulation pumps and controller characterization during charging and discharging when the VRB SOC is between 6.65 and 7.05 is shown in Fig. 8. During this SOC range, when the VRB terminal power is between 0 and 1,500 W, the pumps and controller appear to be in stage 2 at approximately 273 W. The pumps then appear to switch to stage 3 at approximately 316 W total load when the VRB terminal power is between 1,500 and 3,000 W. Finally, the pumps appear to switch to stage 5 at approximately 445 W total power between 3,000 and 4,000 W. During this range, insufficient data was collected due to the maximum charging line being reached at approximately 2,000 W.
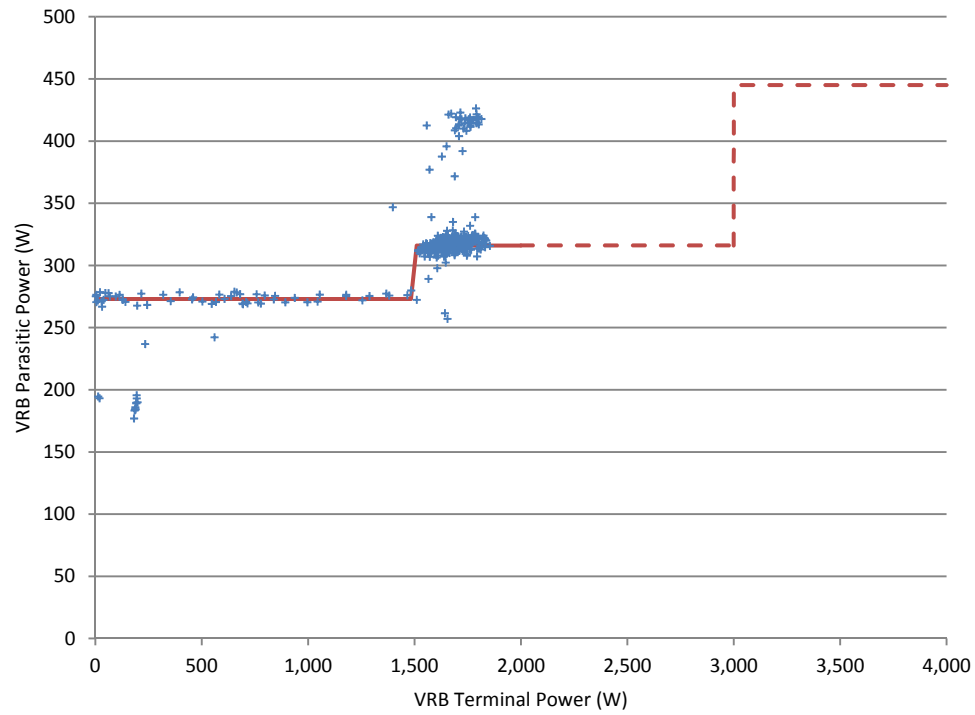
Fig. 8. VRB circulation pump power characterization during charging/ discharging, SOC 6.65-7.05.

Characterization of the VRB circulation pumps and controller during charging and discharging when the VRB SOC is between 7.05 and 10 is shown in Fig. 9. During this SOC range, when the VRB terminal power is between 0 and 1,500 W, the pumps and controller appear to be in stage 1 at approximately 212 W. The pumps then appear to switch to stage 3 at approximately 316 W total load when the VRB terminal power is between 1,500 and 3,000 W. Finally, the pumps appear to stay in stage 3 when the total power is between 3,000 and 4,000 W. However, insufficient data was collected during this range due to the maximum charging line being reached at approximately 1,900 W.
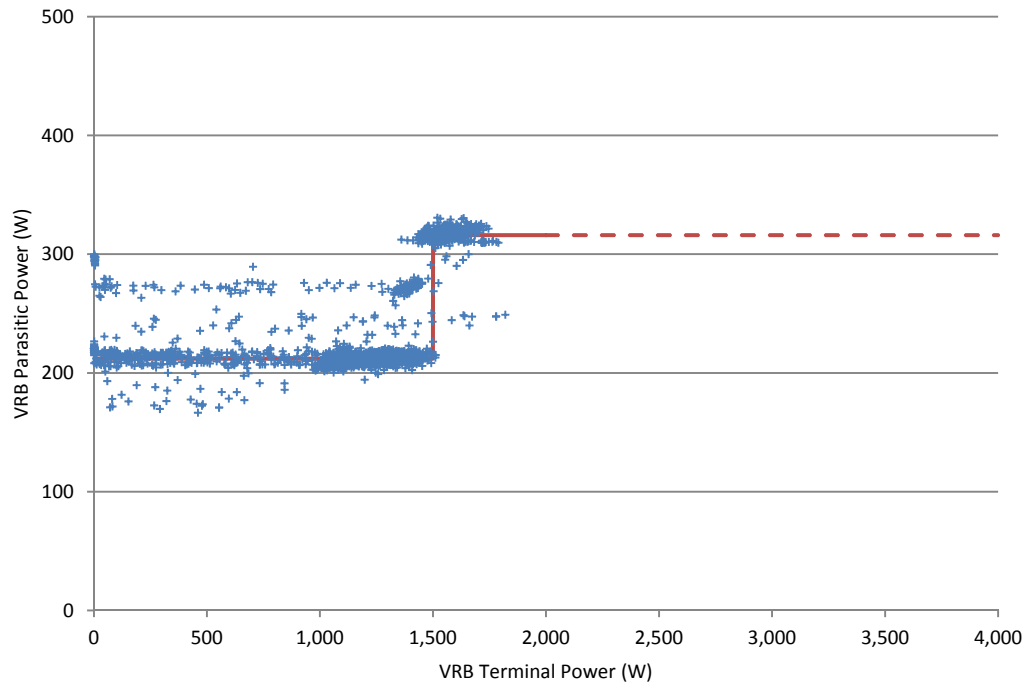
Fig. 9. VRB circulation pump power characterization during charging/ discharging, SOC 7.05-10.

D. VRB HVAC. VRB HVAC is required to ensure the electrical equipment is not exposed to extreme ambient temperatures. Current system layout consists of the VRB being contained in its own enclosure provided by Prudent Energy, which contains its own HVAC to regulate temperatures within the enclosure (T_{VRB}) between 4°C and 29°C. Ambient temperature($T_{Amb.}$), T_{VRB}, and VRB HVAC power (P_{HVAC}) were monitored from June 2011 through October 2011 in order to determine a correlation. An equation to determine P_{HVAC} is shown in (10).

$$P_{HVAC} = f\{T_{Amb.}, T_{Adj.}\} \tag{10}$$

VRB HVAC power is plotted as a function of ambient temperature multiplied by the adjusted temperature $(T_{Adj.})$ in Fig. 10. Adjusted temperature is calculated by taking the ambient temperature minus the VRB container temperature. A linear correlation between the ambient temperature multiplied by the adjusted temperature and the HVAC power follow the line $y = 0.32x - 132.16$ with a R^2 of 0.79, where y is the ambient temperature multiplied by the adjusted temperature and x is the VRB HVAC power.
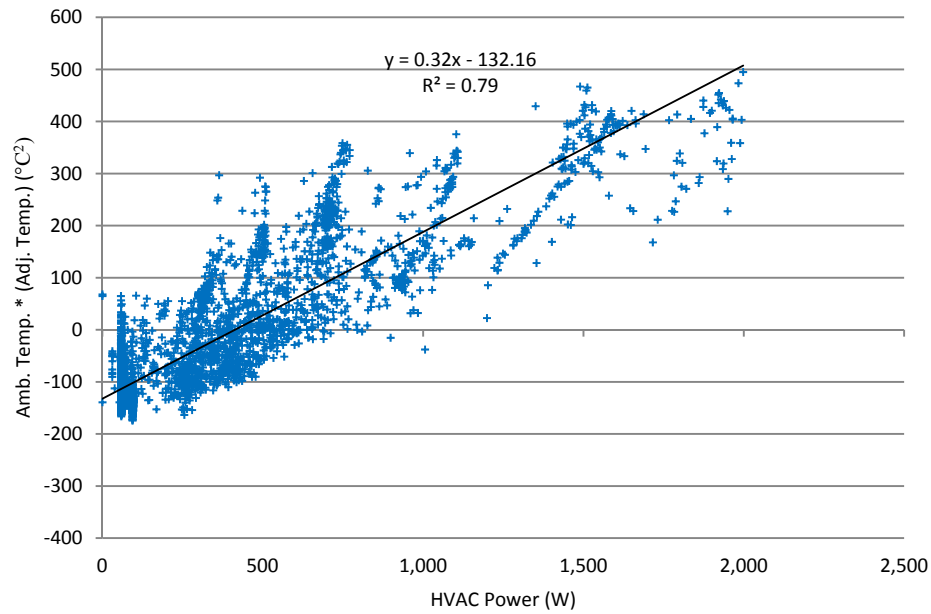
Fig. 10. Ambient temperature times adjusted temperature versus HVAC power.

E. Model. A model was created using the correlations previously stated in Section IV, which allows input of the time step, sample interval, solar insolation, ambient temperature, VRB temperature, and VRB SOC in order to determine the available peak

DC or AC load as well as VRB efficiency. VRB efficiency calculations are shown in (11) and (12),

$$h_{VRB\ discharge} = \frac{P_{VRB}}{P_{VRB}+P_{Pump}+P_{HVAC}}$$ (11)

$$h_{VRB\ charge} = \frac{P_{VRB}-P_{Pump}-P_{HVAC}}{P_{VRB}}$$ (12)

where $h_{VRB\ discharge}$ is the efficiency of the VRB during discharging, and $h_{VRB\ charge}$ is the efficiency of the VRB during charging [11]. The model also allows examination of the incremental change in power over its time period, and calculates the composite energy generation/consumption of each component of the microgrid system.

V. CASE STUDY

A case study was completed based on field results taken during operation on August 10 to18, 2011. During this time, the system operated using a low load of an approximately 600 W submersible pump and an approximately 90 W fan. Field measurements of sample interval, solar insolation, ambient temperature, VRB temperature, and VRB SOC were imported into the model for this time period, and incremental powers, composite energy, and VRB efficiencies determined by the model were analyzed and compared to field data measured directly through appropriate sensors. Fig. 11 presents the modeled cumulative power results, and Fig. 12 presents the actual cumulative power results over the same time period. Both graphs examine available power with heat loss, power into MPPT, VRB power, and total available loads. Modeled results for each power source appear to approximate the actual results. However, the

modeled available loads appear to have both positive and negative peaks, while the actual available loads contain only positive peaks due to small variations during the modeled calculations.
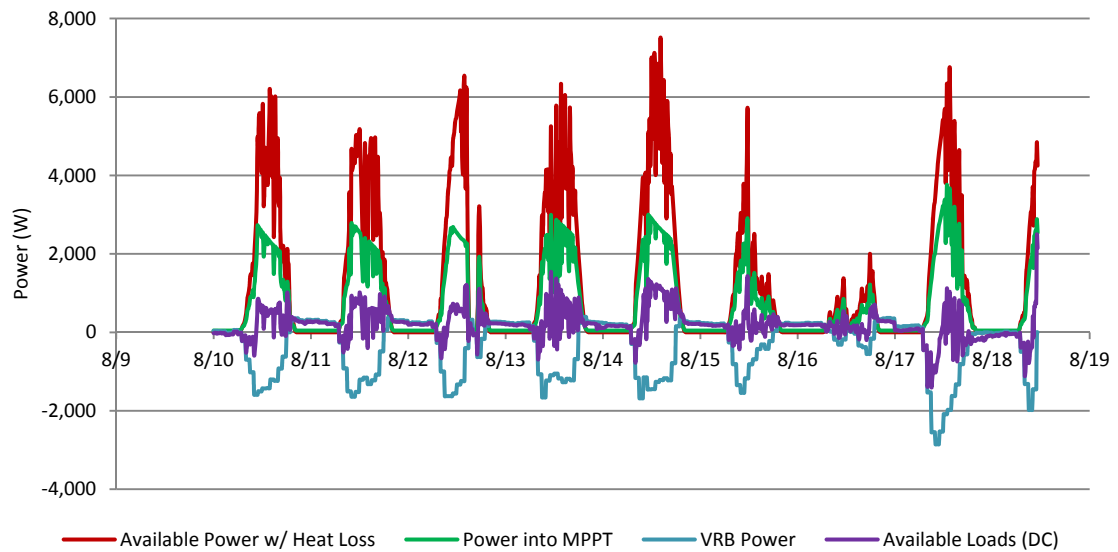
Fig. 11. Modeled cumulative power results versus time.
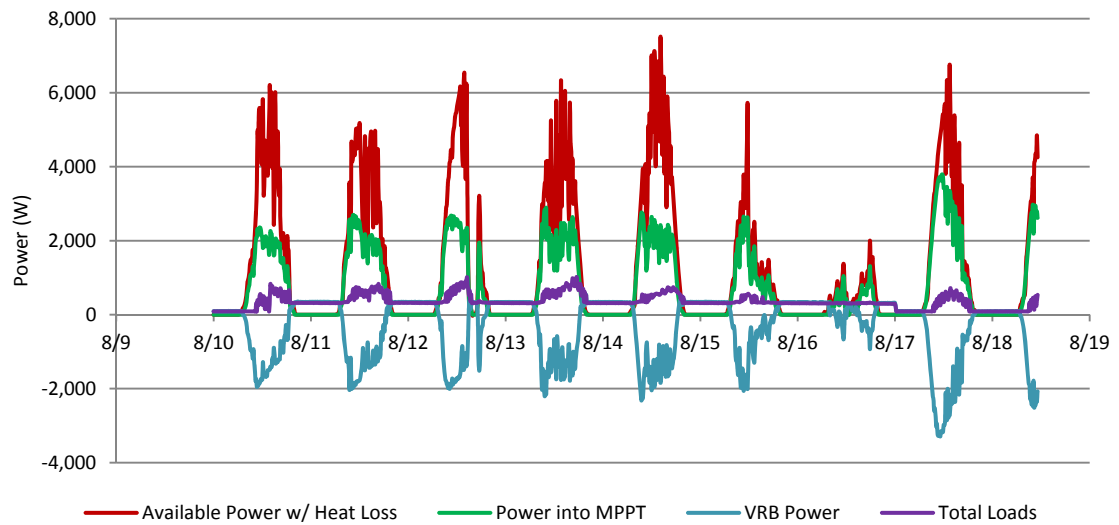
Fig. 12. Actual cumulative power results versus time.

Modeled and actual total parasitic load power (which includes the VRB circulating pumps, controller, and HVAC) versus time is presented in Fig. 13. Modeled parasitic power appears to approximate actual parasitic power, although the modeled power results do not appear to reach the corresponding peak of the actual HVAC power during large demand periods for several days. The model also appears blocky in nature with sharper changes during stages versus the actual parasitic power curves.
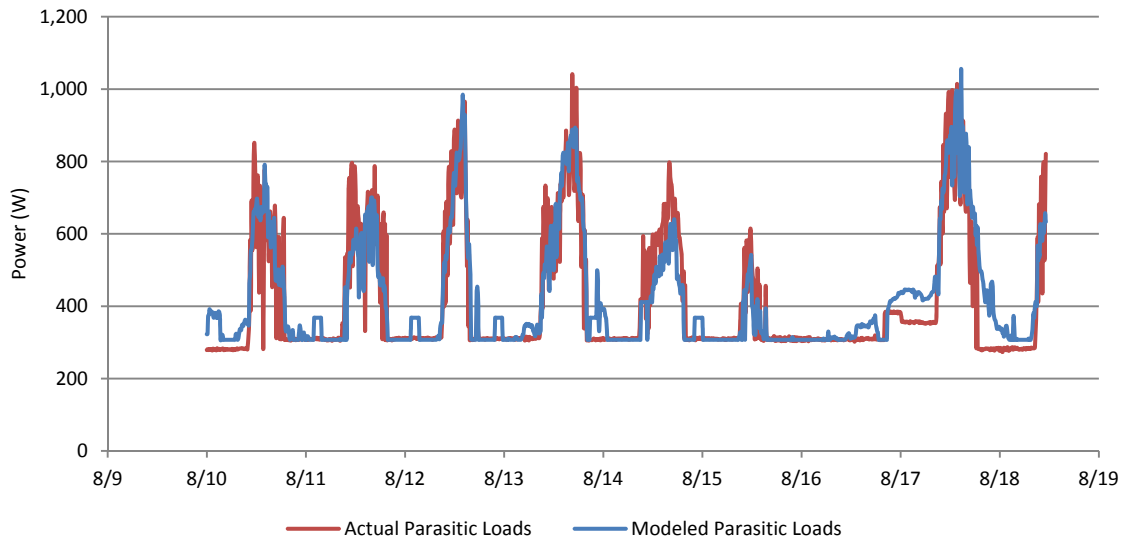
Fig. 13. Modeled and actual parasitic loads versus time during case study.

Modeled and actual cumulative energy produced/consumed by each associated system power component previously described is presented in Table I. Energy consumed/produced by each component during the model approximates within a minimum of 90% of the actual cumulative energy produced/consumed during the same cumulative time period.

The actual and modeled charging and discharging VRB efficiencies during the case study time period is shown in Fig. 14. Modeled efficiency results appear to approximate actual efficiency results, with a peak charge efficiency of approximately 80 percent. This efficiency drops down to approximately zero percent during changes in state of the VRB, and maintains a relatively constant efficiency at approximately 50 percent during discharge of the VRB. Modeled efficiency results vary slightly from the actual results during charge periods due to modeled results appearing to slowly drop to approximately 40 percent towards the end of the charge cycle, while the actual results

appears to stay constant at around approximately 50 percent. The VRB efficiency during

discharge would be greater than 50 percent if a larger load was used than during this case

study.

Table I
Cumulative energy results during case study

	Modeled Results (kWh)	Actual Results (kWh)
Available energy w/o heat loss	264	264
Available energy w/ heat loss	259	259
Energy into MPPT	149	149
Energy out of MPPT	147	145
VRB energy	71	73
VRB Circulating pumps energy	50	49
VRB HVAC energy	35	35
Total energy available for powering loads	41	37
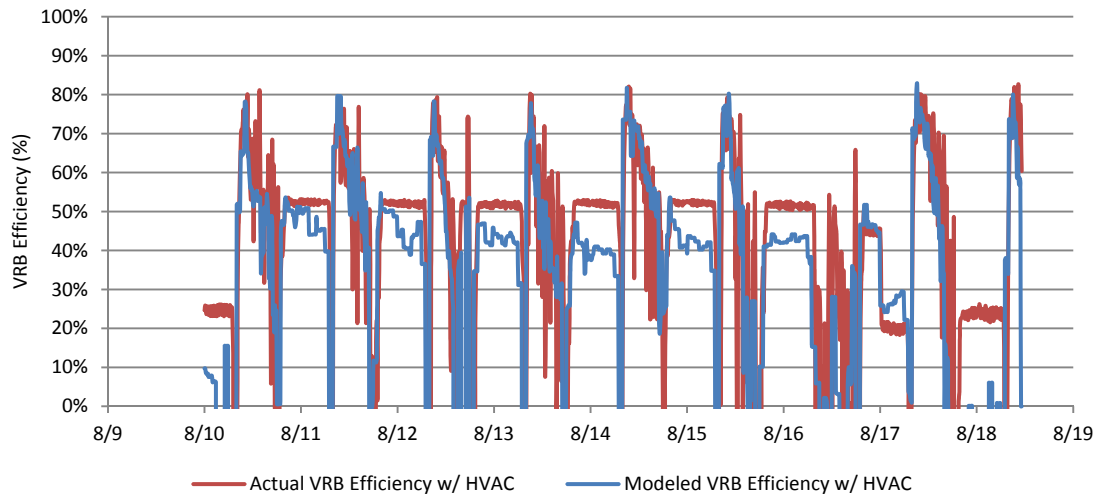
Fig. 14. Actual and modeled VRB efficiency versus time during charging/discharging

VI. CONCLUSIONS

Correlations for predictive power prior to MPPT, MPPT efficiency, circulation

pumps and controller power usage, and VRB HVAC usage present the user a procedure

to accurately model the system power production/consumption. This predictive model

allows you to effectively predict peak available AC/DC load as well as VRB efficiencies

based on climatic field measurements and VRB SOC. This model also allows for the

adjustment of the VRB SOC in order to meet required AC or DC loads. The maximum

available power decreases linearly with increasing VRB SOC. Therefore, the VRB

should be oversized in terms of faceplate power rating to provide maximum energy

density for a constant load. The appropriate PV power rating for VRB charging only is

less than the VRB faceplate power rating. Therefore, the PV array should be sized

according to the constant baseline load (which is typically less than the nominal VRB

power rating) and the incremental intermittent discretionary load. Appropriate sizing of

the VRB should be based on maximum power output at the required energy density. This model also allows appropriate sizing of discretionary loads considering PV power available above the VRB power value associated with the maximum SOC.

This work provides the basis for future analysis which would characterize VRB performance based on VRB SOC in order to accurately model system performance without requiring the VRB SOC to be known. Performance predictions could then occur prior to deployment of the system . This would allow more effective sizing estimations in order to decrease system operation and maintenance as well as transportation costs.

VII.   REFERENCES

[1]   U.S. Defense Science Board. "More capable war fighting through reduced fuel burden. Task force on improving fuel efficiency on weapons platforms." Office of the Under Secretary of Defense for Acquisition, Technology, and Logistics, Washington, D.C.

[2]   R.L. Boswell, "The Impact of Renewable Energy Sources on Forward Operating Bases," M.S. thesis, Air Command and Staff College, Air University, Maxwell Air Force Base, Alabama, 2007.

[3]   S. Booth, J. Barnett, K. Burman, J. Hambrick, and R. Westby. "Net zero energy military installations: a guide to assessment and planning." National Renewable Energy Laboratory, Golden, CO, Tech. Rep. 782-48876, 2010.

[4]   P. Denholm, E. Ela, B. Kirby, and M. Milligan, "The role of energy storage with renewable electricity generation," National Renewable Energy Laboratory, Golden, CO, Tech. Rep. 6A2-47187, Jan. 2010.

[5]   J. Chahwan, C. Abbey, and G. Joos, "VRB modeling for the study of output terminal voltages, internal losses, and performance," in *Proc. 2007 IEEE Canada Electrical Power Conf.*, pp. 387-392.

[6]   C. Blanc and A. Rufer, "Multiphysics and energetic modeling of a vanadium redox flow battery," in Proc. 2008 IEEE International Conference on Sustainable Engineering Technologies, pp. 696-700.

[7]   Brightwatts, Inc., Brightwatts BI-156-200W-G27V 200 Watt Module Data Sheet.

[8]   R. Messer and J. Venter, *Photovoltaic Systems Engineering*. (2nd Edition), CRC Press, LLC., Boca Raton, FL, 2004, p. 455.

[9]   G. Notten, C. Cristofari, M. Mattei, and P. Poggi. "Modeling of a double-gloss photovoltaic module using finite differences." Applied Thermal Engineering, 25:2854-2877, 2005.

[10]   Outback Power Systems, Inc., "FlexMax 80 maximum power point tracking charge controller user's guide: installation, programming and user's manual," Arlington, WA, p. 81.

[11]   K.W. Knehr and E.C. Kumbur, "Open circuit voltage of vanadium redox flow batteries: Discrepancy between models and experiments," *Electrochemistry Communications, vol. 13, pp. 342-345, 2011.*

VIII.   BIOGRAPHIES

Joe David Guggenberger II graduated from the University of Missouri-Rolla with his B.S. and M.S. degrees in geological engineering. He was employed as an environmental engineer with CDM, Inc., Kansas City, Missouri where he specialized in soil and groundwater characterization and remediation. He was then employed as an environmental manager with SRG Global, Farmington, Missouri where he specialized in environmental compliance and green engineering. He is currently completing his Ph.D. degree in geological engineering at the Missouri University of Science and Technology. He is a Registered Professional Engineer.

Andrew Curtis Elmore graduated from the University of Missouri-Rolla with a B.S. degree in geological engineering, and he completed his M.S. and Ph.D. degrees in civil engineering at the University of Arizona. He was employed as a consulting engineer with URS Group, Overland Park,

Kansas where he specialized in green and sustainable environmental remediation. He is currently an associate professor of geological engineering at the Missouri University of Science and Technology.

Jerry L. Tichenor (S'94, M'96) received his B.S.E.E., and M.S.E.E. degrees in electrical engineering from the University of Missouri – Rolla, in 1994, and 1996, respectively. Currently, he is an Associate Research Engineer at the Missouri University of Science and Technology. His research interests include power electronics and renewable energy systems.

M. L. Crow (S'83, M'90, SM'94, F'10) received the B.S.E. degree from the University of Michigan, Ann Arbor, and the Ph.D. degree from the University of Illinois, Urbana/Champaign. She is currently the Director of the Energy Research and Development Center and the F. Finley Distinguished Professor of Electrical Engineering at the Missouri University of Science and Technology. Her research interests include computational methods for dynamic security assessment and the application of power electronics in bulk power systems. She is a Registered Professional Engineer and a Fellow of the IEEE.

II. MICROGRID LOAD CHARACTERIZATION USING LONG-TERM WEATHER DATA

J.D. Guggenberger[1], A.C. Elmore[1] , and M.L. Crow[2]

[1]Department of Geological Engineering, Missouri University of Science and

Technology – Rolla, Missouri, U.S.A. 65401

[2]Department of Electrical and Computer Engineering, Missouri University of Science

and Technology – Rolla, Missouri, U.S.A. 65401

Email: jguggenb@mst.edu, elmoreac@mst.edu, crow@mst.edu

ABSTRACT

Microgrids have proven to be a valuable technique for meeting energy demands at FOBs. Characterizing system performance pre-deployment would allow the system to be appropriately sized to meet all required electrical loads at a given renewable source operational time frequency, which would decrease capital, transportation costs, and quantity of emergency fuel required. An iterative model was derived to incrementally predict microgrid system performance. This model requires incremental values of solar insolation, ambient temperature, and VRB temperature to predict VRB SOC. VRB SOC operational boundaries were added to restrict diesel operation to emergency situations. Calibration of the model was performed to determine accurate PV panel and inverter efficiencies. A case study was performed to estimate the constant loads the system could power at varying renewable source probabilities. Additionally, load characterization at

three locations was performed for periods where climatic control is not required**.**

INDEX TERMS

Energy efficiency, energy management, energy storage, load management, load modeling, photovoltaic power systems, prediction methods, statistics

I.   INTRODUCTION

FOBs have proven to be an effective method of troop deployment to active battlefields [1]. FOBs are typically located in areas without grid access, and are commonly powered by diesel generators. Diesel generators, which are not cost effective due to rising fuel and fuel transportation costs, may put soldiers in harm's way. Fuel tankers have been proven to be an effective target of enemies' improvised explosive devices [2]. The development of renewable energy-powered microgrids as power sources at FOBs would allow energy demands to be met in a portable and effective manner, while limiting diesel fuel consumption to periods of emergency power.

Renewable energy-based microgrids allow energy demands to be met through a variety of energy generation and storage devices, such as wind turbines and PV panels. Typical energy storage technologies such as lead acid batteries provide low energy density at a high mass, which prohibits effective transportation to global locations. Therefore, developing effective energy storage technologies is proving to be a critical aspect in the optimization of portable, scalable microgrids as an effectively deployable technology [3]. VRBs have the potential to be a viable energy storage technology due to their high efficiency, high scalability, fast response, long life, and low maintenance

requirements [4]. During charging and discharging of the VRB, electrolyte is circulated through a power cell using a series of pumps. VRBs must also have temperature control, in the form of HVAC, to ensure the electrical equipment is not exposed to ambient temperatures below 4 °C or above 29°C. Past research focused on electrochemical characterization of VRB performance [4] and modeling VRB terminal voltage output for use in power smoothing in wind systems [5].

One issue with deploying renewable energy-based microgrids globally is sizing the systems to meet required parasitic and discretionary electrical loads pre-deployment without site specific climatic data. Solar radiation and/or wind speeds are not constant from one site to another. Therefore, designers are inclined to oversize the microgrid electrical generation and storage devices in order to meet all necessary electrical loads [6]. Over sizing is cost ineffective for both materials and transportation. Characterizing system performance to meet all necessary electrical loads pre-deployment would allow appropriate sizing of a system prior to deployment. This would limit system design to only appropriate hardware, thus reducing the cost of system components as well as transportation. Predicting the appropriate generator operating frequency would define the appropriate diesel quantity to keep on hand at the FOB. This would limit risks associated with explosions in addition to limiting fuel transportation costs.

Past research on microgrid system performance focused on analyzing performance of a battery-free PV-diesel powered microgrid [6], appropriately sizing wind/PV hybrid systems to power households in Inner Mongolia [7], and appropriate sizing of energy storage for use with variable energy resources [8]. Past research on load

characterization focused on analyzing turbulent wind loads [9], and using geographic information systems (GIS) to characterize wind energy potential [10].

This paper focuses on the development of a computer model that characterizes the performance of a microgrid system prior to deployment. This allows the designer to select the appropriate PV array size given a specific location and a given load. The empirically derived model incrementally calculates VRB SOC and capacity, which allows proper determination of emergency generator operating frequency necessary to meet a given load.

II.   MICROGRID DESCRIPTION

A microgrid was constructed at a FOB training area at Location 1. Site coordinates for Location 1 are presented in Table I, and a system diagram is presented as Fig. 1. This system applied various experimental scenarios through the use of multiple energy generation and storage technologies. The work provided in this study only used the PV array and diesel generator during analysis.

Table I
Site coordinates, sampling timeframe and frequency

	Location 1	Location 2	Location 3
Site Location	TA-246, FLW, MO	Hypoint, Rolla, MO	Troop I, Rolla, MO
Latitude	37.740071	37.980862	37.955678
Longitude	-92.165898	-91.722416	-91.790795
Start Date	4/20/11	11/11/10	11/14/10
End Date	2/3/12	5/11/11	8/3/11
Sampling Frequency	5 seconds	5 seconds	5 seconds
Recording Frequency	10 minutes	10 minutes	1 hour
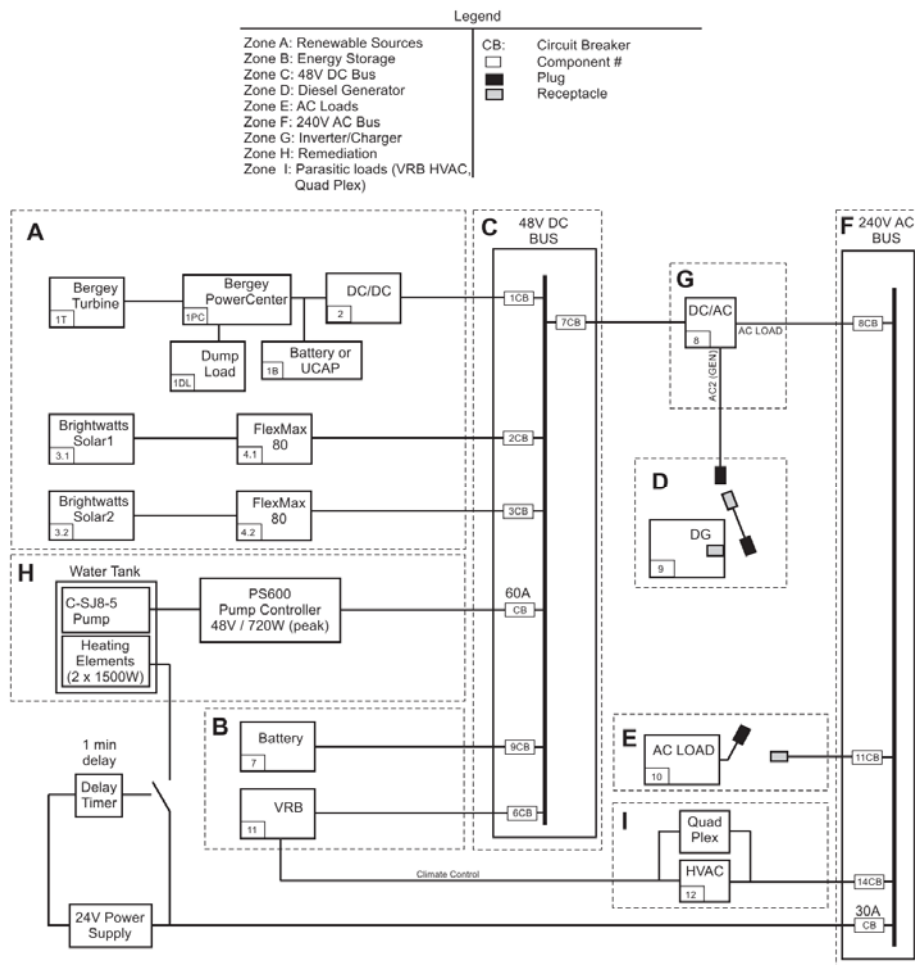
Fig. 1. Electrical schematic for microgrid system

The energy generation configuration of the microgrid consisted of a PV array with a diesel generator for supplemental energy generation. The 6 kW PV array consisted of 30 - 200 W Brightwatts Inc. solar panels (model BI-156-200W-G27V) connected to two Outback FlexMax 80 charge controllers. The PV array was electrically separated into two 3 kW arrays, and was mounted at a fixed horizontal angle of 38 degrees facing south. Each PV array was then connected to a 48 V DC bus, which maintained voltage control through four Sun-Xtender sealed AGM batteries.

A three cylinder Kubota diesel engine was connected to a Leroy Somer 6 kW brushless self-regulated type generator. This generator was then connected to the 48 V bus via a Xantrex DC/AC inverter charge controller.

Variable loads used during experimentation included a Lorentz PS600 HR/C submersible water pump with controller, two 1,500 W heating elements, and the VRB HVAC (Carrier Performance Series XPower ductless high wall system with inverter technology).

The primary storage technology used during experimentation was a nominal 5 kW Prudent Energy VRB rated at an energy density of 20 kWh, which was connected to the 48 V bus. VRB SOC is a measurement (recorded in V) that is linearly correlated to the energy capacity of the VRB, where 0.5 V SOC equals 0 kWh of capacity and 9.5 V SOC equals 20 kWh of capacity.

Solar insolation was measured at Location 1 using one Apogee SP-110 pyranometer facing south with a 38 degree tilt, and a second pyranometer horizontally mounted at a height of 3 m. One Campbell Scientific 107-L temperature probe was located on the 3 m weather station, and a second temperature probe was located inside the

VRB. LEM LA55-P current and LEM LV25-P voltage sensors were used to measure the power of the PV arrays prior to and after the charge controllers, diesel generation, VRB HVAC, VRB pumps, submersible pump, and heating elements. The pyranometers and power sensors were connected to a Campbell Scientific Model CR1000 datalogger.

A weather station was also installed at Location 2. Site coordinates for Location 2 are presented in Table I. Solar insolation was measured at this location using an Apogee SP-110 pyranometer horizontally mounted on a 3 m weather station. One Campbell Scientific 107-L temperature probe was located on the 3 m weather station. The pyranometer and temperature probe were connected to a Campbell Scientific Model CR1000 datalogger.

Another weather station was installed at Location 3. Site coordinates for Location 3 are presented in Table I. A 3 m weather station at this location included one Apogee SP-110 pyranometer horizontally mounted and one Campbell Scientific 107-L temperature probe; both were connected to a Campbell Scientific Model CR1000 datalogger.

III.   DATA COLLECTION

Data collection for model development was performed using two separate power generation sources to charge the VRB under three variable load conditions over an extended time period. The first power generation scenario, characterizing diesel generator performance, was completed in May 2011. This process involved using the diesel generator to charge the VRB to simulate emergency power conditions. Voltage and current prior to and after the inverter were monitored, as well as VRB voltage and

current. The second power generation scenario, characterizing PV performance without supplement from the diesel generator, involved using the PV array to charge the VRB and occurred from June 2011 through October 2011. The PV array charged the VRB over an extended time period to simulate seasonal and daily solar radiation conditions.

Three load scenarios were applied independently during both charging conditions which allowed simulation of variable load requirements for the microgrid. The first load consisted of only the approximately 600 W submersible pump. The second load consisted of the submersible pump combined with one 1,500 W heating element (2,100 W total). The third load consisted of the submersible pump combined with two 1,500 W heating elements (3,600 W total). The HVAC temperature set point was variably adjusted to determine the most energy efficient setting that kept the VRB container temperature below 29°C. Once this set point was obtained, it was consistently applied during all remaining testing scenarios. Voltage and current were continuously monitored for each power generation device, storage device, parasitic load, and required load. Analysis of this data accurately determined the power usage of each component of the microgrid system during charging and discharging conditions.

Ambient temperature and solar insolation were continuously monitored at Location 1. Sampling timeframe and frequency are presented in Table I, where samples' values are averaged and recorded over a given time period. The temperature of the VRB container was also continuously measured at this location from May 17, 2011 through February 3, 2012. All recorded weather data at Location 1 was correlated to the power usage of the VRB HVAC.

Monitoring of the ambient temperature and solar insolation was also performed at Location 2 and Location 3, with sampling frequency and timeframe as presented in Table I.

IV.   MODEL DEVELOPMENT

A microgrid prediction performance model was created to fully characterize the efficiencies and associated losses for each microgrid system component using Microsoft Excel. System losses are associated with panel efficiencies, panel heat loss, charge controller/MPPT losses, inverter losses, and VRB parasitic losses which include the VRB pump and controller, HVAC climate control, and associated sensors.

The model was based on the power balance equation shown in (1),

$$P_{Out\ MPPT} + P_{VRB} + P_{DC\ Load} = (P_{HVAC} + P_{AC\ Load} + P_{Generator}) * h_{Inverter} \quad (1)$$

where $P_{Out\ MPPT}$ is the power available to the system after the MPPT, P_{VRB} is the power charged/discharged from the VRB, $P_{DC\ Load}$ is the peak DC load available to the system, P_{HVAC} is the power used by the VRB's HVAC system, $P_{AC\ Load}$ is the peak AC load available to the system, and $h_{Inverter}$ is the efficiency of the inverter.

The energy balance equation to calculate the change in VRB capacity ($\Delta VRB\ Capacity$) is shown in (2),

$$\Delta VRB\ Capacity = E_{Panels} + E_{Generator} - E_{Parasitic} - E_{HVAC} - E_{AC\ or\ DC\ Loads} \quad (2)$$

where E_{Panels} is the energy produced by the PV array, $E_{Generator}$ is the energy produced by the diesel generator, $E_{Parasitic}$ is the energy loss due to the VRB parasitic pumps and

controller, E_{HVAC} is the energy loss due to the HVAC and AC sensors, and $E_{AC\ or\ DC\ Loads}$ is the energy used by the associated AC or DC loads powered by the system. The model can then predict VRB capacity over time by adding $\Delta VRB\ Capacity$ calculated for each sample period to a known VRB capacity at the start of the modeling period. The VRB capacity can then be converted to VRB SOC using (3).

$$VRB\ SOC = \left[\frac{9}{20} * \left(VRB\ Capacity + \frac{10}{9}\right)\right] \tag{3}$$

Data analysis characterization is described in separate sections detailing the calculations of available PV power to the system, VRB power, VRB loads, VRB HVAC power, and diesel generator power.

A. PV Power Available. Power generated by the PV array prior to heat loss is calculated using (4),

$$P_{Predicted} = I_{Solar} * h_{panel} * A_{array} \tag{4}$$

where $P_{Predicted}$ is the available power produced by the panels, I_{Solar} is the solar insolation in units of power per unit area (kW/m^2), h_{panel} is the panel efficiency, and A_{array} is the area of the PV array. Panel efficiency is an independent variable which is originally set to 15.5 percent [11] prior to calibration, in accordance with manufacturer's recommendations.

Panel power production is decreased during periods of increased cell temperature above normal operating conditions due to a decrease of the open circuit voltage of a panel [12].

The cell temperature, T_c, is calculated using (5),

$$T_c - T_A = \frac{NOTC - 25°C}{0.8} * G \qquad (5)$$

where T_A is the ambient temperature, $G = 0.8$ kW/m², and $NOTC$ is the temperature the cells will reach when operated at open circuit in an ambient temperature of 25°C, which was estimated to be approximately 40°C. The wind speed must be assumed to be less than 1 m/s to meet this criterion.

Power loss (P_{loss}) associated with an increase in cell temperature is calculated using (6),

$$P_{loss} = (T_c - 25°C) * (TS_{panel}) \text{ when } T_c > 25°C \qquad (6)$$

where TS_{panel} is the temperature sensitivity of the panel, which is approximately -1.00 W/°C [11]. Panel temperatures have been proven to reach as high as 70°C, which can cause noticeable power loss [13]. Total projected power available to the system prior to the charge controller ($P_{After\ HL}$) can then be calculated by using (7).

$$P_{after\ HL} = P_{Predicted} - P_{loss} \qquad (7)$$

$P_{After\ HL}$ was calculated from solar isolation data collected during system operation from June through October 2011. This data was plotted as a function of the VRB SOC / VRB capacity in Fig. 2. The calculated $P_{After\ HL}$ values ranged from 0 to approximately 7,000 W and do not appear to be a function of VRB SOC. Array power measured prior to the charge controller was then plotted as a function of VRB SOC in Fig. 2. The maximum measured power prior to the charge controller appears to be a linear function of VRB SOC, which ranges from approximately 1,800 W at a VRB SOC

of 9.5 V to 5,000 W at a VRB SOC of 0.5 V. As the SOC increased, the VRB cell

voltage approaches the charging voltage of 59 V. The resultant voltage drop decreases as

the VRB cell voltage approaches the charging voltage, which lowers the current draw and

power demand. The maximum power accepted prior to the charge controller can be

calculated as a function of VRB SOC using the equation (8).

$$P_{In\ MPPT} = -380.98 * (VRB\ SOC) + 5.227.8 \qquad (8)$$
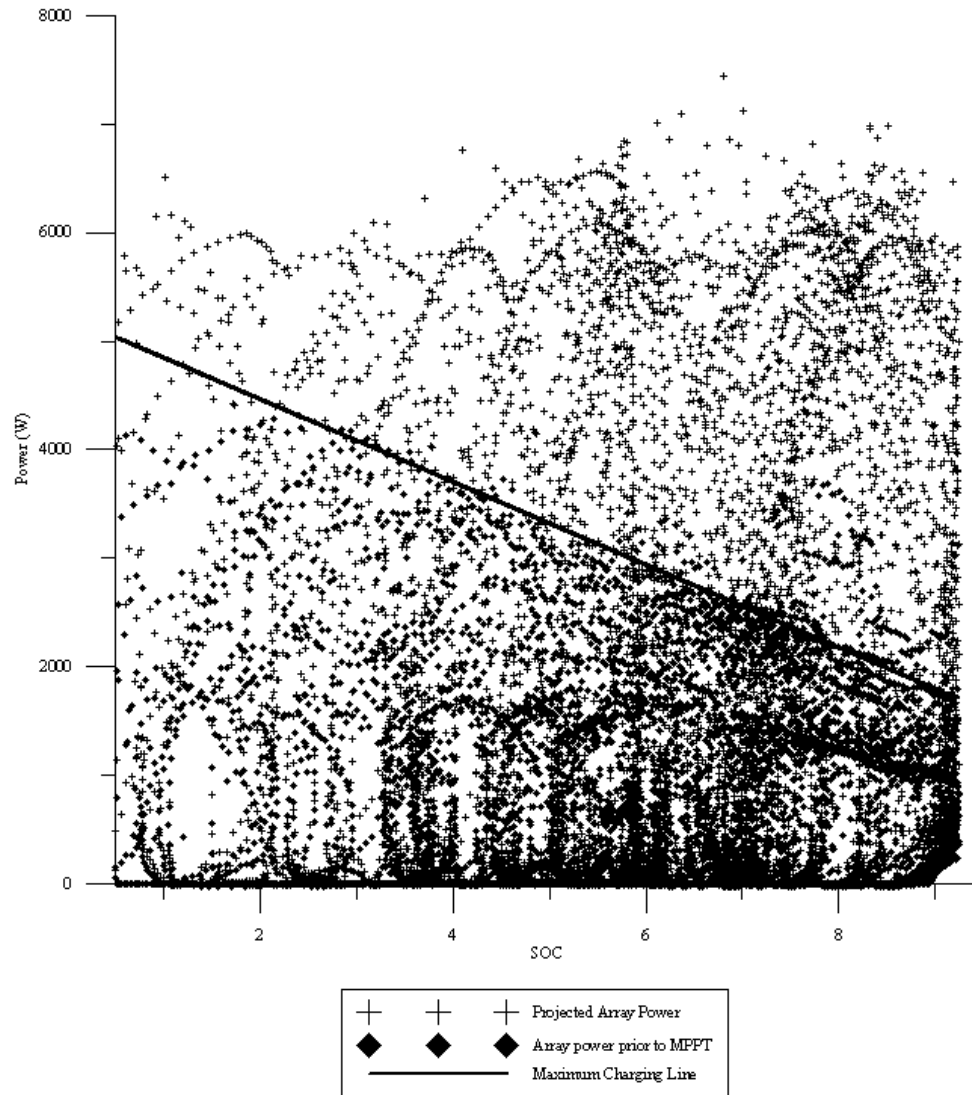
Fig. 2. PV power generation analysis.

Under conditions of high power demand, such as when the SOC is low, both charge controllers will provide as much power as is required. As the SOC increases, the power produced approaches the maximum charging line as displayed in Fig. 2. During this period, the charge controllers function under a master/slave relationship and no longer provide the same power. While the master charge controller remains near its

capacity, the slave charge controller contributes significantly less power. Therefore, variation in power produced by the master and slave charge controllers can be used to identify if power production approaches the maximum charging line, which is assumed to have a power production variation of greater than ±10 percent during calculations. A linear correlation was performed between $P_{after\,HL}$ and $P_{In\,MPPT}$ during periods when $P_{In\,MPPT}$ is below the maximum charging line. This correlation equation, which is presented in (9), has a R^2 of 0.89.

$$P_{after\,HL} = 0.5861 * P_{In\,MPPT} + 44.758 \tag{9}$$

Efficiency of the charge controllers (h_{MPPT}) is calculated using (10),

$$h_{MPPT} = \frac{P_{Out\,MPPT}}{P_{In\,MPPT}} \tag{10}$$

where $P_{Out\,MPPT}$ is the power after the charge controllers. The charge controller efficiency was determined to be 96.8 percent based on data obtained from June through October 2011 with a R^2 of 1.0. This is approximately equal to the manufacturer's specification of 0.975 [14].

B. VRB Parasitic Loads. Parasitic losses associated with VRB usage include a constant load for the controller and a variable load for the pumps required to circulate the electrolyte solution. VRB circulation pump power (P_{pumps}) is calculated using (11) during both charge and discharge periods.

$$P_{pumps} = f\{SOC, P_{VRB}\} \tag{11}$$

Characterization of the VRB circulation pumps was performed by using an empirical analysis of pump loads. Programmable pump logic controls the pump stage based on the VRB SOC, and five pump stages were observed. Combined circulation pump power and controller power were measured as approximately 212 W in the first stage, 273 W in the second stage, 286 W in the third stage, 316 W in the fourth stage, and 445 W in the fifth stage. The selection of the pump stage is function of both SOC and instantaneous VRB power. The stage selection was consistent during both charge and discharge periods. Table II shows the parasitic losses as a function of SOC and VRB terminal power.

Table II
VRB parasitic losses as a function of VRB SOC and VRB terminal power

VRB SOC (V)	VRB Terminal Power (W)		
	0-1,500	1,500-3,000	>3,000
0.5 - 3	286	445	445
3 - 6.65	212	316	445
6.65 - 7.05	273	316	NA
7.05 – 9.5	212	316	NA

C. VRB HVAC. Ambient temperature ($T_{Amb.}$), T_{VRB}, and VRB HVAC power (P_{HVAC}) were monitored from June through October, 2011 to determine a correlation between HVAC power and ambient and VRB temperature. The equation used to calculate P_{HVAC} is shown in (12).

$$P_{HVAC} = f\{T_{Amb.}, T_{Adj.}\} \tag{12}$$

Adjusted temperature is calculated by subtracting VRB container temperature from the ambient temperature. A linear correlation between the ambient temperature multiplied by the adjusted temperature and the HVAC power follow the line described by (13) with a R^2 of 0.79.

$$P_{HVAC} = \left. \frac{T_{Amb.} * T_{Adj.} + 132.16}{} \right/ 0.32 \qquad (13)$$

D. Diesel Generator. The model assumes that the diesel generator turns on when the VRB SOC falls below 3V in order to maintain adequate storage capacity. The generator charges the system in unison with the PV array until the VRB SOC reaches 8 V. At that time, the diesel generator is turned off and the PV array assumes the full charging responsibility for the entire system.

V.   SYSTEM CALIBRATION

Model calibration is performed to improve model predictions by comparing modeled VRB SOC data to actual VRB SOC values observed in the field. Data used during calibration was collected during system operation from August 9 to August 15, 2011. The system was calibrated by adjusting the independent variables panel efficiency and inverter efficiency to produce predicted values of VRB SOC (P_i) for each sample interval during the calibration time period. The model results were then compared to the measured, or observed values of VRB SOC (O_i).

The statistic used during calibration was the coefficient of determination (CD) which is the proportion of variability between a modeled data set and an observed data set. The CD was selected because it gives equal weight to the entire data set whereas

other statistics only give proportional rate to the largest differences within the data. The CD ranges from 0 to 1, with 0 showing no correlation and 1 showing perfect correlation. The CD calculation is shown in (14),

$$CD = \left.\frac{\sum_{i=1}^{n}(O_i - \bar{O})^2}{\sum_{i=1}^{n}(P_i - \bar{O})^2}\right. \tag{14}$$

where $\bar{O}$ is the mean of the observed SOC, and n is the number of observations during the calibration time period [15].

The manufacturer-provided efficiency of the panels was 15.5 percent and inverter efficiency s 89.4 percent, and these values served as the point of departure for the calibration. The CD was 0.53 using these initial values. An iterative process was used to arrive at the values of 13.2 percent for the panel efficiency, and inverter efficiency of 79.3 percent for a maximum CD value of 0.83. The panels were 14.8 percent less efficient and the inverter was 11.3 percent less efficient than the manufacturers' ratings. The calibration results are shown in Fig. 3.

VI.   LOAD CHARACTERIZATION

After model development and calibration, load characterization was performed in order to calculate the percent of time that a constant load can be powered by the PV panels without requiring diesel generation. The loads were assumed to be constant over the entire sample period.
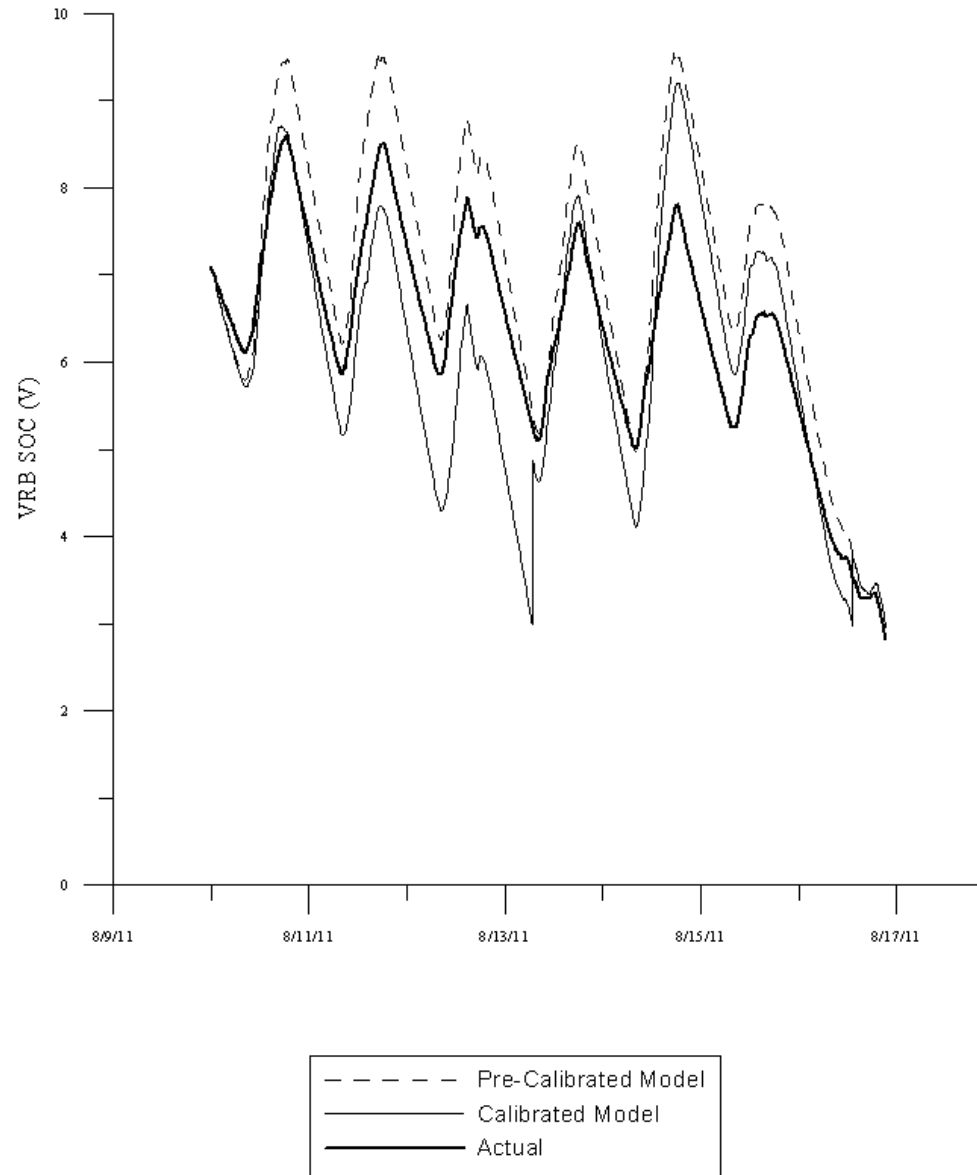
Fig. 3. Model calibration versus actual performance.

To properly characterize the load that could power the microgrid to a certain time frequency, a record of VRB temperature must be available or estimated to calculate HVAC power requirements. If it is assumed that the VRB operating temperature range can be maintained passively without the need for self-powered HVAC, then a load

characterization can be performed prior to deployment based on solar insolation and ambient temperature from nearby weather stations. Appropriate sizing of the system can then be performed to allow known loads to fit in the range of diesel generator operational frequency.

Load characterization assuming no HVAC power load was performed for three locations using weather data obtained from local weather stations, which are presented in Table III. Predicted AC loads at each location, calculated as a function of the time frequency that the emergency diesel generator must operate to power, are shown in Table IV. Without any external loads, the system is able to operate via PV sources 99.91 percent of the time at Location 1, 99.90 percent of the time at Location 2, and 99.94 percent of the time at Location 3. Operational times are significantly lower when self-powered HVAC is necessary to maintain VRB temperatures. Significant differences occur during periods when system operation requires diesel generator operation 5 percent of time at Location 1. During this period, the AC load showed an increase from 71 W when HVAC was required to 502 W when HVAC was not required. This difference was less significant during periods when diesel generator operations increased to 50 percent, where the AC load with HVAC was 2,310 W and the AC load without HVAC was 2,693 W. Variations between locations varied from 40 percent during periods of one percent and 2.5 percent diesel generator operation frequency to 5.3 percent during periods of 50 percent diesel generator operational frequency. This difference could be associated with sample location, date of sampling, as well as sample frequency.

Table III

Predicted AC energy loads to meet known generator operational time frequencies with HVAC at Location 1

	AC Load	DC Load
3.8% of Time Generator Operates	0 W	0 W
5% of Time Generator Operates	71 W	90 W
10% of Time Generator Operates	360 W	454 W
15% of Time Generator Operates	599 W	755 W
25% of Time Generator Operates	1,100 W	1,383 W
50% of Time Generator Operates	2,310 W	2,909 W

Table IV

Predicted AC loads to meet known generator operational time frequencies at known locations without HVAC

	Location 1	Location2	Location 3
% of time Generator Operates at 0 W Load	0.09%	0.10%	0.06%
1% of Time Gen. Operates	191 W	165 W	115 W
2.5% of Time Gen. Operates	365 W	262 W	220 W
5% of Time Gen. Operates	502 W	409 W	369 W
10% of Time Gen. Operates	691 W	629 W	583 W
15% of Time Gen. Operates	1,010 W	899 W	837 W
25% of Time Gen. Operates	1,457 W	1,373 W	1,350 W
50% of Time Gen. Operates	2,693 W	2,572 W	2,551 W

Characterization of DC loads was also performed at three locations, which are described in Table I. This DC load characterization is shown in Table V. The system can power a DC load from 144 W at Location 3 to 239 W at Location 1 when at a one percent diesel generator operational frequency. During periods when a five percent diesel generator operational frequency is allowed, the DC load at Location 1 showed an increase from 90 W when HVAC was required to 632 W when HVAC was not required.

When the allowed diesel generator operational frequency increased to 50 percent, the DC

load with HVAC was 2,909 W and the DC load without HVAC was 3,392 W.

Table V
Predicted DC loads to meet known generator operational time frequencies at known
locations without HVAC

	Location 1	Location 2	Location 3
% of time Generator Operates at 0 W Load	0.09%	0.10%	0.06%
1% of Time Gen. Operates	239 W	210 W	144 W
2.5% of Time Gen. Operates	460 W	330 W	280 W
5% of Time Gen. Operates	632 W	516 W	466 W
10% of Time Gen. Operates	872 W	792 W	734 W
15% of Time Gen. Operates	1,273 W	1,133 W	1,055 W
25% of Time Gen. Operates	1,838 W	1,731 W	1,699 W
50% of Time Gen. Operates	3,392 W	3,241 W	3,216 W

VII. CONCLUSIONS

Renewable energy-based microgrid operational performance at a known location

can be relatively accurately modeled using solar insolation, ambient temperature, and

VRB temperature data. The model can be used to select the appropriate PV array size for

a given load by estimating the percent of time that the PV generation would need to be

supplemented by diesel generation.

The microgrid component efficiencies were shown to be significantly less than

manufacturer's specifications. For example, the VRB can only be charged to the

manufacturer's 5 kW specified charge rate at low SOC periods. This is due to the charge controller which only allowed high current throughput at low SOCs and decreased the throughput at high SOC. The VRB only reached approximately 40 percent of its rated efficiency as the VRB SOC approaches its maximum value.

The VRB HVAC is shown to greatly reduce the microgrid system performance. Modeled system performance with the HVAC was shown to range from 14 percent to 86 percent of the VRB load during periods when self-powered HVAC was assumed to be unnecessary.

The microgrid is shown to meet load values significantly below the panel and VRB optimal performance values (6 kW PV array and 5 kW VRB), especially during low diesel generation operational time frequencies. When HVAC is included, the microgrid can only meet 1.3 percent of the rated panel load at a five percent diesel generator operational frequency. This increases to 43 percent of the rated load at a diesel generator operational frequency of 50 percent.

VIII. REFERENCES

[1] R.L. Boswell, "The Impact of Renewable Energy Sources on Forward Operating Bases," M.S. thesis, Air Command and Staff College, Air University, Maxwell Air Force Base, Alabama, 2007.

[2] S. Booth, J. Barnett, K. Burman, J. Hambrick, and R. Westby. "Net zero energy military installations: a guide to assessment and planning." National Renewable Energy Laboratory, Golden, CO, Tech. Rep. 782-48876, 2010.

[3] P. Denholm, E. Ela, B. Kirby, and M. Milligan, "The role of energy storage with renewable electricity generation," National Renewable Energy Laboratory, Golden, CO, Tech. Rep. 6A2-47187, Jan. 2010.

[4] C. Blanc and A. Rufer, "Multiphysics and energetic modeling of a vanadium redox flow battery," in Proc. 2008 IEEE International Conference on Sustainable Engineering Technologies, pp. 696-700.

[5] J. Chahwan, C. Abbey, and G. Joos, "VRB modeling for the study of output terminal voltages, internal losses, and performance," in *Proc. 2007 IEEE Canada Electrical Power Conf.*, pp. 387-392.

[6] S. Pelland, D. Turcotte, G. Colgate, and A. Swingler. "Nemiah Valley photovoltaic-diesel mini-grid: system performance and fuel saving based on one year of monitored data." *IEEE Transactions on Sustainable Energy*, 3(1), 167-175, January 2012.

[7] C.D. Barley, D.J. Lew, and L.T. Flowers. "Sizing Wind/Photovoltaic Hybrids for Households in Inner Mongolia." Presented at Windpower '97 Conference. National Renewable Energy Laboratory, Golden, Colorado, 1997.

[8] Y.V. Makarov, P. Du, M.C.W. Kintner-Meyer, C. Jin, and H.F. Illian. "Sizing energy storage to accommodate high penetration of variable energy resources." *IEEE Transactions on Sustainable Energy*, 3(1), 34-40, January 2012.

[9] N.D. Kelley and H.E. McKenna, "The evaluation of a turbulent loads characterization system." National Renewable Energy Laboratory, Golden, CO. Tech. Paper 442-20164, 1996.

[10] D.M. Heimiller and S.R. Haymes. "Geographic information systems in support of wind energy activities at." National Renewable Energy Laboratory, Golden, CO, Conf. Paper CP-500-29164,. 2001.

[11] Brightwatts, Inc., Brightwatts BI-156-200W-G27V 200 Watt Module Data Sheet.

[12] R. Messer and J. Venter, *Photovoltaic Systems Engineering.* (2nd Edition), CRC Press, LLC., Boca Raton, FL, 2004, p. 455.

[13] G. Notten, C. Cristofari, M. Mattei, and P. Poggi. "Modeling of a double-gloss photovoltaic module using finite differences." Applied Thermal Engineering, 25:2854-2877, 2005.

[14] Outback Power Systems, Inc., "FlexMax 80 maximum power point tracking charge controller user's guide: installation, programming and user's manual," Arlington, WA, p. 81.

[15] K. Loague and R.E. Green. "Statistical and graphical methods for evaluating solute transport models: Overview and application." Journal of Contaminant Hydrology, 7:51-73, 1991.

IX.   BIOGRAPHIES

Joe David Guggenberger II graduated from the University of Missouri-Rolla with his B.S. and M.S. degrees in geological engineering. He was employed as an environmental engineer with CDM, Inc., Kansas City, Missouri where he specialized in soil and groundwater characterization and remediation. He was then employed as an environmental manager with SRG Global, Farmington, Missouri where he specialized in environmental compliance and green engineering. He is currently completing his Ph.D. degree in geological engineering at the Missouri University of Science and Technology. He is a Registered Professional Engineer.

Andrew Curtis Elmore graduated from the University of Missouri-Rolla with a B.S. degree in geological engineering, and he completed his M.S. and Ph.D. degrees in civil engineering at the University of Arizona. He was employed as a consulting engineer with URS Group, Overland Park, Kansas where he specialized in green and sustainable environmental remediation. He is currently an associate professor of geological engineering at the Missouri University of Science and Technology.

M. L. Crow (S'83, M'90, SM'94, F'10) received the B.S.E. degree from the University of Michigan, Ann Arbor, and the Ph.D. degree from the University of   Illinois, Urbana/Champaign. She is currently the Director of the Energy Research and Development Center and the F. Finley Distinguished Professor of Electrical Engineering at the Missouri University of   Science and Technology. Her research interests include computational methods for dynamic security assessment and the application of power electronics in bulk power systems. She is a Registered Professional Engineer and a Fellow of the IEEE.

III.   PREDICTING PERFORMANCE OF A RENEWABLE ENERGY-POWERED MICROGRID THROUGHOUT THE UNITED STATES USING TYPICAL METEOROLOGICAL YEAR 3 DATA

J.D. Guggenberger[1], A.C. Elmore[1] , and M.L. Crow[2]

[1]Department of Geological Engineering, Missouri University of Science and

Technology – Rolla, Missouri, U.S.A. 65401

[2]Department of Electrical and Computer Engineering, Missouri University of Science

and Technology – Rolla, Missouri, U.S.A. 65401

Email: jguggenb@mst.edu, elmoreac@mst.edu, crow@mst.edu

ABSTRACT

Natural disasters, as well as the costs associated with them, are increasing in

frequency throughout the U.S. Long term power outages frequently result from natural

disasters, which leads to people relying on gasoline or diesel powered generators to meet

their energy needs which are inefficient and not cost effective. The development of

deployable renewable energy-powered microgrids as power sources would allow energy

demands to be met in portable and effective way, while limiting diesel fuel consumption

to emergency periods. Characterizing system performance of renewable energy-powered

microgrids pre-deployment would allow a system to be appropriately sized to meet all

required electrical loads at a given backup diesel generator operational time frequency,

which would decrease system operation and transportation costs as well as define the

appropriate amount of fuel to be kept on hand. This paper focuses on developing figures

that represent the quantity of external AC or DC load a microgrid could supply as a function of intermittent backup diesel generator operational percentage. TMY3 data from 217 Class I locations throughout the U.S. was inserted into a model developed by Guggenberger et al. (2012) to determine the quantity of external AC and DC load the system could supply at intermittent diesel generator operational percentages of 1 percent, 5 percent, 10 percent, 25 percent, and 50 percent. Ordinary block Kriging analysis was performed using ArcGIS to interpolate AC and DC load power between TMY3 Class I locations for each diesel generator operating percentages. Figures representing projected AC and DC external load were then developed for each diesel generator operating frequency.

HIGHLIGHTS

- A model was created to accurately model microgrid performance, as well as characterize the AC or DC load the system could supply at a given generator operating frequency.

- TMY3 data was imported into the model, and constant AC and DC loads were calculated for varying generator operating frequencies.

- Each load was imported into GIS based on latitude and longitude.

- Kriging analysis was performed to determine constant loads powered by the microgrid throughout the U.S.

KEY WORDS

Renewable energy, load characterization, TMY3 data, vanadium redox battery, photovoltaics, Kriging analysis

1. INTRODUCTION

Natural disasters impact every region of the U.S., and have increased in frequency and severity over the last 40 years [1]. Common natural disasters throughout the U.S. include extreme weather events such as hurricanes, flooding, tornadoes, earthquakes, volcano eruptions, and landslides. The U.S. government set a record in 2011 for disaster declarations, with aggregate damage totaling approximately $55 billion [2]. During natural disasters, power outages are common occurrences and can last up to several months if connection to the utility grid is interrupted during the event [3]. Approximately $150 billion is lost each year in the U.S. due to power outages and blackouts [4].

During blackout periods, most homeowners rely on portable gasoline or diesel-powered generators to keep their refrigerators running and perhaps operate a light and a small fan for a few hours each night [1]. Gasoline and diesel-powered generators are commonly supplied by insurers during periods of long-term power outages resulting from natural disasters. Fossil fuel-powered generators are not cost effective due to rising fuel costs, require large quantities of nonrenewable fossil fuels, and cause an increase in carbon monoxide emissions as well as fire hazards [2]. The development of deployable renewable energy-powered microgrids as power sources during long term power outages would allow energy demands to be met with portable and effective way, while limiting diesel fuel consumption to emergency periods.

Microgrids can be powered by a variety of renewable energy generation and storage technologies. The most common renewable energy generation technologies are wind turbines and PV panels. Due to the inherent intermittency of renewable energy powered microgrids, a diesel generator is used to provide emergency power. Common energy storage technologies such as lead acid batteries prohibit effective transportation due to their low energy density and large mass. New energy storage technologies are emerging that are proving to be more effective for deployable systems due to their high energy density. VRBs are an emerging and promising energy storage technology for deployable microgrids due to their high efficiency, high scalability, fast response, long life, and low maintenance requirements [5]. A VRB converts electrical energy to chemical energy via a conversion stack and two electrolyte tanks. During operation, ions are transferred along a thin membrane in the conversion stack between the two electrolyte tanks, which aid in the oxidation/reduction reactions during charging and discharging [6]. No liquid is actually mixed between the two tanks, but electrolyte is circulated across the membrane via a series of pumps. HVAC must be provided inside the VRB enclosure to ensure electrical equipment is not exposed to ambient temperatures below 4°C or above 29°C.

Variations in solar radiation and wind occur globally due to changes in location, season, and weather conditions. Therefore, renewable energy-powered microgrids cannot provide constant power from one location to another. Proper sizing of renewable energy-based microgrids to meet necessary loads prior to deployment without site specific climatic data has proven to be challenging. Over sizing microgrids is cost ineffective due to extra equipment leading to high capital and transportation costs. Under sizing

microgrids requires systems to rely heavily on backup diesel generation. Proper characterization of the system would allow appropriate sizing of the energy generation and storage devices prior to deployment, which would decrease system capital and transportation costs. Intermittent generator operational frequency is the percentage of run time the generator must operate in order to meet a given constant load. Predicting this frequency would allow accurate prediction of fuel usage. This would allow total system costs to be calculated effectively and define the appropriate quantity of fuel to be kept on hand during operation, which would limit fuel transportation costs.

Past research on characterization of renewable energy-powered microgrids includes analysis of individual components of the microgrid system. Cameron et al. [7] focused on comparing modeled PV system performance from the SAM program developed by NREL to measured system performance during operation. Marion et al. [8] defined performance parameters that calculated the performance of a grid-connected PV system. Yildiz et al. [9] determined the energetic performance of a PV-powered closed loop heat exchanger for use in solar greenhouse cooling. Research on VRB characterization focused on electrochemical characterization of VRB performance [10] and modeling VRB terminal voltage output for use in power smoothing in wind systems [11].

Past research also focused on characterization of microgrid system performance. This includes analyzing the performance of a battery-free PV-diesel powered microgrid [12], appropriately sizing wind/PV hybrid systems to power households in Inner Mongolia [13], and appropriate sizing of energy storage for use with variable energy resources [14]. Guggenberger et al. [15] developed a model to predict performance of a

PV-powered microgrid with a VRB for energy storage. Guggenberger et al. [16] further developed this model to allow characterization of microgrid operation based on long-term site specific data, and allowed accurate determination of the intermittent operational frequency of the backup diesel generator as a function of external load.

This paper focuses on characterizing performance of a PV-powered microgrid system throughout the U.S. as a function of the intermittent backup generator operational frequency. TMY3 data was imported into the model developed by Guggenberger et al. [16], and Kriging analysis was performed to interpolate system performance in locations between TMY3 locations. Figures were developed that represent constant AC and DC loads that can be powered by the microgrid as a function of intermittent generator operational frequency throughout the U.S. This allows a quick and accurate prediction of microgrid operational performance prior to deployment anywhere within the continental U.S.

2.   MICROGRID DESCRIPTION

A renewable energy-powered microgrid was constructed at latitude 37.71 degrees and longitude -92.15 degrees in FLW. The microgrid energy generation source was a 6 kW PV array consisting of 30 - 200 W Brightwatts Inc. solar panels (model BI-156-200W-G27V) mounted at a fixed horizontal angle of 38 degrees facing south. The PV array was electrically separated into two 3 kW arrays, and was connected to two Outback FlexMax 80 charge controllers. Emergency energy generation was provided by a three cylinder Kubota diesel engine connected to a Leroy Somer 8 kW brushless self-regulated type generator. Energy storage for the microgrid consisted of a nominal 5 kW Prudent

Energy VRB rated at an energy density of 20 kWh. VRB SOC, which is measured in V, can be used to calculate VRB capacity in kWh using (1).

$$VRB\ SOC = \left[\frac{9}{20} * \left(VRB\ Capacity + \frac{10}{9}\right)\right] \tag{1}$$

External loads used during experimentation included a 720 W Lorentz PS600 HR/C submersible water pump with controller, two 1,500 W heating elements, and the VRB HVAC. AC energy sources such as VRB HVAC and the diesel generator were connected to the VRB through a Xantrex DC/AC inverter charge controller.

Solar insolation was measured using Apogee SP-110 pyranometers mounted horizontally and at 38 degrees south facing, which were located on a nearby 3 m weather station. Campbell Scientific 107-L temperature probes were located on the 3 m weather station and inside the VRB. Power was measured throughout the VRB using LEM LA55-P current and LEM LV25-P voltage sensors. These sensors were mounted at the following locations: prior to the charge controllers, after the charge controllers, the VRB, diesel generator, and associated external loads. The pyranometers and power sensors were connected to a Campbell Scientific Model CR1000 datalogger. Sensor readings were measured at 5 second intervals, and 10 minute average values were recorded to the datalogger.

The model developed by Guggenberger et al. [15] is able to iteratively determine the performance of a PV-powered microgrid with a VRB for energy storage. This model calculated the efficiency of the VRB to be a function of VRB SOC and charging/discharging power. Losses associated with the VRB HVAC were determined to be a function of ambient temperature and the VRB container temperature. The VRB

circulation pumps were determined to operate as five stage gear pumps that switched between stages as a function of VRB SOC and charging/discharging power.

Guggenberger et al. [16] further developed this model to iteratively calculate the potential load that the microgrid system could supply as a function of solar insolation and ambient temperature. This model characterized the frequency at which the backup diesel generator must operate in order to meet an assigned AC or DC load over a known time period. The model was also calibrated to determine actual efficiencies of the PV panels and the inverter.

3.   MICROGRID PERFORMANCE MODEL

The model developed by Guggenberger et al. [15] iteratively predicts the performance of a PV-powered microgrid with a VRB for energy storage. This model determined the efficiency of the VRB to be a function of VRB SOC and charging/discharging power. Losses associated with the VRB HVAC were determined to be a function of ambient temperature and the VRB container temperature.

The model was expanded to iteratively calculate the potential load that the microgrid system could supply as a function of solar insolation and ambient temperature [16]. This operation frequency prediction model characterized the frequency at which the backup diesel generator must operate in order to meet an assigned AC or DC load over a known time period.

4.   DATA ANALYSIS

The U.S. Department of Renewable Energy National Solar Radiation Data Base (NSRDB) is a ready source for hourly irradiance data for more than 1,000 U.S. locations throughout the U.S. TMY3 data are the most current and accurate data files in the NSRDB, as described by Wilcox and Marion in [17]. TMY3 data are based on meteorological data from 1961 to 1990, which is represented by 12 typical meteorological months (January through December) that are concatenated essentially without modification to form a single year with a serially complete data record for primary measurements [17]. TMY3 data are separated into three classes of data, and only Class I data (lowest uncertainty) were used in this analysis. There are 217 Class I TMY3 locations throughout the 48 continental U.S. as shown in Figure 1.

The GHI TMY3 data set for all 217 TMY3 Class I locations throughout the continental U.S. were transformed to GII values using SAM, assuming a south-facing PV array set at the latitude of each location [18]. Data was analyzed for hourly periods from January 1 through December 31, which provided 8,760 sample intervals for each TMY3 Class I location. These GII data were used as input for the operation frequency prediction model [16].

Characterization was performed to determine the quantity of AC and DC external load power the microgrid could meet with intermittent generator operational frequencies of 1 percent, 5 percent, 10 percent, 25 percent, and 50 percent. Statistical analysis of data from the AC load characterization for all TMY3 Class I locations for each generator operational frequency (DG) described above is presented in Table 1. Statistical analysis for data from the DC load characterization for all TMY3 Class I locations for each

generator operational frequency are presented in Table 2. AC load characterization is performed by multiplying the DC load by a constant inverter efficiency loss of 20.7 percent [16]. Therefore, the projected DC load is approximately 20.7 percent higher than the projected AC load for each generator operational frequency analyzed at each location. Minimum values for AC and DC load characterization were measured at a weather station located near Olympia, WA for 1 percent diesel generator operational frequency and at Quillayute, WA for 5 percent, 10 percent, 25 percent, and 50 percent diesel generator operator frequencies. Maximum values for AC and DC load characterization were measured in Daggette, CA for all generator operational frequencies.

Table 1: Statistical analysis of projected AC power model results

	1% DG	5% DG	10% DG	25% DG	50% DG
Number of data points	217	217	217	217	217
Minimum Value (W)	86	330	552	1,202	2,227
25th Percentile Value (W)	170	423	596	1,286	2,313
50th Percentile Value (W)	205	464	610	1,319	2,346
75th Percentile Value (W)	247	489	620	1,341	2,370
Maximum Value (W)	420	570	656	1,454	2,465

Table 2: Statistical analysis of projected DC power model results

	1% DG	5% DG	10% DG	25% DG	50% DG
Number of data points	217	217	217	217	217
Minimum Value (W)	109	414	695	1,516	2,807
25th Percentile Value (W)	213	534	752	1,621	2,914
50th Percentile Value (W)	259	585	769	1,664	2,958
75th Percentile Value (W)	311	617	782	1,693	2,988
Maximum Value (W)	523	719	826	1,830	3,104

5. MAP DELINEATION

External loads for all TMY3 Class I locations were imported into ArcMap version 9.3 in separate layers for each generator operational frequency. Latitude and longitude values for each location were provided by NSRDB for each location. Interpolation was performed between TMY3 Class I data points using Kriging analysis. Global deterministic interpolation techniques were used to calculate predictions using the entire data set. Ordinary block Kriging with spherical variogram model was used during analysis. Chosen blocks are 0.19 m, and thus pixel support is 0.19 x 0.19 m^2. Contour intervals were developed in 50 W increments over the entire range of data for each layer.

6. RESULTS

Figures were created that depict constant DC and AC loads that can be powered by the microgrid throughout the U.S. with intermittent generator operating frequencies of 1 percent, 5 percent, 10 percent, 25 percent, and 50 percent. Figures depicting AC loads of 5 percent, 25 percent, and 50 percent are considered the most common operating frequencies, and thus are the figures presented and described in detail below. Since DC loads are directly proportional to AC loads, contour intervals for AC loads approximate the same shape as DC loads for each generator operational frequency. Therefore, the DC load that can be powered by the microgrid at a 5 percent diesel generator operating frequency is the only one presented and described in detail in this section.

A figure depicting a constant AC load that can be powered by the PV-powered microgrid throughout the U.S. with an intermittent diesel generator operating frequency of 5 percent is presented as Figure 1. Contour lines showing power intervals of 350 W, 400 W, 450 W, 500 W, and 550 W are shown on this figure. The area with the highest

projected constant power interval of 550 W to 600 W is located in southeastern California, southern Nevada, Arizona, and southwestern New Mexico. The area with the lowest projected constant power interval of 300 W to 350 W is located in northwestern Washington. Areas of each projected power contour interval throughout the U.S. and percentages of total area for each contour interval are presented in Table 3. The projected power contour interval of 450 W to 500 W has the largest area throughout the U.S. at 43 percent of the total area.

A figure showing projected constant AC power that can be provided by the microgrid at a 25 percent intermittent diesel generator operating frequency is presented as Figure 2. Contour lines of 1,250 W, 1,300 W, 1,350 W, 1,400 W, and 1,450 W are shown on the figure. The contour interval with the highest projected power of 1,450 W to 1,500 W is located in southern California. The contour interval with the lowest projected power of 1,200 W to 1,250 W is located in western Washington. Areas for each projected contour interval and percentages of total area for each contour interval are presented in Table 4. The projected power interval of 1,300 W to 1,350 W has the largest area at 45 percent of the total area.
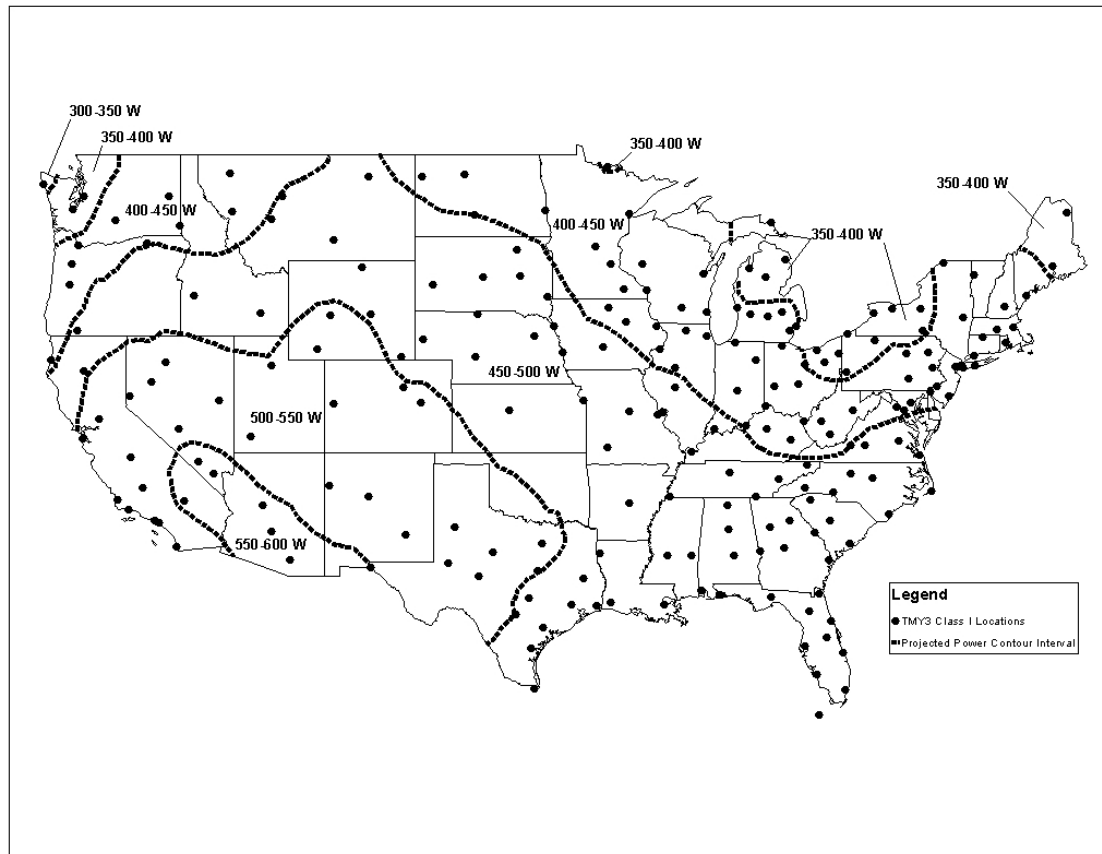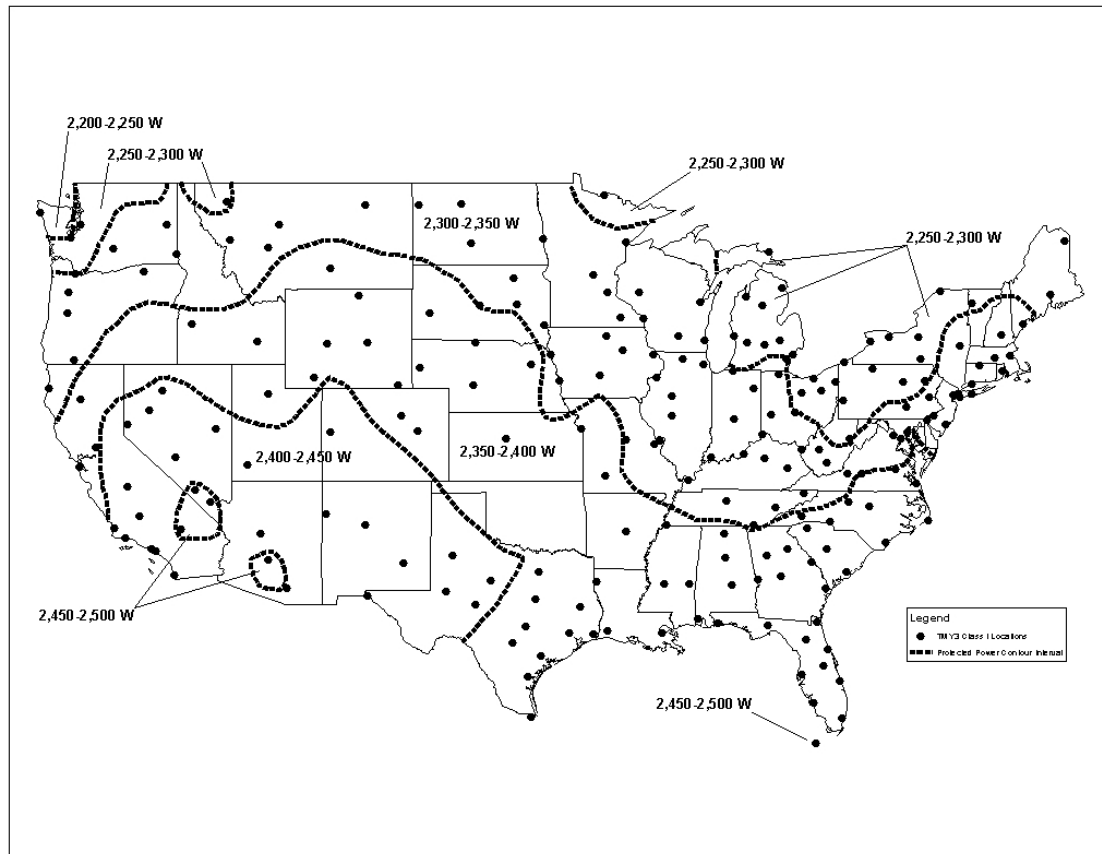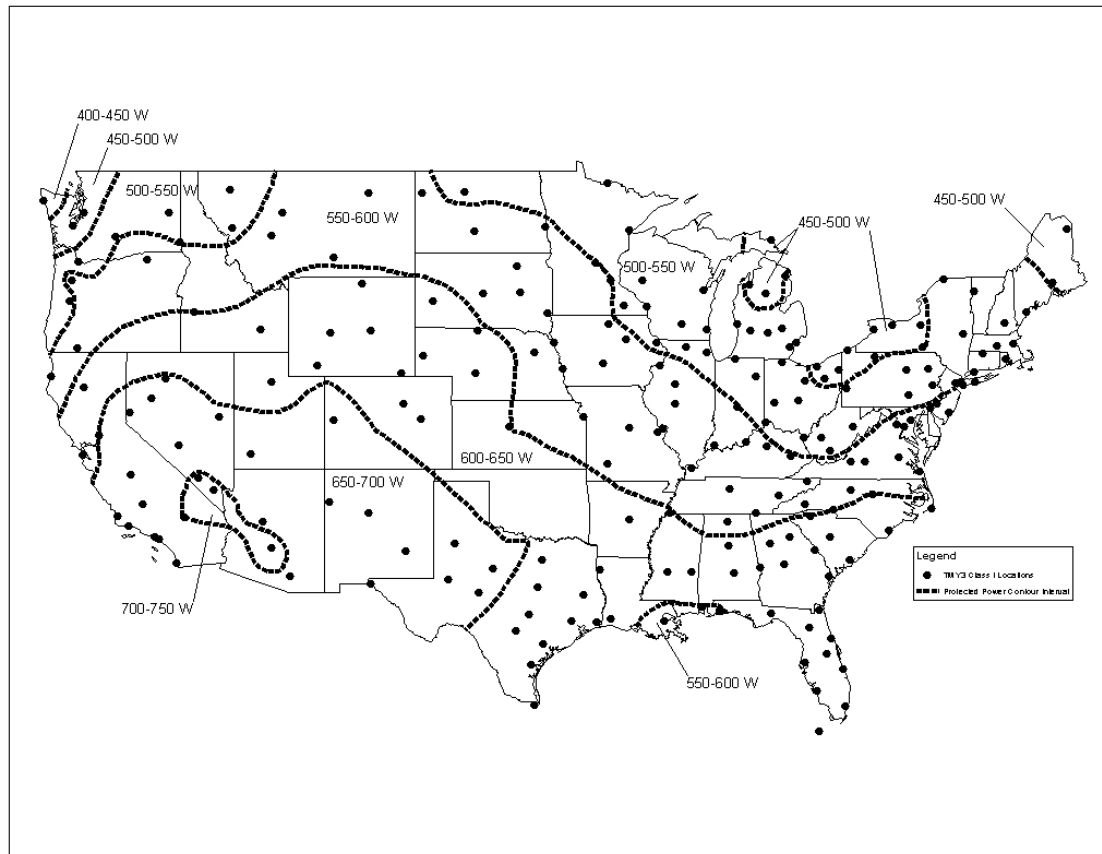
Figure 1: Projected AC power at 5 percent diesel generator operating frequency

Table 3: Area of projected AC power contour intervals for a 5 percent diesel generator operating frequency

Projected Power Interval (W)	Area (m^2)	Percent of Total Area (%)
550-600	4.5 x 10^{11}	3.4
500-550	3.1 x 10^{12}	23
450-500	5.8 x 10^{12}	43
400-450	3.4 x 10^{12}	25
350-400	6.0 x 10^{11}	4.6
300-350	6.4 x 10^9	0.0
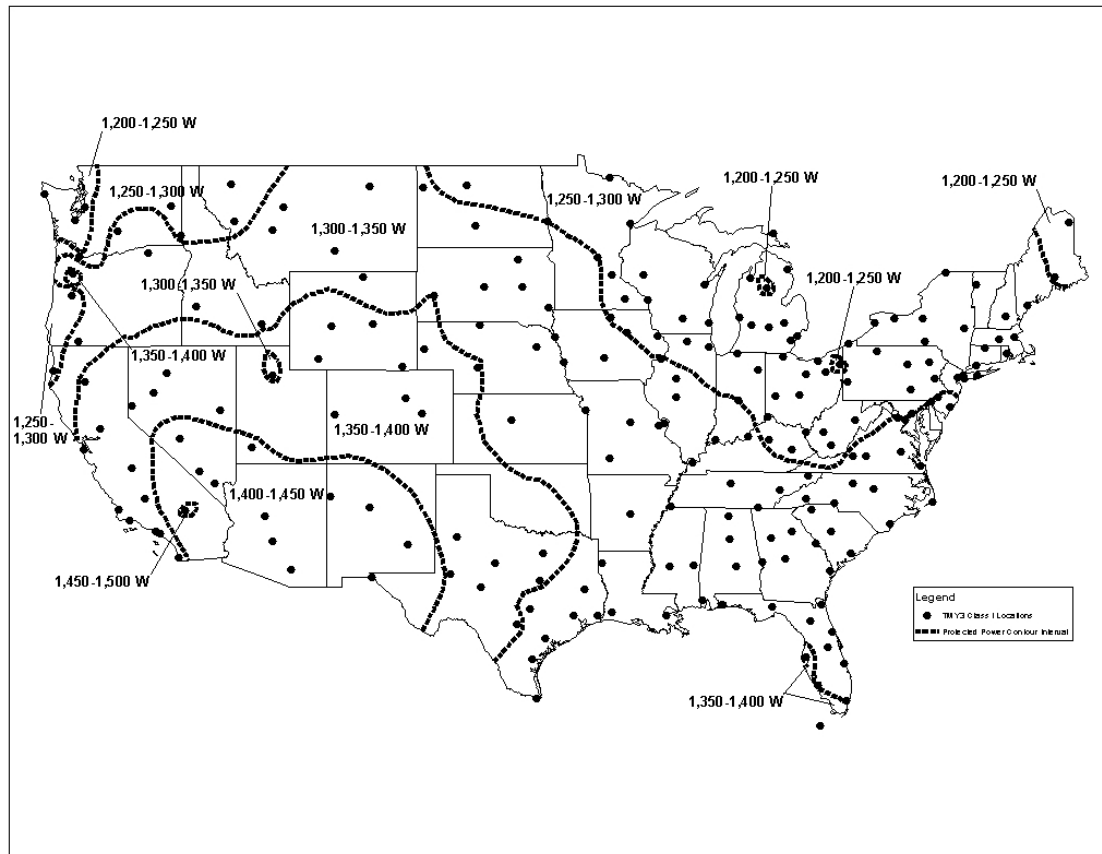
Figure 2: Projected AC power at 25 percent diesel generator operating frequency

Table 4: Area of projected AC power contour intervals for a 25 percent diesel generator operating frequency

Projected Power Interval (W)	Area (m^2)	Percent of Total Area (%)
1450-1500	6.4×10^9	0.0
1400-1450	1.3×10^{12}	10
1350-1400	2.9×10^{12}	22
1300-1350	5.9×10^{12}	45
1250-1300	2.9×10^{12}	22

A figure showing projected AC power that can be powered by the microgrid at a 50 percent generator operating frequency is presented as Figure 3. Contour lines of 2,250 W, 2,300 W, 2,350 W, 2,400 W, and 2,450 W are shown on this figure. The two contour intervals with the highest projected power of 2,450 W to 2,500 W are located in southern California, southern Nevada, and Arizona. The contour interval with the lowest projected power of 2,200 W to 2,250 W is located in western Washington. Areas of contour intervals for each projected power interval and percentages of total area for each contour interval are presented in Table 5. The projected power interval of 2,350 W to 2,400 W has the largest area at 38 percent of the total area.

A figure showing projected DC power that can be powered by the microgrid at a 5 percent diesel generator operating percentage is presented as Figure 4. Contour lines of 450 W, 500 W, 550 W, 600 W, 650 W, and 700 W are shown on this figure. The contour interval with the highest projected power of 700 W to 750 W is located in southern California, southern Nevada, and Arizona. The contour interval with the lowest projected power of 400 W to 450 W is located in western Washington. Areas of contour intervals for each projected power interval and percentages of total area for each contour interval are presented in Table 6. The projected power interval of 600 W to 650 W has the largest area at 30 percent of the total area.

Figure 3: Projected AC power at 50 percent diesel generator operating frequency

Table 5: Area of projected AC power contour intervals for a 50 percent diesel generator operating frequency

Projected Power Interval (W)	Area (m^2)	Percent of Total Area (%)
2,450-2,500	1.1×10^{11}	0.9
2,400-2,450	2.6×10^{12}	19
2,350-2,400	5.0×10^{12}	38
2,300-2,350	4.4×10^{12}	33
2,250-2,300	1.1×10^{12}	8.3
2,200-2,250	3.8×10^{10}	0.3

Figure 4: Projected DC power at 5 percent diesel generator operating frequency

Table 6: Area of projected DC power contour intervals for a 5 percent diesel generator operating frequency

Projected Power Interval (W)	Area (m^2)	Percent of Total Area (%)
700-750	1.4×10^{11}	1.1
650-700	2.5×10^{12}	19
600-650	4.1×10^{12}	30
550-600	3.7×10^{12}	28
500-550	2.5×10^{12}	19
450-500	4.4×10^{11}	3.3
400-450	1.6×10^{10}	0.1

7. CONCLUSIONS

A figure developed by NREL [19] to depict the average daily solar radiation throughout the U.S. is presented as Figure 5. This figure was based on daily average GII data collected from 239 TMY3 Class I and II locations from 1961 to 1990. Projected power contours depicted in Figures 1 through 4 approximate solar radiation contours depicted in Figure 5, which shows that TMY3 data used in conjunction with the model developed by Guggenberger et al. [16] accurately predicts projected AC and DC power as a function of available solar radiation. Differences between power contour intervals in Figures 1 through 4 and those in Figure 5 could be attributed to differences in averaging solar insolation data and model power calculations. Figure 5 is based on average daily solar radiation, while Figures 1 through 4 are based on 12 typical meteorological months. The model developed by Guggenberger et al. [16] calculates average power over a typical year, which includes PV power as well as intermittent generator power. Therefore, projected power represented in Figures 1 through 4 is not solely reliant on solar insolation, which could lead to differences in contour intervals as those represented in Figure 5.

TMY3 data files are available globally, which would allow this method to predict operational performance for various locations throughout the world.
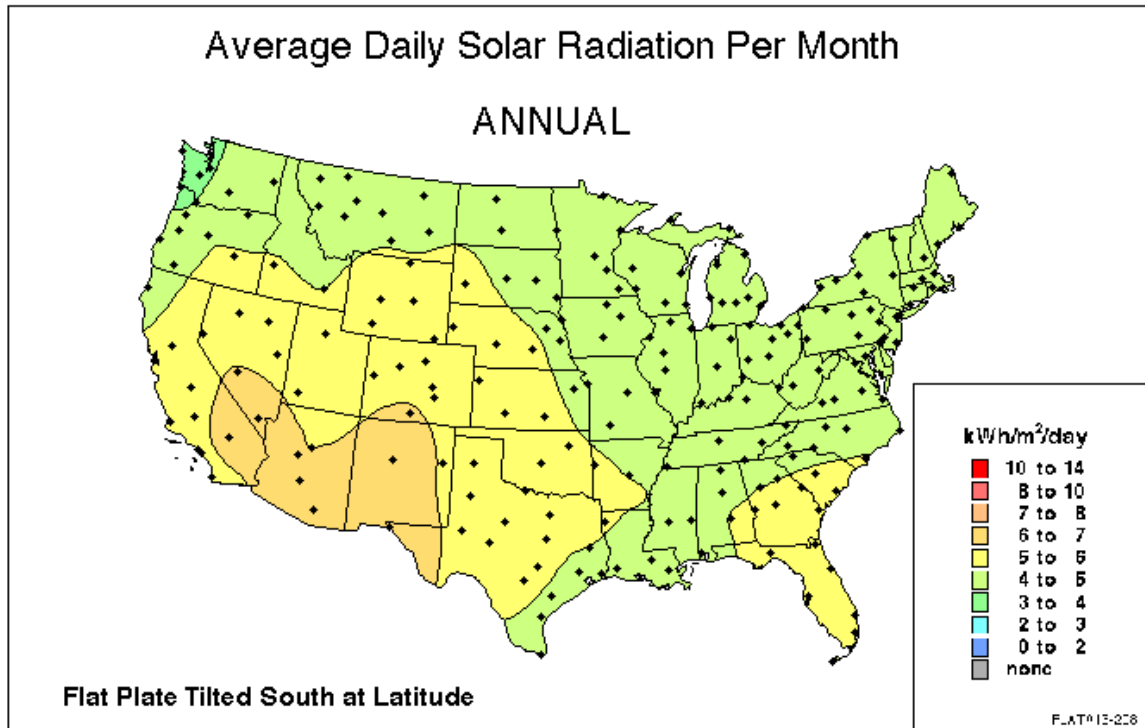
Figure 5: Average daily solar radiation throughout U.S. [19]

ACKNOWLEDGEMENTS

REFERENCES

[1]   Deering, A., & Thornton, J. P. (1999). Applications of solar technology for catastrophe response, claims management, and loss prevention. National Renewable Energy Laboratory, Retrieved April 10, 2012, from http://www.nrel.gov/docs/fy99osti/25866.pdf

[2]   National Oceanographic and Atmospheric Administration National Climatic Data Center . (2012). Billion dollar U.S. weather / climate disasters. Retrieved April 10, 2012, from http://www.ncdc.noaa.gov/soa/reports/billionz.html

[3]   Congress of the U.S. Office of Technology Assessment. Physical Vulnerability of Electric Systems to Natural Disasters and Sabotage. Technical Report OTA-E-453. 1990.

[4]   U.S. Energy Information Administration. Electric Power Annual 2009 - State Data Tables. 2011.

[5]   Blanc and A. Rufer, "Multiphysics and energetic modeling of a vanadium redox flow battery," in Proc. 2008 IEEE International Conference on Sustainable Engineering Technologies, pp. 696-700.

[6]   Fabjan, Ch. et al, 2001 Institute for Electrochemical Technology and Solid State Chemistry, Vienna University of Technology "The vanadium redox-battery: An efficient storage unit for photovoltaic systems"

[7]   Cameron, C.P., Boyson, W.E., Riley, D.M. Comparison of PV system performance-model predictions with measured PV system performance. 33rd IEEE Photovoltaic Specialists Conference Proceedings. 2008.

[8]   Marion, B., Adelstein, J., Boyle, K., Hayden, H., Hammond, B., Fletcher, T., Canada, B., Narang, D., Shugar, D., Wenger, H., Kimbler, A., Mitchell, L., Rich, G., Townsend, T. Performance parameters for grid-connected PV systems. 31st IEEE Photovoltaics Specialists Conference and Exhibition Presentation NREL/CP-520-37358. 2005.

[9]   Yildiz, A., Ozgener, O., Ozgener, L. Energetic performance analysis of a solar photovoltaic cell (PV) assisted closed loop earth-to-air heat exchanger for solar greenhouse cooling: An experimental study for low energy architecture in Aegean Region. Renewable Energy 44: 281-87. 2012.

[10]   Blanc, C., Rufer, A., Multiphysics and energetic modeling of a vanadium redox flow battery. Proc. 2008 IEEE International Conference on Sustainable Engineering Technologies, pp. 696-700.

[11]   Chahwan, J., Abbey, C., Joos, G., VRB modeling for the study of output terminal voltages, internal losses, and performance. in *Proc. 2007 IEEE Canada Electrical Power Conf.*, pp. 387-392.

[12]   Pelland, S., Turcotte, D., Colgate, G., Swingler, A. Nemiah Valley photovoltaic-diesel mini-grid: system performance and fuel saving based on one year of monitored data. *IEEE Transactions on Sustainable Energy*, 3(1):167-175. January 2012.

[13]   Barley, C.D., Lew, D.J., Flowers, D.T.   Sizing Wind/Photovoltaic Hybrids for Households in Inner Mongolia. Presented at Windpower '97 Conference. National Renewable Energy Laboratory, Golden, Colorado, 1997.

[14]   Makarov, Y.V., Du, , Kintner-Meyer, M.C.W, Jin, C., Illian, H.F.   Sizing energy storage to accommodate high penetration of variable energy resources. *IEEE Transactions on Sustainable Energy*, 3(1), 34-40, January 2012.

[15]   Guggenberger, J.D.*, Elmore, A.C., Crow, M.L.   In review. Microgrid load characterization using long-term weather data. Submitted to *IEEE Transactions on Sustainable Energy* on March 14, 2012.

[16]   Guggenberger, J.D., Elmore, A.C., Tichenor, J.L., Crow, M. In review. Performance prediction of a vanadium redox battery for use in portable, scalable microgrids. Submitted to *IEEE Transactions on Smart Grid Special Issue on Microgrids* on November 30, 2011.

[17]   Wilcox, S., Marion, W. Users Manual for TMY3 Data Sets. National Renewable Energy Laboratory Technical Report NREL/TP-581-43156. 2008.

[18]   Blair, N., Mehos, M., Christensen, C. Sensitivity of concentrating solar power through performance, cost, and financing with the solar advisor model. 14th Biennial CSP Solar Power and Chemical Energy Systems Symposium, NREL/CD-550-42709. 2008.

[19]   National Renewable Energy Laboratory. U.S. Solar Radiation Resource Maps: Atlas of the Solar Radiation Data Manual for Flat-Plate and Concentrating Collectors. Retrieved April 17, 2012, from http://rredc.nrel.gov/solar/old_data/nsrdb/1961-1990/redbook/atlas/

APPENDIX A.

MICROGRID SYSTEM PHOTOGRAPHS

Figure A.1. Microgrid system

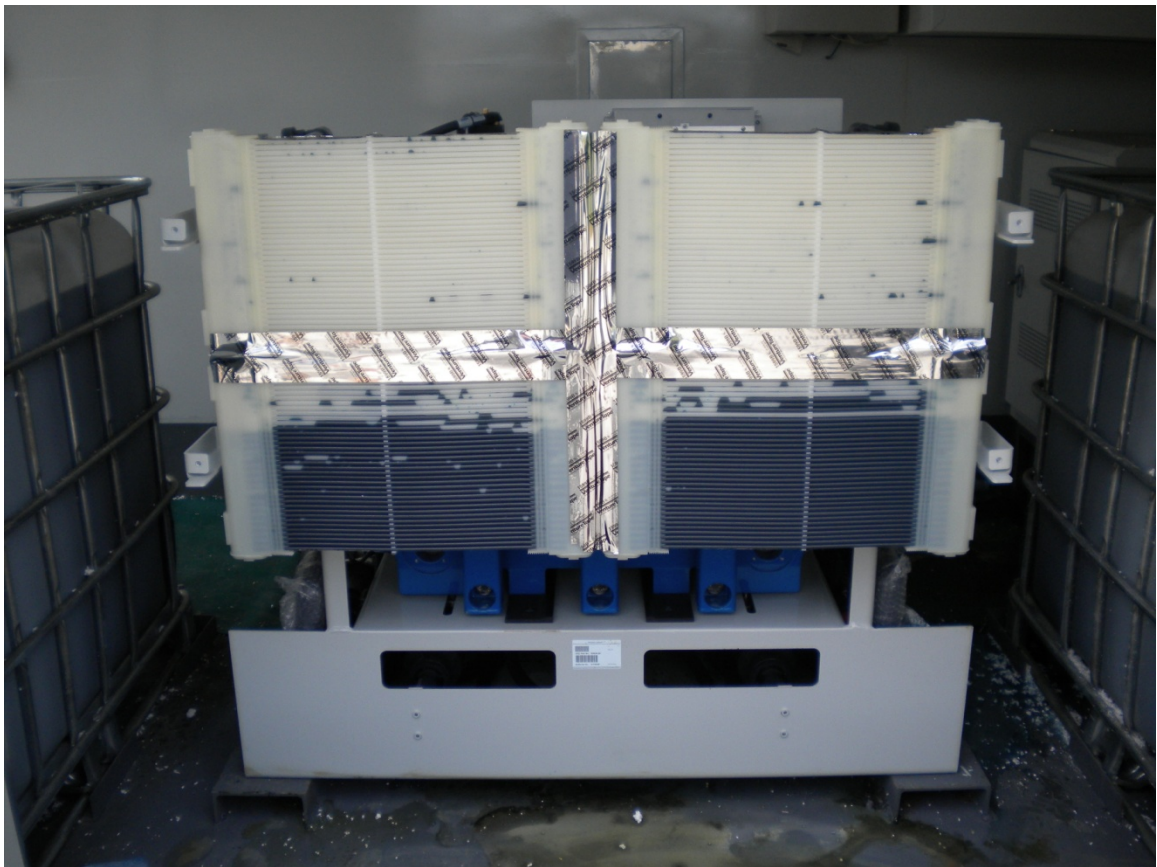**Figure A.2** PV array mounted on main container

Figure A.3. VRB container

Figure A.4. VRB electrolyte tanks and stack
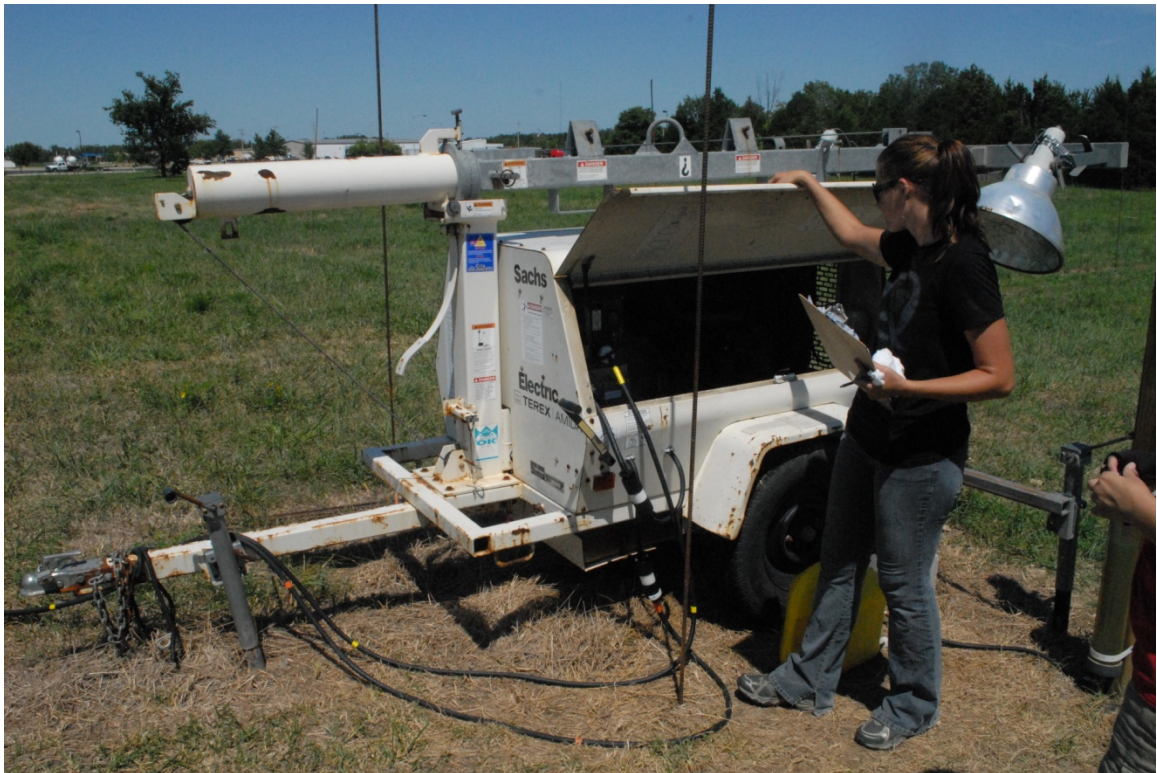
Figure A.5. VRB stack

Figure A.6. Main container layout

Figure A.7. System electrical components

Figure A.8. Diesel generator
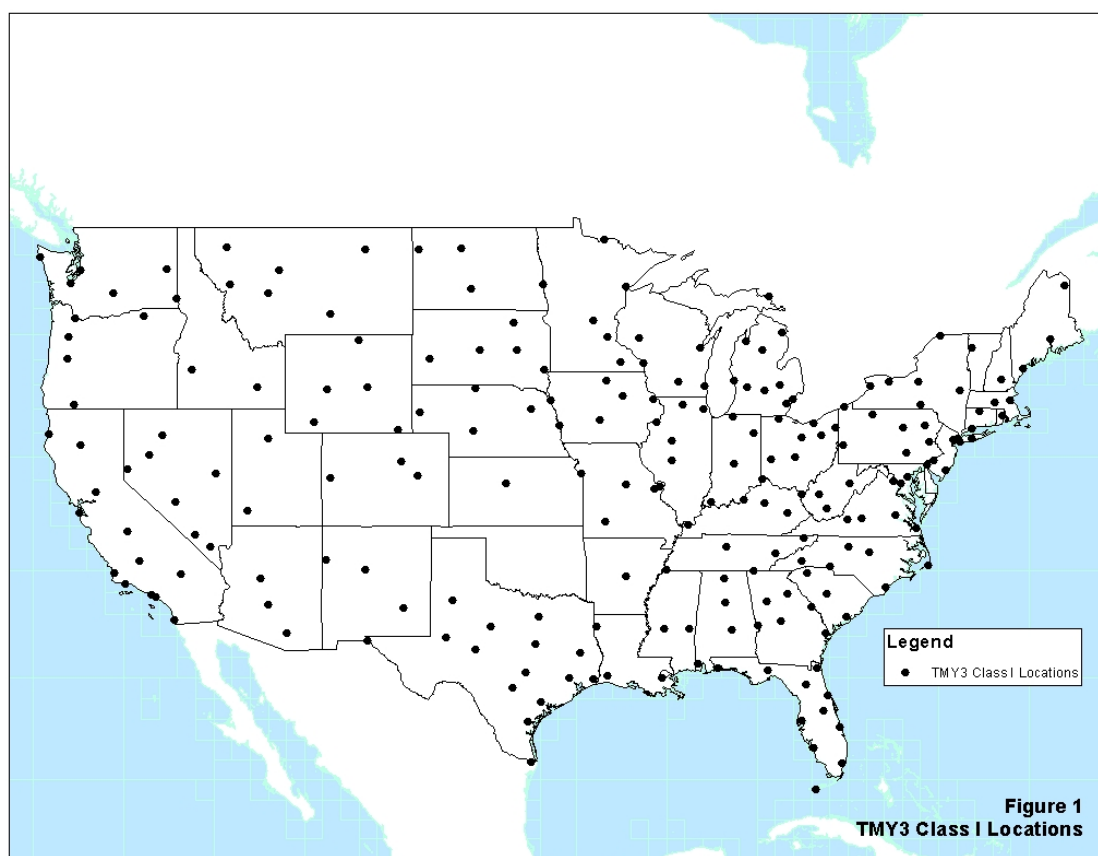
Figure A.9. FLW weather station
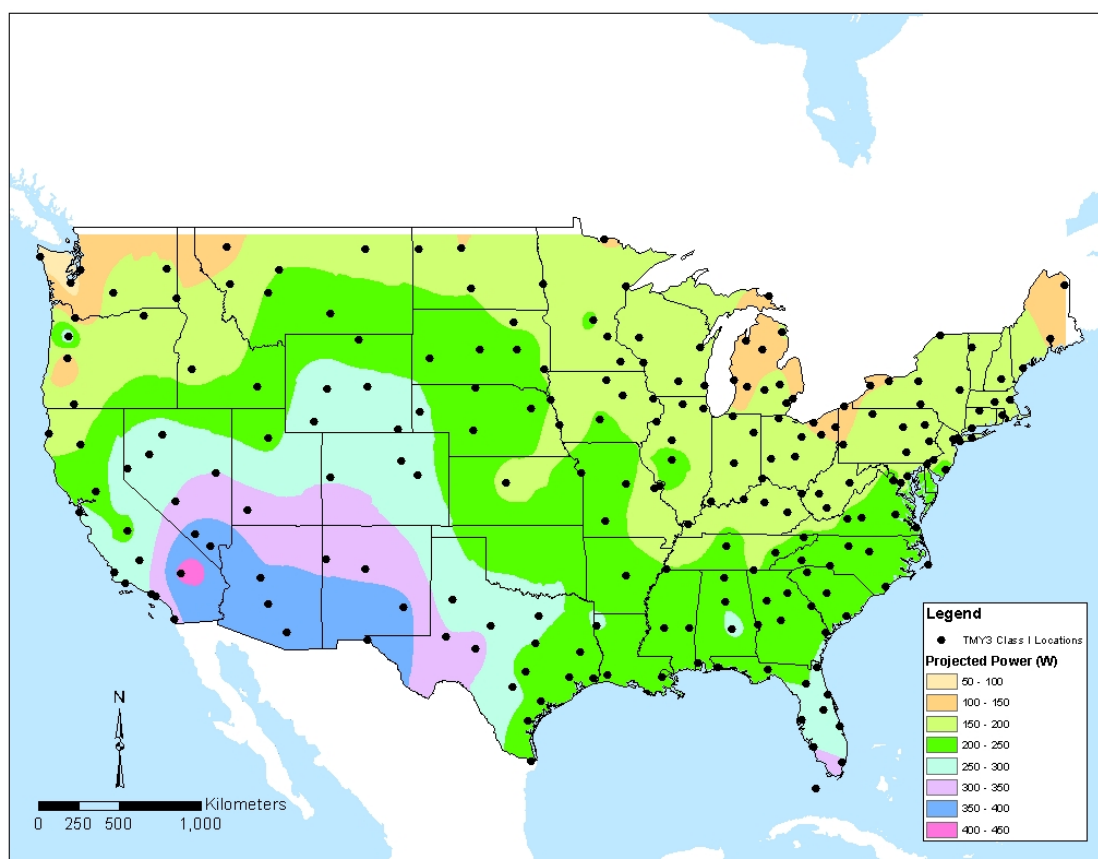
Figure A.10. Bergey Xl.1 wind turbine
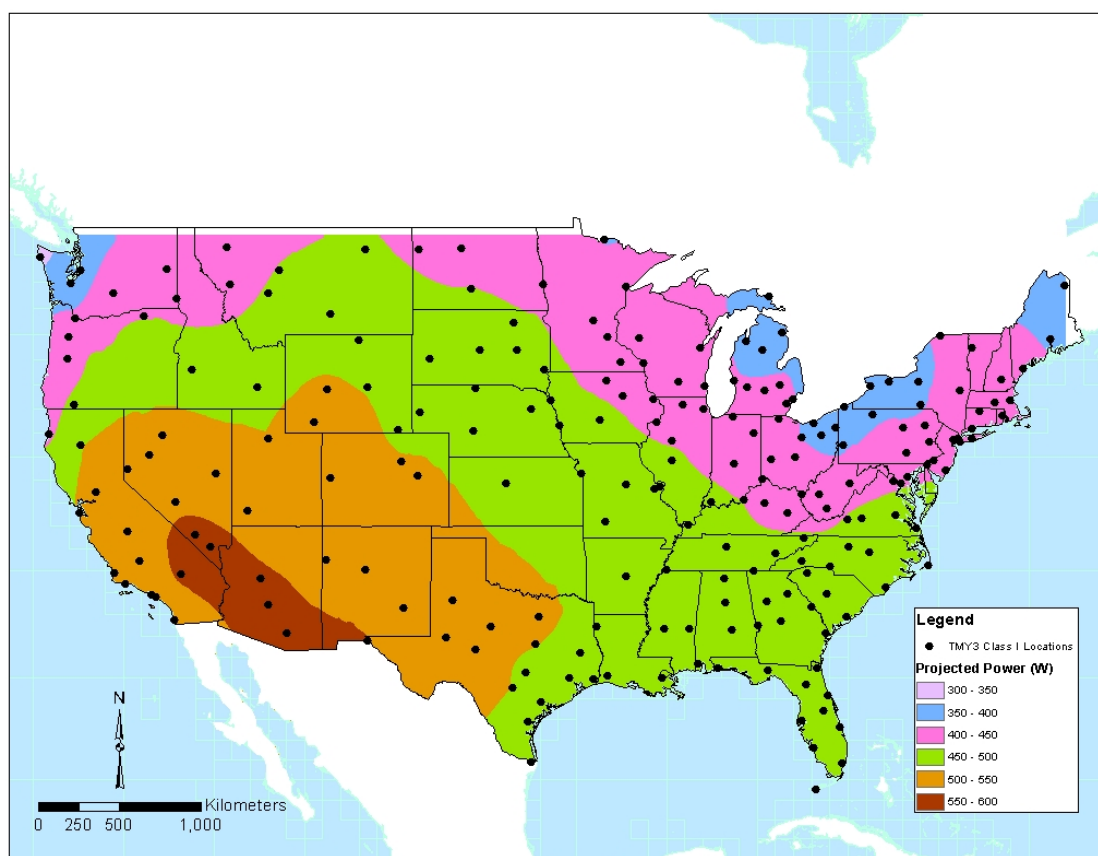
APPENDIX B.

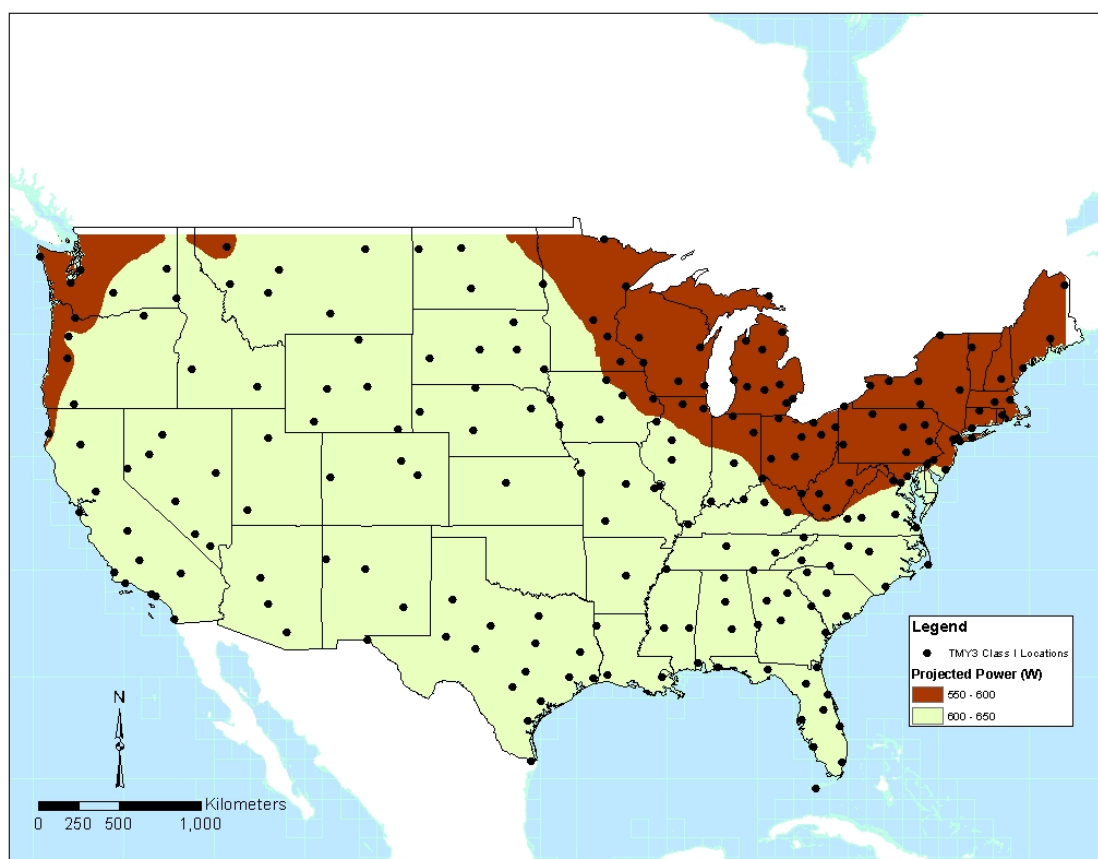PROJECTED MICROGRID EXTERNAL LOAD THROUGHOUT THE U.S.

Figure B.1. TMY3 Class 1 locations

Figure B.2. Projected AC power at 1 percent generator operating frequency
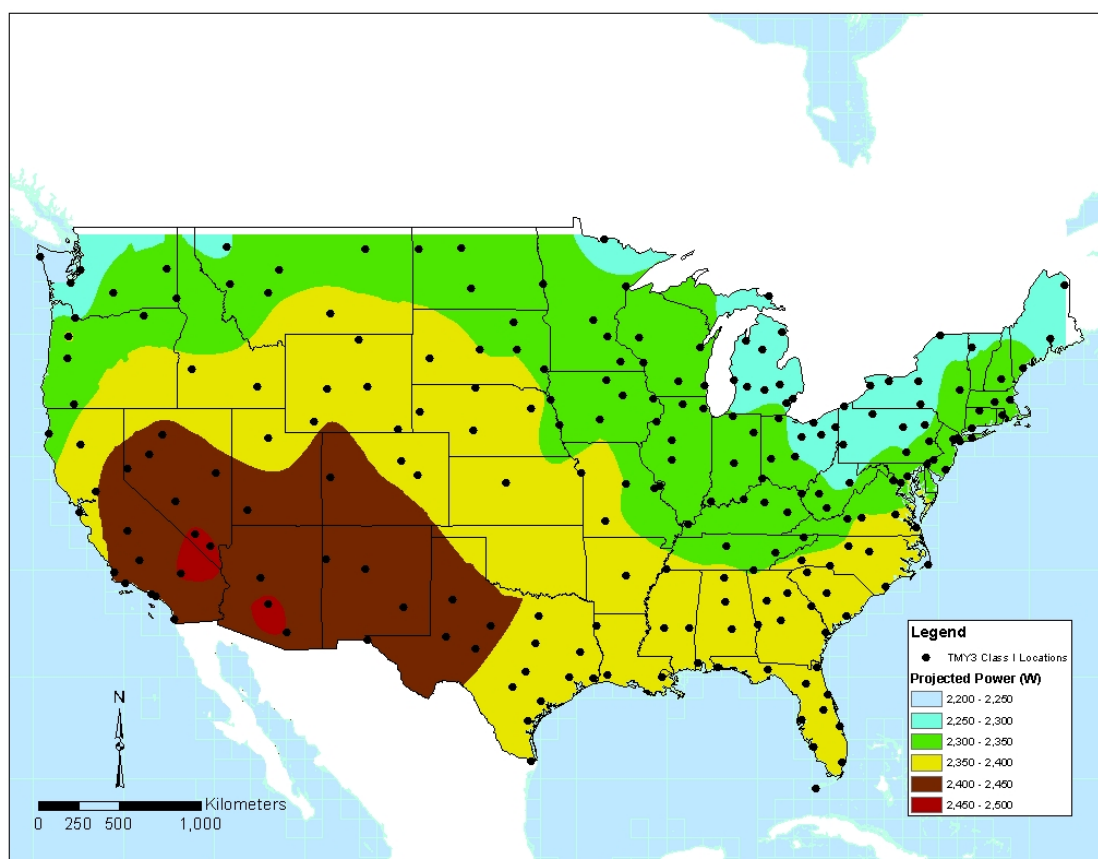
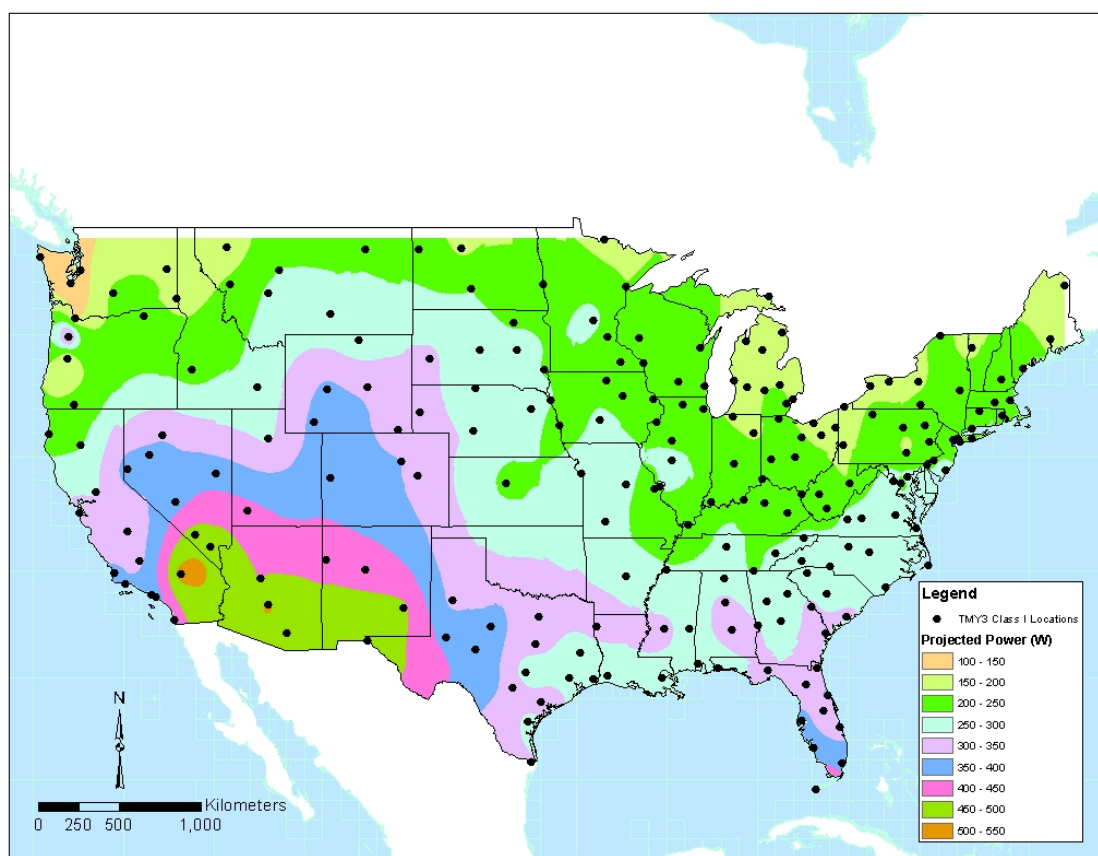**Figure B.3.** Projected AC power at 5 percent generator operating frequency

Figure B.4. Projected AC power at 10 percent generator operating frequency
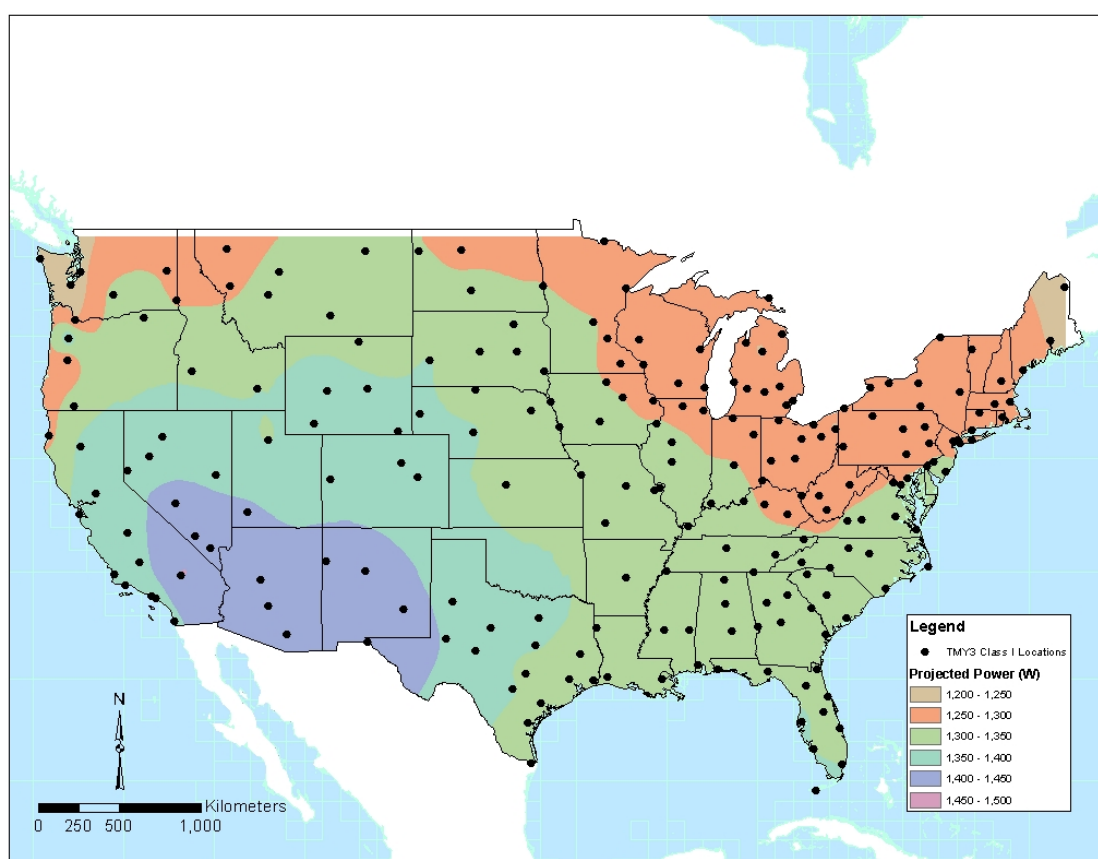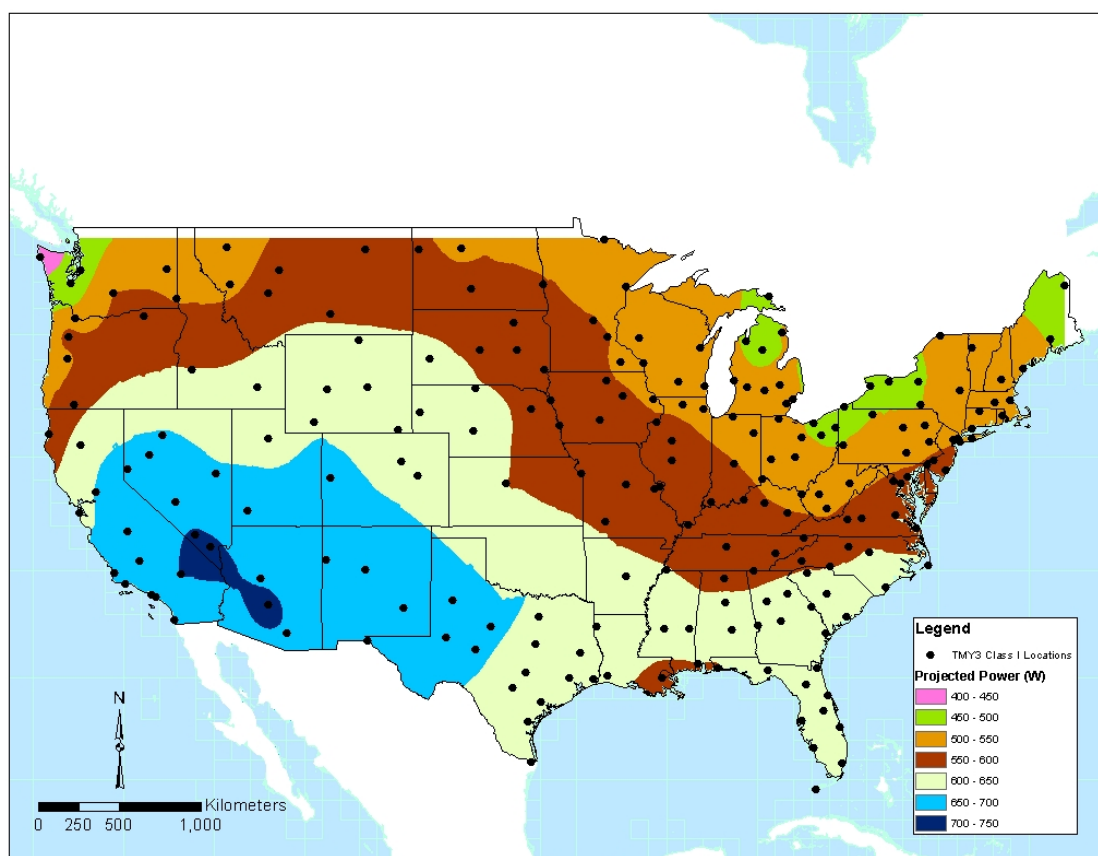
Figure B.5. Projected AC power at 25 percent generator operating frequency
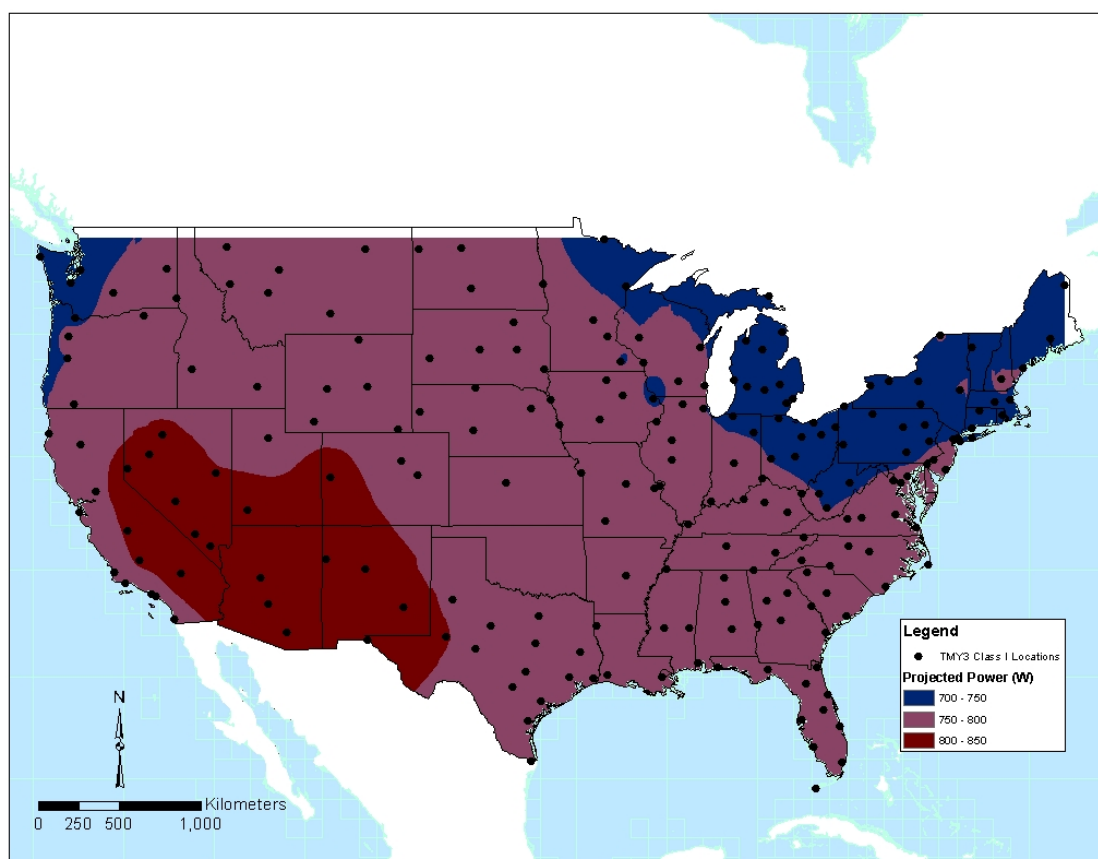
Figure B.6. Projected AC power at 50 percent generator operating frequency

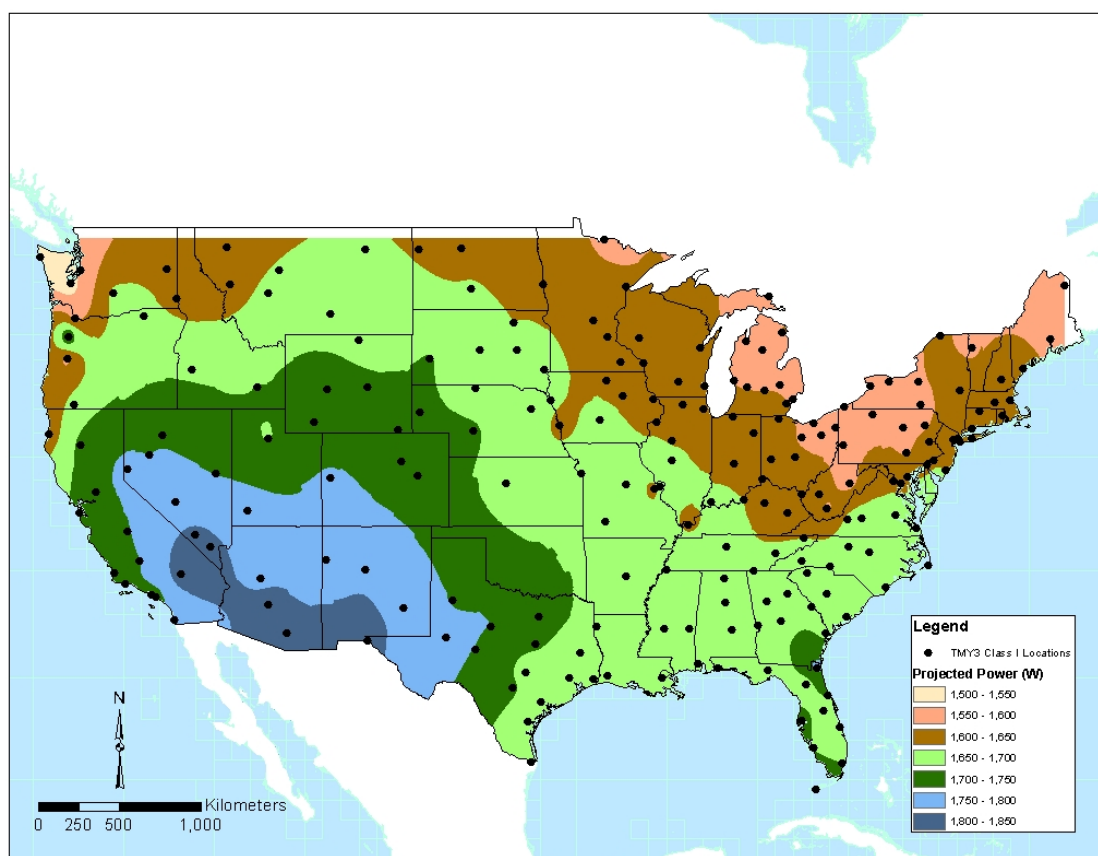**Figure B.7.** Projected DC power at 1 percent generator operating frequency

Figure B.8. Projected DC power at 5 percent generator operating frequency
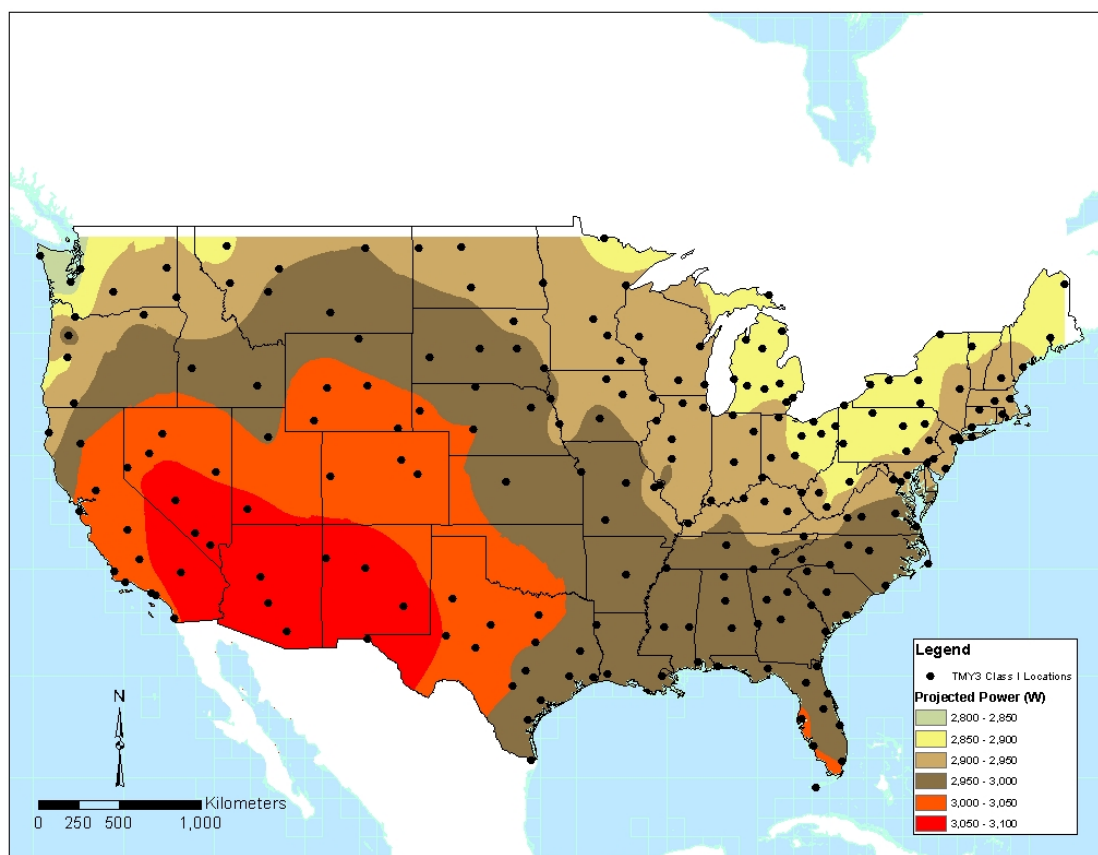
Figure B.9. Projected DC power at 10 percent generator operating frequency

Figure B.10. Projected DC power at 25 percent generator operating frequency

Figure B.11. Projected DC power at 50 percent generator operating frequency

APPENDIX C.

EXPLANATION OF THEORY

C.1   WIND ENERGY CALCULATIONS

Wind turbine energy power production is calculated using the following equation (C.1):

$$P = A \times \frac{\rho}{2} \times v^3 \tag{C.1}$$

where P is the power generated from the wind turbine, A is the cross-sectional area of the wind turbine blades, ρ is the air density, and v is the wind velocity. This calculation assumes that the subject air is an incompressible fluid. This calculation shows that power output of a wind turbine is a cubed function of the wind velocity. Doubling the wind velocity will increase the power output by a factor of eight.

Wind turbine energy production (E) is calculated using the following equation (C.2) (Elmore and Gallagher 2009):

$$E = \sum_{i=1}^{n}(f_{v_i} \times P(v_i) \times T) \tag{C.2}$$

where power output of the wind turbine (P) has been separated into n bins according to wind velocity (v), where v_i is the effective velocity for each bin (i). f_{v_i} is the frequency that the wind velocity is between v_i and v_{i+1}. $P(v_i)$ is the effective wind turbine power output and T is the length of time.

Currently, wind frequency is estimated using a two parameter Weibull probability distribution based on an average wind velocity (Manwell et al. 2002). A two parameter Weibull probability distribution (PDF) was calculated using the following equation (C.3) (Haldar and Mahadevan 2000).

$$f_v(v) = \frac{k}{c} \times \left(\frac{v}{c}\right)^{k-1} \times e^{\left[-\left(\frac{v}{c}\right)^k\right]}$$

(C.3)

where k is the Weibull shape factor and c is the Weibull scale factor. The mean wind velocity (μ) is calculated using the following equation (C.4):

$$\mu = c \times \Gamma\left(1 + \frac{1}{k}\right)$$

(C.4)

where $\Gamma(\ )$ is the gamma function. This equation can be substituted into equation (C.3) and rewritten as a function of the mean wind velocity and Weibull shape factor as equation (C.5) (Elmore and Gallagher 2009):

$$f_v(v) = \frac{k \times \Gamma\left(1 + \frac{1}{k}\right)}{\mu} \times \left(\frac{v \times \Gamma\left(1 + \frac{1}{k}\right)}{\mu}\right)^{k-1} \times e^{\left[-\left(\frac{v \times \Gamma\left(1 + \frac{1}{k}\right)}{\mu}\right)^k\right]}$$

(C.5)

Typical wind velocity k values range from 1.5 to 3.0, with 2.0 frequently assumed during calculations. Therefore, this equation can be used in conjunction with the wind turbine energy production equation to predict energy output of a wind turbine output as a function of mean wind velocity (Elmore and Gallagher 2009).

Since there is a small variation of the gamma function compared to corresponding changes to the variable k, this equation can be simplified. Gallagher and Elmore (2009) simplified this equation where the gamma function is replaced with an average value of 0.89, which is shown in the following equation (C.6):

$$f_v(v) = \frac{k}{\frac{\mu}{0.89}} \times \left(\frac{v}{\frac{\mu}{0.89}}\right)^{k-1} \times e^{\left[\frac{-v}{\frac{\mu}{0.89}}\right]^k}$$

(C.6)

Since anemometers and wind turbines are installed at multiple heights, it is important to be able to project wind speeds at variable heights based on wind speeds collected at different elevations. Johnson (1985) developed an equation to relate wind velocity as a function of height, which is shown in the following equation (C.7):

$$\frac{v_2}{v_1} = \left(\frac{h_2}{h_1}\right)^{\alpha} \tag{C.7}$$

where v_2 and v_1 are the velocities at height 2 (h_2) and height 1 (h_1), respectively, and α is the wind shear exponent. Wind shear exponent values typically range from 0.1 to 0.32 for various ground terrains (Elliot et al. 1986).

Effective wind turbine power output [P(v)] was calculated based on ideal wind turbine power functions at sea level conditions (P_T) adjusted for wind turbine elevation (H) to account for changes in atmospheric air in the following equation (C.8):

$$P(v) = (1 - TF) \times (1 + A) \times P_T \times v \tag{C.8}$$

where TF is the turbulence factor , and A=H$^{0.0000918}$. Typical turbulence typically factors vary from 10 to 15 percent depending on site conditions.

C.2 SOLAR ENERGY CALCULATIONS

Sunlight, or solar radiation, is converted to electrical energy by PV cells. This process occurs by the cells absorbing light, which converts the incident photon (i.e. heat) to electrical energy due to certain properties of the semiconductor material of these cells. PV cells are constructed of semiconductor materials such as silicon, germanium, or gallium-arsenate. These cells are "doped" with materials such as boron on one side and

germanium on the other in order to create a pn junction. The pn junction causes electrons to travel to one side of the junction and electron holes to travel to the other side of the junction. This results in a voltage being created across the panel, which generates a DC electric current.

Solar radiation can reach earth through three different pathways. The most common pathway is direct beam solar radiation, which refers to radiation that travels directly from the sun to the ground surface. The second pathway is diffuse radiation, which refers to the radiation that travels through translucent materials such as clouds or aerosols. These materials can alter the pathway of the solar radiation before it would reach the earth, sometimes to great effects. The third pathway is reflected radiation, which refers to solar radiation that completely reflects off objects such as mountains, buildings or clouds before it approaches earth's surface.

The sun provides energy by converting hydrogen to helium in a massive thermonuclear fusion reaction. As a result of this reaction, the surface of the sun is maintained at a temperature of approximately 5,800 Kelvin (K). This energy is radiated away from the sun uniformly in all directions following Planck's blackbody radiation formula (C.9) stated below:

$$w_\lambda = \frac{2 \times \pi \times h \times c^2 \times \lambda^{-5}}{e^{\frac{h \times c}{\lambda \times k \times T}} - 1} \qquad (C.9)$$

where h is Planck's constant of 6.63 x 10^{-34} watt sec^2, K is the Boltzmann's constant of 1.38 x 10^{-23} joules/K, c is the speed of light, λ is the wavelength, T is the temperature of the black body, , and w is the frequency (in hertz).

Horizontal beam radiation (I_h) is radiation that approaches earth directly from the sun. This radiation can be calculated for any location based on the following equation (C.10):

$$I_h = I \times \sin \theta \qquad \text{(C.10)}$$

where I is the radiation reaching the ground and θ is the degree from which this radiation approaches earth, which is measured parallel to the ground surface. The units for I_h and I are watts per square meter (W/m^2).

Solar radiation leaving the sun loses energy while traveling through the atmosphere. This energy loss is shown in the following equation (C.11):

$$I = \tau_B \times I_o \qquad \text{(C.11)}$$

where τ_B is the atmospheric transmittance and I_o is the extraterrestrial radiation. The amount of sunlight either absorbed or scattered depends on the length of the path in the atmosphere. This path is typically compared to a vertical path directly at sea level, which is called an air mass (AM). In general, the air mass through which sunlight passes is directly proportional to the secant of the zenith angle (θ_z), which is the angle measured between the direct beam and the vertical. The intensity of the global radiation is typically 1,367 W/m^2 at the top of the atmosphere to approximately 1,000 W/m^2 at sea level. A calculation to determine the intensity of solar radiation at the earth's surface is shown in the following equation (C.12):

$$I = 1367 \times (0.7)^{AM} \qquad \text{(C.13)}$$

This equation shows that the intensity of sunlight is reduced to approximately 70 percent at one atmosphere compared to its value above the atmosphere. This calculation isn't as precise when comparing air masses from different thicknesses as compared to the following equation (C.14):

$$I = 1367 \times (0.7)^{AM^{0.678}} \tag{C.14}$$

To calculate the amount of solar irradiation for a given day based on calendar date (n), you can use the following equation (C.15):

$$I_o = SC \left(1 + 0.033 \times cos\left(\frac{360\,n}{365}\right)\right) \tag{C.15}$$

where SC is the solar constant of 1,353 W/m^2 .and n is the calendar date with January 1st being day 1.

Due to earth constantly rotating around the sun at a declination of 23.45 degrees, direct beam solar radiation will reach earth at differing angles based on the time of the year. At spring and fall equinoxes, direct beam radiation is directed perpendicular to areas located at the Equator. The radiation will be tilted from perpendicular directly proportional to your latitude. If you are approximately 38 degrees north of the Equator as we are in Rolla, Missouri, the sun's rays will be directed at 38 degrees south of perpendicular during equinoxes. During summer solstice, solar rays are directed at the Tropic of Cancer, which is approximately 23 degrees north of the equator, and will be tilted from the perpendicular proportional to your latitude from this point. During summer solstice, direct beam radiation is 23.45 degrees north of perpendicular at the Equator and 15 degrees south of perpendicular in Rolla, Missouri. During winter

solstice, solar radiation is directed at the Tropic of Capricorn, which is 23.45 degrees south of the Equator, and will also be tilted from the perpendicular proportional to your latitude away from this location. During winter solstice, direct beam radiation is 23.45 degrees south of perpendicular at the Equator and approximately 53 degrees south of perpendicular in Rolla, Missouri. The declination (δ) previously described can be calculated in the following equation (C.16):

$$\delta = 23.45° \times sin\left(\frac{360 \times (n-80)}{365}\right) \tag{C.16}$$

where n is the day of the year with n=1 on January 1st.

Since the earth rotates around the sun once per year in an elliptical orbit, the distance from the sun to the earth is given in the following equation (C.17), with units in m:

$$d = 1.5 \times 10^{11} \times \left\{1 + 0.017 \times sin\left[\frac{360 \times (n-93)}{365}\right]\right\} \tag{C.17}$$

The zenith angle (θ_z) is the angle between the sun and the zenith. This angle is directly measured at solar noon since this is the point that the sun is at its highest point in the sky. This zenith angle is calculated in both the northern and southern hemispheres using the following equation (C.18):

$$\theta_z = \phi - \delta \tag{C.18}$$

where ϕ is the site latitude. As shown in this equation, the declination can be positive or negative based on site location and date.

Since there are 24 hours in the day and the earth rotates 360 degrees per day, the earth then rotates at 15 degrees per hour. This hour angle (ω) can be calculated using the following equation (C.19):

$$\omega = \frac{12-t}{24} \times 360° = 15 \times (12 - T)°$$ (C.19)

where T is the time of day expressed with respect to solar midnight on a 24-hour clock. Since site locations are more specific than a large time zone, precise solar time must be calculated using the following equation (C.20):

$$Solar\ Time = ST + 4 \times (SL + LL) + E$$ (C.20)

where ST is the standard time, SL is the standard longitude, LL is the local longitude, and E is a correction factor. Do not forget to adjust standard time for daylight savings time during these periods by subtracting an hour.

Solar altitude (α) represents the angle between the horizon and the incident solar beam in a plane determined by the zenith and the sun. Solar altitude is therefore the compliment to the zenith angle. Since AM is proportional to secant of the zenith angle, AM is therefore calculated using the following equation (C.21):

$$AM = AM\ (90°) \times \csc \alpha$$ (C.21)

Previous calculations can be adjusted to determine the sunrise angle (ω_s), which is shown in the following equation (C.22):

$$\omega_s = \cos^{-1} (-\tan \phi \tan \delta)$$ (C.22)

This equation implies that sunset is equal to -ω_s. You can then use this value to calculate the incident hour at which sunrise would occur, which would give you the amount of sunlight for a given day (DH) See the following equation (C.23) for details:

$$DH = \frac{48}{360} \times \omega_s = \frac{cos^{-1}(-\tan\phi\tan\delta)}{7.5} \, hr \tag{C.23}$$

You can also determine the solar altitude at a given location at a specific date and time by using the following equation (C.24):

$$\sin\alpha = \sin\delta\sin\phi + \cos\delta\cos\phi\cos\omega \tag{C.24}$$

The azimuth angle (ψ) is the angular deviation of the sun from directly south. This angle measures the sun's angular position east or west of south, and is zero at solar noon and increases toward the west. The azimuth angle is measured as the angle between the intersection of the vertical plane determined by the observer and the sun with the horizontal and the horizontal line facing directly south from the observer, assuming the path of the sun is to the south of the observer. This azimuth angle can be calculated for a given location at a specific date and time using the given equation (C.25) below:

$$\cos\psi = \frac{\sin\alpha\sin\phi - \sin\delta}{\cos\alpha\cos\phi} \tag{C.25}$$

C.3 REFERENCES

Elmore, A.C. and Gallagher, R. (2009) *Using Regional Climate Center Data to Predict Small Wind Turbine Performance.* Practice Periodical of Hazardous, Toxic, and Radioactive Waste Management; 13(1):14-19

Gallagher, R. and Elmore, A.C. (2009). *Monte Carlo Simulations of Wind Speed Data.* Wind Engineering; 33(6):661-673.

Haldar, A., and Mahadevan, S. (2000). *Probability, Reliability, and Statistical Methods in Engineering Design,* Wiley, New York.

Johnson, G.L. (1985). *Wind Energy Systems.* Prentice Hall, Englewood Cliffs, New Jersey

Manwell, J., Mcgowan, J., and Rogers, A. (2002). *Wind Energy Explained – Theory, Design and Application*, Wiley, West Sussex, U.K.

VITA

Joe David Guggenberger II obtained his B.S. and M.S.in Geological Engineering from the University of Missouri-Rolla (currently Missouri University of Science and Technology) in 2003 and 2004, respectively. He received his Ph.D. in Geological Engineering from the Missouri University of Science and Technology in August 2012.

Mr. Guggenberger was employed as an associate research engineer and graduate research assistant at the Missouri University of Science and Technology. During this time, he was part of a team that designed and built two working renewable energy-powered microgrids, as well as completed research which led to this dissertation. Prior work experience included approximately 2.5 years as an environmental manager with Siegel-Robert Automotive (currently SRG Global) in Farmington, Missouri. He was also employed for approximately 3 years as an environmental engineer with CDM, Inc. in Kansas City, Missouri.

Mr. Guggenberger is a member of Engineers without Borders, Missouri Society of Professional Engineers, and the American Society of Civil Engineers. He is a registered Professional Engineer in the states of Missouri and Colorado, and a Certified Hazardous Materials Manager.